T.C.

MARMARA UNIVERSITY

INSTITUTE FOR GRADUATE STUDIES IN

PURE AND APPLIED SCIENCES

PRODUCTION OF NANOSCALE $Ba(Zn_{1/3}Nb_{2/3})O_3$ MICROWAVE DIELECTRIC CERAMICS BY POLYMERISED COMPLEX METHOD

Duygu SERT

THESIS

FOR THE DEGREE OF MASTER OF SCIENCE

IN

METALLURGY AND MATERIALS ENGINEERING

SUPERVISOR

Assoc. Prof. Dr. Ayhan MERGEN

İSTANBUL 2010

T.C.

MARMARA UNIVERSITY

INSTITUTE FOR GRADUATE STUDIES IN

PURE AND APPLIED SCIENCES

PRODUCTION OF NANOSCALE $Ba(Zn_{1/3}Nb_{2/3})O_3$ MICROWAVE DIELECTRIC CERAMICS BY POLYMERISED COMPLEX METHOD

Duygu SERT

(141103520070355)

THESIS

FOR THE DEGREE OF MASTER OF SCIENCE

IN

METALLURGY AND MATERIALS ENGINEERING

SUPERVISOR

Assoc. Prof. Dr. Ayhan MERGEN

İSTANBUL 2010

ACKNOWLEDGEMENT

I would like to thank all people who have helped and inspired me during my master study.

I especially want to thank my advisor, Assoc. Prof. Dr. Ayhan MERGEN, for his guidance during my research and study at Marmara University. His perpetual energy and enthusiasm in research had motivated all his students, including me. In addition, he was always accessible and willing to help his students with their research. Therefore, his encouragement, guidance and support from the initial to the final level enabled me to develop an understanding of the subject.

Prof. Dr. Arif N. GULLUOGLU deserves special thanks for his guidance during my undergraduate and postgraduate days and also for recommending me as a research assistant to work with Assoc. Prof. Dr. Ayhan MERGEN for the research project of The Scientific and Technological Research Council of Turkey (TUBITAK).

I was delighted to interact with Prof. Dr. Arif N. GULLUOGLU, Assoc. Prof. Dr. Seval GENC, Prof. Dr. Altan TURKELI and Assoc. Prof Dr. Cevat SARIOGLU by attending their classes during my post graduate education.

All my lab buddies at Marmara University, Metallurgical and Materials Science Engineering Laboratory made it a convivial place to work. In particular, I would like to thank Oğuz ÖZYOLDAŞ for his friendship and help in the past years. All other folks, including Esin KORKMAZ and Nisa BAKIR, had inspired me in research and life through our interactions during the long hours in the lab.

Lastly, I would like to give my great thanks to The Scientific and Technological Research Council of Turkey (TUBITAK) for financial support of this investigation under the Project grant number 107M372.

June, 2010 **Duygu SERT**

CONTENTS

ABSTRACT

PRODUCTION OF NANOSCALE $Ba(Zn_{1/3}Nb_{2/3})O_3$ MICROWAVE DIELECTRIC CERAMICS BY POLYMERISED COMPLEX METHOD

Dielectric materials, a kind of electronic ceramics, have various applications such as communication technology. Dielectric materials used in communication technology are microwave dielectrics which are applicable at high frequencies. The primary applications of microwave dielectrics in communication technology are resonators and filters. The other important application of microwave dielectrics is multi layer ceramic capacitors and detectors. Microwave dielectric ceramics require high relative permittivity (ε_r>30), low dielectric loss, high quality factor (Q~1/tanδ>20.000 at 2 GHz), temperature and frequence stability good mechanical and thermal stability.

$Ba(Zn_{1/3}Nb_{2/3})O_3$ (BZN) ceramic is one of the material that can be used as microwave dielectric in communication systems. BZN ceramic has high dielectric constant, low dielectric loss and high electrical resistivity (ε_r=38, Q×f=90 THz). However, BZN ceramics have high sintering temperatures of 1350°C which inhibits them to be co-fired with Cu or Ag electrodes with low melting temperature. In addition, the temperature coefficient of resonant frequency of BZN ceramic is high (τ_f=30 ppm/K) which restrict the use of these ceramics in microwave applications. In this respect, production of BZN ceramics with superior microwave dielectric properties and low sintering temperatures will encourage the usage of these ceramics.

In this study, nanosized BZN ceramics with low sintering temperature were produced by chemical method which is suitable for nanoscale powder production. Various parameters were used to produce nanosized, homogeneous powders without agglomeration. Synthesized powders were characterized to demonstrate the effect of different parameters in chemical processing.

June, 2010 **Duygu SERT**

ÖZET

POLİMERİZE KOMPLEKS METHOD İLE NANOBOYUTTA $Ba(Zn_{1/3}Nb_{2/3})O_3$ MİKRODALGA DİELEKTRİK SERAMİKLERİNİN ÜRETİMİ

Elektronik seramik grubu içerisindeki dielektrik malzemeler farklı kullanım alanlarına sahip olup, bunlardan biri haberleşme teknolojisidir. Haberleşme teknolojisinde kullanılan dielektrik malzemeler yüksek frekanslarda kullanılmaya uygun mikrodalga dielektriklerdir. Haberleşme sistemlerinde mikrodalga dielektrik seramiklerin temel uygulama alanları rezonatorler ve filtrelerdir. Mikrodalga dielektrik seramiklerin diğer önemli uygulama alanı da çok katlı seramik kapasitörler ve farklı alanlarda ihtiyaç duyulan dedektörlerdir. Mikrodalga dielektrik seramiklerin yüksek dielektrik katsayısına (ε_r>30), düşük dielektrik kayıplarına veya yüksek kalite faktörüne (Q~1/tanδ>20.000 2 GHz'de), geniş spektral aralıkta iyi bir frekans ve sıcaklık stabilitesine, iyi mekanik ve ısıl stabiliteye sahip olması gerekmektedir.

Haberleşme endüstrisinde mikrodalga dielektrik malzeme olarak kullanılma potansiyeli olan seramiklerden biri de $Ba(Zn_{1/3}Nb_{2/3})O_3$ (BZN) seramiğidir. BZN seramiği yüksek dielektrik sabitine, düşük dielektrik kaybına ve yüksek dirence sahiptir (ε_r=38, Q×f=90 THz). Ancak BZN seramiği 1350 °C gibi yüksek sinterlenme sıcaklığına sahip olup, bu durum BZN seramiğinin Cu ve Ag gibi düşük ergime sıcaklıklı elektrotlarla kullanımını imkansız hale getirmektedir. Ayrıca, BZN seramiğinin rezonans frekans sıcaklık katsayısı (τ_f=30 ppm/K) relatif olarak yüksek olup, bu durum BZN seramiklerinin mikrodalga uygulamalarında kullanımlarını kısıtlamaktadır. Bu nedenle ütün mikrodalga dielektrik özelliklere ve düşük sinterlenme sıcaklığına sahip BZN seramiğinin üretilmesi bu seramiklerin kullanılma potansiyelini arttıracaktır.

Yapılan çalışmada, düşük sinterlenme sıcaklığına sahip BZN seramiklerin üretilmesi amacıyla nano boyutta toz üretimine uygun kimyasal yöntemle BZN seramikleri üretilmiştir. Nano boyutta, aglomerasyon içermeyen homojen dağılıma sahip BZN seramik tozlarının üretilebilmesi için farklı parametreler kullanılmıştır. Üretilen tozlar kimyasal üretimde farklı parametrelerin etkisini vurgulayacak şekilde karakterize edilmiştir.

Haziran, 2010 **Duygu SERT**

SYMBOLS

°C : Degree Celsius

Å : Angstrom (10^{-10} m)

A : Infrared ıntensity in terms of absorbance

a : Lattice parameter (Å, Angstrom)

AC : Alternating current

am : Attometer (10^{-18} m)

B : Full-width at half-maximum

cm : Centimeter (10^{-2} m)

d : Separation of the positive and negative ends of the dipole

GHz : Giga Hertz (10^{9} Hertz)

h : hour

J : Joule

k : a constant taken as 0.9

kHz : Kilo Hertz (10^{3} Hertz)

kV : Kilovolt

M : Molarity

MHz : Mega Hertz (10^{6} Hertz)

mm : milimeter (10^{-3} m)

N : Normality

N : Number of dipoles

n : Refractive index

nm : Nanometer (10^{-9} m)

P : Polarization, dipole moment per unit volume

pH : Power of hydrogen

q : Electrical charge

Qxf : Quality Factor (Hz, Hertz)

T : Infrared ıntensity in terms of transmittence

tan γ : Dielectric loss tangent

V : Volume (cm^3)

W_D : Dray weight

$\mathbf{W_S}$: Weight after suspension

$\mathbf{W_w}$: Weight measured in air

$\boldsymbol{\alpha_L}$: Linear thermal expansion coefficient of the dielectric material (ppm/°C)

$\boldsymbol{\varepsilon_r}$: Relative permittivity

$\boldsymbol{\theta}$: Diffraction angle

$\boldsymbol{\kappa}$: Dielectric constant

$\boldsymbol{\lambda}$: Wavelength of the X-ray radiation (1.5406Å for Cu Kα)

$\boldsymbol{\lambda_0}$: Wavelenght in air

$\boldsymbol{\lambda_d}$: Wavelength in the dielectric

$\boldsymbol{\mu}$: Dipole moment

$\boldsymbol{\mu m}$: Micrometer (10^{-6} m)

$\boldsymbol{\tau_f}$: Temperature coefficient of resonant frequency (ppm/K, ppm/°C)

$\boldsymbol{\tau_\varepsilon}$: Temperature coefficient of the permittivity

ABBREVIATIONS

BCN : $Ba(Co_{1/3}Nb_{2/3})O_3$

BF : Brightfield

BGT : $Ba(Ga_{1/2}Ta_{1/2})O_3$

BMN : $Ba(Mg_{1/3}Nb_{2/3})O_3$

BMT : $Ba(Mg_{1/3}Ta_{2/3})O_3$

BNN : $Ba(Ni_{1/3}Nb_{2/3})O_3$

BSE : Backscattered electron

BZCN : $Ba[(Zn,Co)_{1/3}Nb_{2/3}]O_3$

BZN : $Ba(Zn_{1/3}Nb_{2/3})O_3$

BZN-1 : Powders that were synthesized by citrate gel method with citric acid/metal cations mol ratio as 5

BZN-2 : Powders that were synthesized by citrate gel method with citric acid/metal cations mol ratio as 2

BZN-3 : Powders that were synthesized by citrate gel method with citric acid/metal cations mol ratio as 1

BZN-4 : Powders that were synthesized by citrate gel method with citric acid/metal cations mol ratio as 0.5

BZT : $Ba(Zn_{1/3}Ta_{2/3})O_3$

CA : Citric acid

CZN : $Ca(Zn_{1/3}Nb_{2/3})O_3$

DF : Dark-field

DTA : Differential thermal analysis

EDS : Energy dispersive X-Ray spectroscopy

ESR : Electron spin resonance spectroscopy

FTIR : Fourier Transform Infrared

FWHM : Full-width at half-maximum

IR : Infrared

MC : Metal cation

SE : Secondary electron

SEM : Scanning electron microscopy

SZN : $Sr(Zn_{1/3}Nb_{2/3})O_3$

TEM : Transmission electron microscopy

TEOA : Titanium triethanolamine

TG : Thermogravimetry

TGA : Thermogravimetric analysis

XRD : X-ray diffractometer

FIGURES

PAGE NO

TABLES

PAGE NO

CHAPTER I

INTRODUCTION AND AIM

Although there has been considerable amount of work in the area of dielectric oxides in the past 50 years, dielectric materials continue to remain a significant area of scientific research due to their wide range of applications such as resonators, filters and tuners. Most of these dielectric materials are formed by the connection of metal-oxygen octahedras to each other to form principally three-dimensional structures. Among these dielectric oxides, $BaTiO_3$ which has a simple perovskite type structure and has wide ranging applications in electronic industry is probably the best dielectric ceramic of the century [1]. In addition to simple perovskites, complex perovskite structures such as niobium and tantalum based $AB_{1/3}B'_{2/3}O_3$ oxides (A=Ba; B=Mg, Zn, Ni; B'=Ta, Nb) are novel microwave dielectric materials that have been used in dielectric applications such as mobile communication, global positioning system and base station filtering technology [2]. Microwave dielectric materials are required to have high dielectric constant (ε_r>30), low dielectric loss, good temperature stability of frequency in a wide spectral range and good mechanical and thermal stability as they are investigated in terms of electrical properties [3]. Beside satellite systems and mobile communication, microwave dielectric materials are used in multi-layer ceramic capacitors and various kinds of detectors such as thermal, pressure, vibration and radiation.

$Ba(B'_{1/3}B''_{2/3})O_3$ microwave dielectric ceramics (B'=Mg, Zn, Ni; B''=Ta, Nb) which have complex perovskite structure have gained a giant importance for the last 20 years after the discovery of $Ba(Zn_{1/3}Ta_{2/3})O_3$ ceramics. The group of ceramics such as $Ba(Zn_{1/3}Ta_{2/3})O_3$, $Ba(Mg_{1/3}Ta_{2/3})O_3$ and $Ba(Mn_{1/3}Ta_{2/3})O_3$ have excellent microwave dielectric properties [4, 5]. Improvement of cheaper materials that have similar properties with $Ba(Zn_{1/3}Ta_{2/3})O_3$ microwave dielectrics has become important since Ta_2O_5 is an expensive oxide. In recent years, one of the materials that has been improved as a result of the studies is the $Ba(Zn_{1/3}Nb_{2/3})O_3$ (BZN) ceramic [6]. As

compared with Ta_2O_5, Nb_2O_5 has the same crystal structure, similar ionic radius (0.64 Å) and electronic structure. The most importantly Nb_2O_5 is rather cheaper than Ta_2O_5.

$Ba(Zn_{1/3}Nb_{2/3})O_3$ oxide is a cubic perovskite ceramic and it is a member of Pm3m space group. High temperature sintering makes $Ba(Zn_{1/3}Nb_{2/3})O_3$ ceramic to have disordered cubic structure, on the other hand sintering below 1350 °C makes it to have ordered hexagonal structure which belongs to P−3m1 space group that introduces lower symmetry [7, 8]. $Ba(Zn_{1/3}Nb_{2/3})O_3$ ceramic has a high dielectric constant, low dielectric loss and high resistivity (ε_r=38, Qxf=90 THz). These electrical properties cause $Ba(Zn_{1/3}Nb_{2/3})O_3$ dielectric ceramic become a popular material in the communication industry and also increase the usage potential in applications such as capacitors and high frequency resonators. However, the temperature coefficient of resonant frequency of $Ba(Zn_{1/3}Nb_{2/3})O_3$ ceramic is high (τ_f=30 ppm/K) which restricts the use of these ceramics in microwave applications. Various methods have been applied to improve the properties of $Ba(Zn_{1/3}Nb_{2/3})O_3$ ceramics such as doping with different elements like Ti [9] or making composite of $Ba(Zn_{1/3}Nb_{2/3})O_3$ ceramics with other $Ba(B'_{1/3}B''_{2/3})O_3$ microwave dielectric ceramics (B'=Mg, Zn, Ni; B''=Ta, Nb) like $Ba(Zn_{1/3}Nb2_{/3})O_3$–$Ba(Ni_{1/3}Nb_{2/3})O_3$ [10]. $0.35(Ba(Ni_{1/3}Nb_{2/3})O_3)$–$0.65(Ba(Zn_{1/3}Nb_{2/3})O_3)$ composite microwave dielectric material which was sintered at 1450 °C for 4 h and annealed at 1300 °C for 72 h exhibited good dielectric properties: temperature coefficient of resonant frequency (τ_f) of +0.6 ppm°C^{-1}, relative permittivity of 35 and quality factor in excess of 25,000 GHz [10]. The other drawback with $Ba(Zn_{1/3}Nb_{2/3})O_3$ ceramics is that they require fairly high sintering temperatures which inhibits these ceramics to be co-fired with Cu or Ag electrodes that have low melting temperature. Therefore, it is important to reduce the sintering temperature of these ceramics. In this respect, different methods such as synthesis by chemical methods or production with additives that were applied to different electronic ceramics can be applied to $Ba(Zn_{1/3}Nb_{2/3})O_3$ ceramic to lower its sintering temperature and improve its microwave properties.

In this thesis, $Ba(Zn_{1/3}Nb_{2/3})O_3$ (BZN) perovskite ceramics were produced from BZN nanoparticles by citrate gel method which is a suitable chemical method for nanoscale powder production and never used before in the production of BZN ceramic. Effect of citric acid content on the BZN phase formation and on the size

and shape of BZN particles was investigated by changing the citric acid to metal cation mol ratio. Fabricated $Ba(Zn_{1/3}Nb_{2/3})O_3$ ceramic powders were characterized by various methods like TG–DTA, XRD, FT-IR, SEM and TEM. BZN single phase perovskite ceramics with high density were sintered from nanoscale BZN powders at lower temperatures as compared with mixed oxide route. Dielectric properties of these ceramics were examined at various frequencies (1 kHz-2 MHz) and temperatures (20-200 °C). The aim was to produce nano sized BZN perovskite ceramics with low cost, better dielectric properties and low sintering temperatures to ensure these ceramics to be co-fired with cheaper and high on conductivity, low melting point electrodes such as Cu or Ag.

CHAPTER II

GENERAL BACKGROUND

II.1 CERAMIC MATERIALS

Ceramics are usually associated with “mixed” bonding—a combination of covalent, ionic, and sometimes metallic. They consist of arrays of interconnected atoms; there are no discrete molecules. The majority of ceramics are compounds of metals or metalloids and nonmetals. Most frequently they are oxides, nitrides, and carbides.

Ceramics generally have specific properties associated with them:

Brittleness - The reason that the majority of ceramics are brittle is the mixed ionic–covalent bonding that holds the constituent atoms together.

Poor electrical and thermal conduction - The valence electrons are tied up in bonds and are not free as they are in metals. In metals it is the free electrons—the electron gas—that determines many of their electrical and thermal properties.

Compressive strength - Ceramics are stronger in compression than in tension, whereas metals have comparable tensile and compressive strengths. This difference is important when we use ceramic components for load-bearing applications. It is necessary to consider the stress distributions in the ceramic to ensure that they are compressive.

Chemical insensitivity - A large number of ceramics are stable in both harsh chemical and thermal environments.

II.1.1 Types of Ceramic and Their Applications

The applications of ceramics are diverse, from bricks and tiles to electronic and magnetic components. These applications use the wide range of properties exhibited by ceramics. Some of these properties are listed in Table II.1 together with examples of specific ceramics and applications. The functions of ceramic products are

dependent on their chemical composition and microstructure, which determines their properties.

Table II.1 Properties and applications for ceramics [11].

Property	*Example*	*Application*
Electrical	$Bi_2Ru_2O_7$	Conductive component in thick-film resistors
	Doped ZrO_2	Electrolyte in solid-oxide fuel cells
	Indium tin oxide (ITO)	Transparent electrode
	SiC	Furnace elements for resistive heating
	$YBaCuO_7$	Superconducting quantum interference devices (SQUIDs)
	SnO_2	Electrodes for electric glass melting furnaces
Dielectric	α-Al_2O_3	Spark plug insulator
	$PbZr_{0.5}Ti_{0.5}O_3$ (PZT)	Micropumps
	SiO_2	Furnace bricks
	$(Ba,Sr)TiO_3$	Dynamic random access memories (DRAMs)
	Lead magnesium niobate (PMN)	Chip capacitors
Magnetic	γ-Fe_2O_3	Recording tapes
	$Mn_{0.4}Zn_{0.6}Fe_2O_4$	Transformer cores in touch tone telephones
	$BaFe_{12}O_{19}$	Permanent magnets in loudspeakers
	$Y_{2.66}Gd_{0.34}Fe_{4.22}Al_{0.69}Mn_{0.09}O_{12}$	Radar phase shifters
Optical	Doped SiO_2	Optical fibers
	α-Al_2O_3	Transparent envelopes in street lamps
	Doped $ZrSiO_4$	Ceramic colors
	Doped (Zn,Cd)S	Fluorescent screens for electron microscopes
	$Pb_{1-x}La_x(Zr_zTi_{1-z})_{1-x/4}O_3$ (PLZT)	Thin-film optical switches
	Nd doped $Y_3Al_5O_{12}$	Solid-state lasers
Mechanical	TiN	Wear-resistant coatings
	SiC	Abrasives for polishing
	Diamond	Cutting tools
	Si_3N_4	Engine components
	Al_2O_3	Hip implants
Thermal	SiO_2	Space shuttle insulation tiles
	Al_2O_3 and AlN	Packages for integrated circuits
	Lithium-aluminosilicate glass ceramics	Supports for telescope mirrors
	Pyrex glass	Laboratory glassware and cookware

It is a common approach to class ceramics as traditional and advance, before dividing them according to their properties and applications:

Traditional ceramics are usually based on clay and silica. There is sometimes a tendency to equate traditional ceramics with low technology, however, advanced manufacturing techniques are often used. Competition among producers has caused processing to become more efficient and cost effective. Complex tooling and machinery is often used and may be coupled with computer-assisted process control.

Advanced ceramics are also referred to as "special," "technical," or "engineering" ceramics. They exhibit superior mechanical properties, corrosion/oxidation resistance, or electrical, optical, and/or magnetic properties.

While traditional clay-based ceramics have been used for over 25,000 years, advanced ceramics have generally been developed within the last 100 years [11].

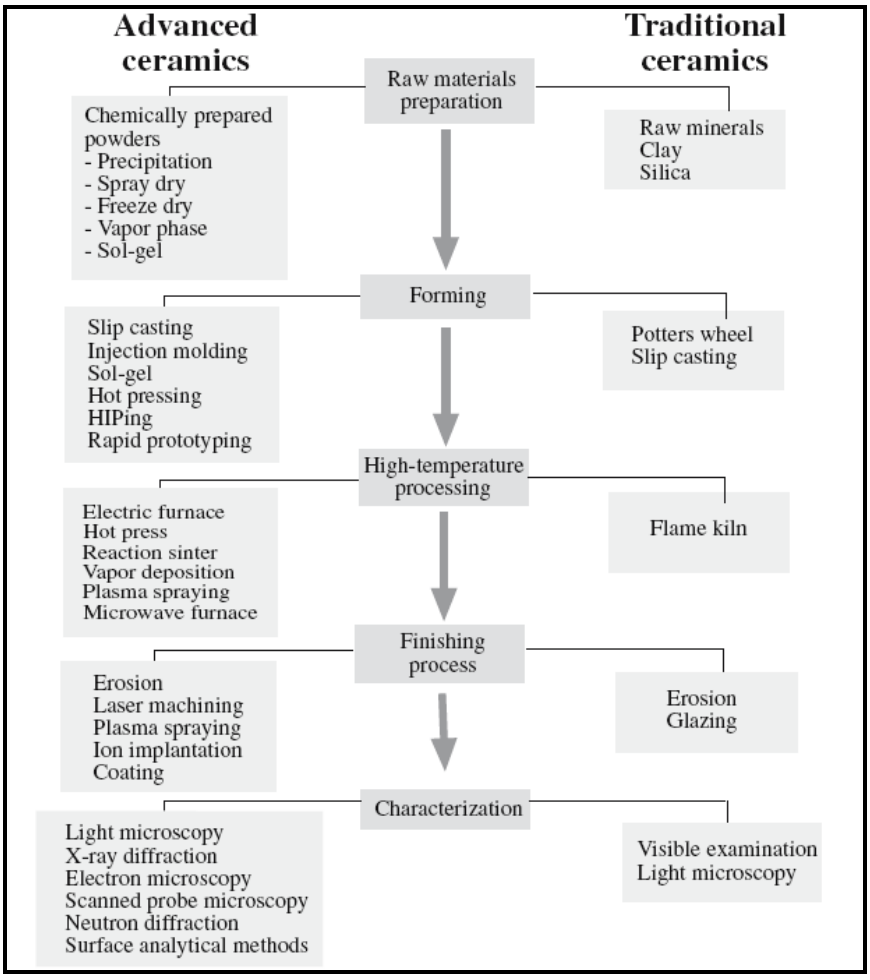

Figure II.1 A comparison of different aspects for traditional and advanced ceramics.

Figure II.1 compares traditional and advanced ceramics in terms of the type of raw materials used, the forming and shaping processes and the methods used for characterization.

II.1.2 Ceramic Powder Processing

Many methods are available for the preparation of ceramic powders. These can be divided into just three basic types: Mechanical, Chemical, Vapor Phase [11].

Mechanical methods use coarse-grained materials that have generally been derived from naturally occurring minerals. They are subjected to a series of processes, collectively referred to as comminution, in which the particle size is gradually reduced. The final step is known as milling, which produces particles of

the desired size. Mechanical methods of powder production are used widely in the production of traditional ceramic products where high purity powders are not required and cost is one of the most important requirements.

Chemical methods, such as sol-gel processing, offer several advantages over mechanical methods because they allow exceptional control over particle size, morphology and purity. In addition, atomic or molecular level homogeneity can be attained by chemical methods. Chemical processes are used widely in the production of advanced ceramic materials.

Vapor-phase processes can be used to produce ceramic powders. They tend to be expensive, but offer many advantages, such as the ability to produce particles of non-oxides such as Si_3N_4 and SiC. In addition, there are several reasons for using vapor-phase reactions to prepare powders, particulary when the below properties are required:

- High purity,
- Discrete and non-aggregated particles,
- Nanoparticles with narrow size distributions,
- Versatility in producing powders of oxides and non-oxides [11].

II.1.2.1 Chemical Processing of Ceramics

The performance and properties of materials depend on atomic structure, composition, microstructure, defects, and interfaces which are controlled by thermodynamics and kinetics of the synthesis and processing. Nanostructured materials, often characterized by a physical dimension (such as particle size or grain size) of less than 100 nm, attract much interest due to their unique properties compared to conventional materials. Current advances in synthesizing and processing of functional materials for high technology emphasize the bottom-up approach to assemble atoms, molecules and particles, from the atomic or molecular scale to the macroscopic scale [12].

Chemical methods such as precipitation [13], sol–gel processing and solvothermal methods [14] can be used to synthesize ceramic nanoparticles. As-synthesized powders, depending on the synthesis technique used, may require subsequent heat treatment for dehydration, removal of organics, and controlled crystallization to form oxides with desirable structure and crystallite size.

Sol-gel processing is one of the chemical methods to produce nanopowders of ceramics with a high surface area, which allows sintering to nearly full density at much lower temperatures than are normally required when the particles have been made by other techniques [11].

Sol–gel processes can be used to make various types of materials such as powders, films, fibers, and monoliths. The conventional sol–gel process involves hydrolysis and condensation of metal alkoxides. Metal alkoxides have the general formula $M(OR)_x$ and an alkoxide ion is the conjugate base of an alcohol. The general synthesis of metal alkoxides involves the reaction of metal species (a metal, metal hydroxide, metal oxide or metal halide) with an alcohol. Metal alkoxides are good precursors because they readily undergo hydrolysis that replaces an alkoxide with a hydroxide group from water and a free alcohol is formed. Once hydrolysis has occurred the sol can react further and condensation (polymerization) occurs, leading to gel formation. In condensation two hydrolyzed fragments join together, releasing either an alcohol or water. Condensation occurs by either nucleophilic substitution or nucleophilic addition [12]. There are several variables in the sol-gel process:

- Rates of hydrolysis and condensation (relative differences in the rates can be used to modify the microstructure of the powder)
- Type of alkoxide (mixing of the alkoxides in the solution is achieved at a molecular level giving the powders a high degree of chemical homogeneity)
- Reaction temperature (affects the degree of polymerization of the gel)
- Amount of water added (affects the degree of polymerization of the gel)
- Solution pH (rates of hydrolysis and condensation can be increased by the addition of acids or bases, respectively)

Gelation times vary from seconds to several days. When the gel forms it may contain only about 5 vol% of the oxide. The dried gel is calcined to completely convert it to oxide. Powders produced by the sol-gel method are amorphous. A crystallization step is required to produce crystalline bodies, which is often performed after sintering [11].

Sol–gel methods can be used to prepare pure, stoichiometric, dense, equiaxed, and uniform particles. For example, uniform anatase TiO_2 particles with average particle size of 5 to 30 nm were prepared by controlled hydrolysis of a titanium

triethanolamine (TEOA) complex [15]. It was found that the pH value of the sol–gel was a decisive factor for controlling the final size, shape, and phase of the particle. The effects of surface chemistry on the morphology and phase stability of titanium dioxide nanoparticles was investigated using a thermodynamic model based on surface free energies and surface tensions. It was suggested that surfaces representing acidic and alkaline conditions had a significant influence on both the shape of the nanocrystals and the anatase-to-rutile transition size [16].

The sol–gel process is particularly attractive for synthesis of multicomponent particles with binary or ternary compositions using double alkoxides (two metals in one molecule) or mixed alkoxides (with mixed metaloxane bonds between two metals). Atomic homogeneity is not easily achieved by coprecipitating colloidal hydroxides from a mixture of salt solutions since it is difficult to construct double metaloxane bonds from metal salts [17]. Hybrid materials such as metal-oxide, organics-oxide can be prepared using the sol–gel approach.

The Pechini method (Pechini, 1967) is very famous as a simple method for preparing metal oxide powders where polymeric precursors are made from metal salts, ethylene glycol and citric acid by low temperature heat-treatment. This method allows the metal cations to be mixed at a molecular level and the stoichiometric compositions to be achieved by chelating the metal ions in solution by citric acid.

Pechini method is based on polymerization of metal citrates using ethylene glycol [18]. It is a commercial process for the preparation of titanates and niobates for the capacitor industry. With slight modifications, it is also referred to as the "citrate gel" process or the "amorphous citrate" process. Figure II.2 shows a flow chart for the preparation of strontium titanate powder by Pechini method. Metal ions from starting materials such as carbonates, nitrates, and alkoxides are complexed in aqueous solution with α-carboxylic acids such as citric acid. When heated with a polyhydroxyl alcohol, such as ethylene glycol, polyesterification occurs. On removal of the excess liquid a transparent resin is formed. The resin is heated to decompose the organic constituents, ground to break up large agglomerates, and finally calcined.

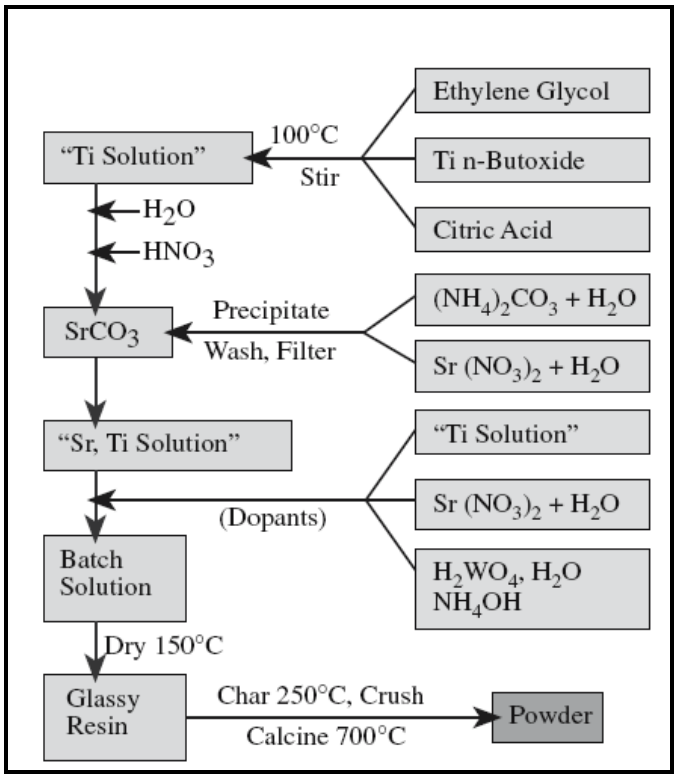

Figure II.2 Flow chart for preparing $SrTiO_3$ powders by the Pechini method [11].

Precipitation is the other chemical method to produce ceramic nanopowders with superior properties. To cause precipitation it is necessary to produce a supersaturated solution. This can be achieved, for example, by changing the pH or the temperature of the solution. A larger quantity of a soluble component (for example, a metal salt) can be dissolved in a solution at high temperature than at a lower temperature [11].

In a solution or mixture, chemical reagents or precursors react to form stable nuclei followed by the growth of particles. Reactants can be solids or liquids and sometimes gases. Aqueous or nonaqueous solvents are used. For coprecipitation of multicomponent particles, attention is required to control the conditions to achieve chemical homogeneity of the final product. Different ions may precipitate under different conditions of pH and temperatures with different solubility product constants.

After a reagent such as a reducing or oxidizing agent is added to the reactant solution or mixture, chemical reactions occur and the solution becomes supersaturated with the product. The supersaturation drives the chemical system to deviate from the minimum free energy configuration. The state of thermodynamic

equilibrium is restored by condensation of nuclei of the reaction product. Homogeneous nucleation does not involve foreign species as nucleating aids. Heterogeneous nucleation however allows formation of nuclei on foreign species.

Kinetic factors compete with the thermodynamics of the system in a growth process. Factors such as reaction rates, transport rates of reactants, accommodation, removal, and redistribution of matter compete with influences of thermodynamics in particle growth. The reaction and transport rates are affected by concentration of reactants, temperature, pH and order of introduction of and degree of mixing of reagents. The structure and crystallinity of particles may be influenced by reaction rates and impurities. Factors such as supersaturation, nucleation and growth rates, colloidal stability and recrystallization and aging processes have effects on the particle size and microstructure. Supersaturation generally shows predominant influence on the morphology of precipitates. At low supersaturation, the particles are small, compact, and well-formed, and the shape depends on crystal structure and surface energies. At high supersaturation, large and dendritic particles form. At even higher supersaturation, smaller but compacted, agglomerated particles form. The interface-controlled growth of a small particle in solution becomes diffusion-controlled after the particle exceeds a critical size [12].

For a supersaturated solution concentration exceeds the threshold for homogeneous nucleation and therefore, a large number of nuclei form suddenly. Their formation lowers the solution concentration below the concentration at which nucleation occurs, but enough excess solute remains for the existing nuclei to grow. If the solution is kept uniform, growth of all the particles proceeds at the same rate, producing powders with extremely uniform size distribution. The variation of solute concentration with time during the nucleation and growth of particles from solution is shown in Figure II.3. This diagram is often referred to as a LaMer diagram.

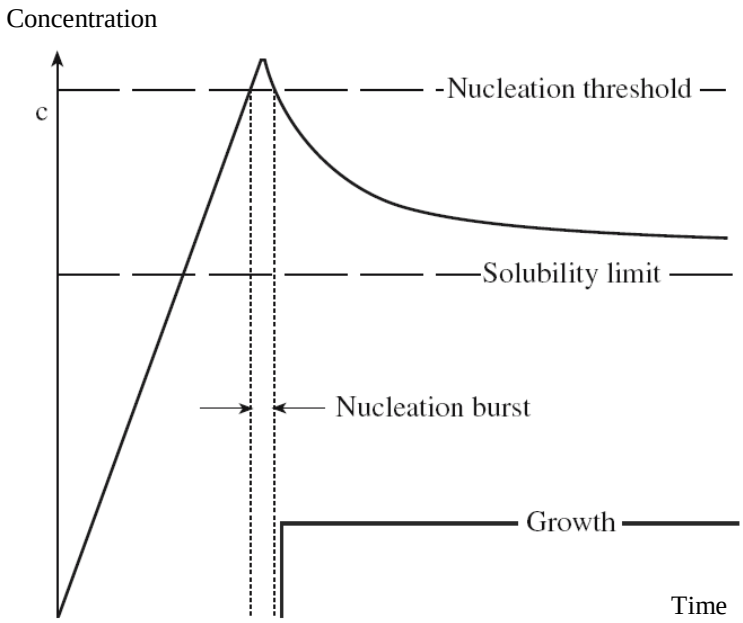

Figure II.3 Concentration versus time for a solution in which the concentration is first increased to the point of nucleation (e.g., by evaporation) and then declines as a precipitate grows [11].

Solvothermal Method is the technique in which the reaction mixture is heated above the boiling point of the solvent in an autoclave or other closed system and the sample is exposed to steam at high pressures. The reactions may be carried out in water or in any other solvent (e.g. methanol, ethanol, polyol). When water is used as a solvent, the process is described as hydrothermal. Compared with synthesis routes at atmospheric pressure, the increased reaction temperature in the solvothermal technique may lead to an accelerated crystal growth accompanied by a narrow particle size distribution and better crystallinity.

A general strategy utilizing the solvothermal technique was reported as a unified approach to the synthesis of a large variety of nanoparticles including noble metal, ceramic, and polymer nanoparticles. In this method, sodium linoleate (or another sodium stearate), linoleic acid (or another fatty acid), and ethanol are added to the aqueous solution of metal ions in an autoclave tube under agitation. At a certain temperature, it is proposed that a cation exchange between the metal ion and sodium linoleate results in formation of metal linoleate. Decomposition of the in-situ generated metal linoleate, under designated reaction conditions, can yield oxide (e.g. TiO_2 and ZnO), ferrite (e.g. Fe_3O_4 and $CoFe_2O_4$), and titanate (e.g. $BaTiO_3$ and $SrTiO_3$) nanoparticles [12].

II.1.3 Ceramic Powder Characterization

Common analytical methods used to characterize ceramic powders include Thermogravimetric (TG) and Differential Thermal Analysis (DTA) for thermal behavior investigations to track phase decompositions and formations, X-Ray Diffraction Analysis for phase formation, particle size and structure analysis, Scanning Electron Microscopy (SEM) and Transmission Electron Microscopy (TEM) for particle size, morphology and chemical composition investigations, Energy Dispersive X-Ray Spectroscopy (EDS) for characterization of the elemental composition for an analyzed volume, Fourier Transform Infrared Spectroscopy (FTIR) for the identification of compounds and sample compositions.

II.1.3.1 Thermal Gravimetric (TGA)/Differential Thermal (DTA) Analysis

TGA measures the change in weight as the sample is heated in an atmosphere of choice. Equipment is capable of reaching above 1500 °C and usually has an air, nitrogen, or an argon atmosphere. TGA is useful in studies such as binder burn-out, desorption, dehydration and thermal decomposition. DTA measures the temperature difference between a sample and an inert material as they are heated. This is useful for locating the temperature where reactions occur such as for melting, phase changes and oxidation. Instruments can measure both the change in weight and the change in temperature.

II.1.3.2 X-Ray Diffraction

X-ray diffraction produces an array of peaks resulting from lattice geometry rather than a spectra of wavelengths. This technique is used to identify the crystalline phase present in the sample. Each phase has a nearly unique diffraction pattern; when the same pattern appears for more than one phase, chemical analysis can aid in sorting. Diffraction is not only widely used for crystal structure analysis, but it is also commonly used in the ceramic laboratory. X-ray analysis are performed by a diffractometer for phase identification, particle or grain size analysis, presence of glass, colloidal particle size and stress analysis. Powders are analyzed for the phases present by a diffractometer. Figure II.4 shows the main components of an X-ray diffractometer [18]. The important features include the following:

X-ray source - Often Cu Kα λ = 0.154184 nm because of its high intensity.

Sample - Usually a powder, but it can be pressed or sintered. Only a few milligrams is needed.

Detector - There are two main types: proportional detectors use photoelectrons generated in Xe (Xenon) ; semiconductor detectors use electron-hole pairs created in p-i-n junctions formed in silicon.

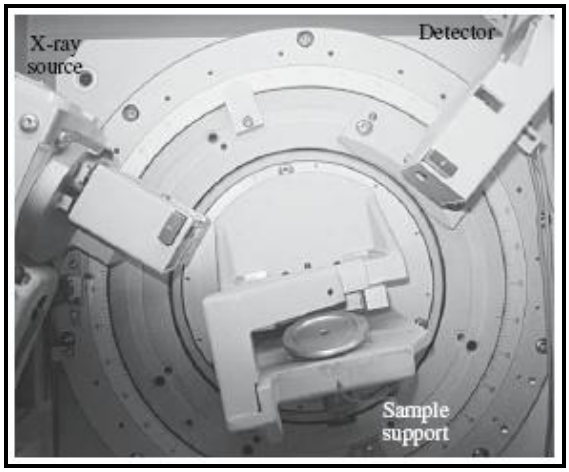

Figure II.4 XRD apparatus showing the location of the source, sample, and detector (Siemens D5005) [11].

X-rays from a source pass through a monochrometer, collimated, and impinge upon the sample being analyzed. The sample is usually powder packed in a rectangular holder, but can also exist as a film on a glass slide or a solid ceramic planer surface. Interplaner spacings in the crystal lattice diffract the beam at different angles. The interference of beam patterns is constructive when the phase shift is a multiple of 2π; this condition can be expressed by Bragg's law:

$$nX = 2d\sin\theta \qquad \text{(II.1)}$$

n: an integer,

λ: wavelength of the incident wave,

d: the spacing between the planes in the atomic lattice,

θ: the angle between the incident ray and the scattering planes.

A sketch of the geometry is presented in Figure II.5. The angles in the instrument shown in Figure II.5 are measured with a shaft-encoder-controlled goniometer that contains a radiation detector to measure ray intensity. Slit widths are

computer-controlled. The amount of a phase present is proportional to the intensity of the diffraction line.

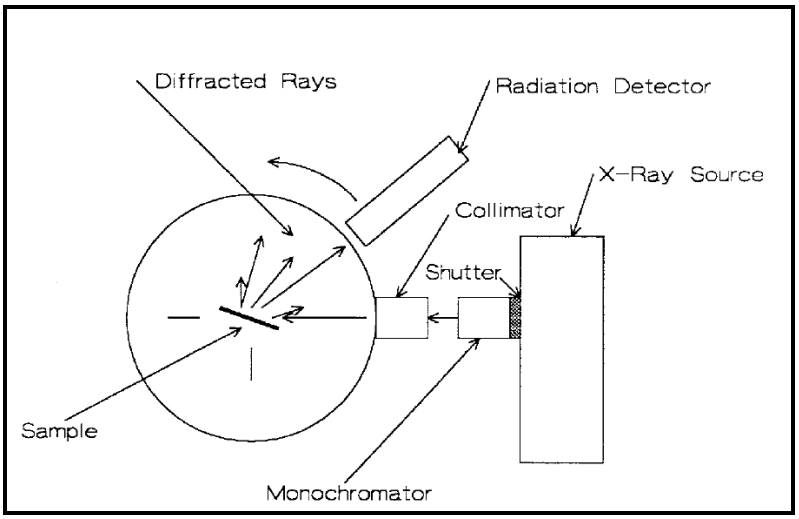

Figure II.5 Sketch, X-Ray Diffraction Geometry. Both the detector and sample rotate during the measurement [19].

II.1.3.3 Imaging in Scanning Electron Microscopy (SEM)

The SEM can have two imaging detectors, one for secondary electrons (SEs) and one for higher-energy backscattered electrons (BSEs). SEM works under high vacuum, because a gas atmosphere rapidly spreads and attenuates electron beams. The vacuum levels of each part of SEM are indicated in Figure II.6. The SEM typically has a resolution in SE mode of 0.7 nm (at 25 kV) and 2.5 nm in BSE mode at 5 kV. In addition to the excellent spatial resolution, the other great advantage of the SEM is that it has a great depth of field. So the images appear more three dimensional. The physical reason for this is that the electron beam is very narrow.

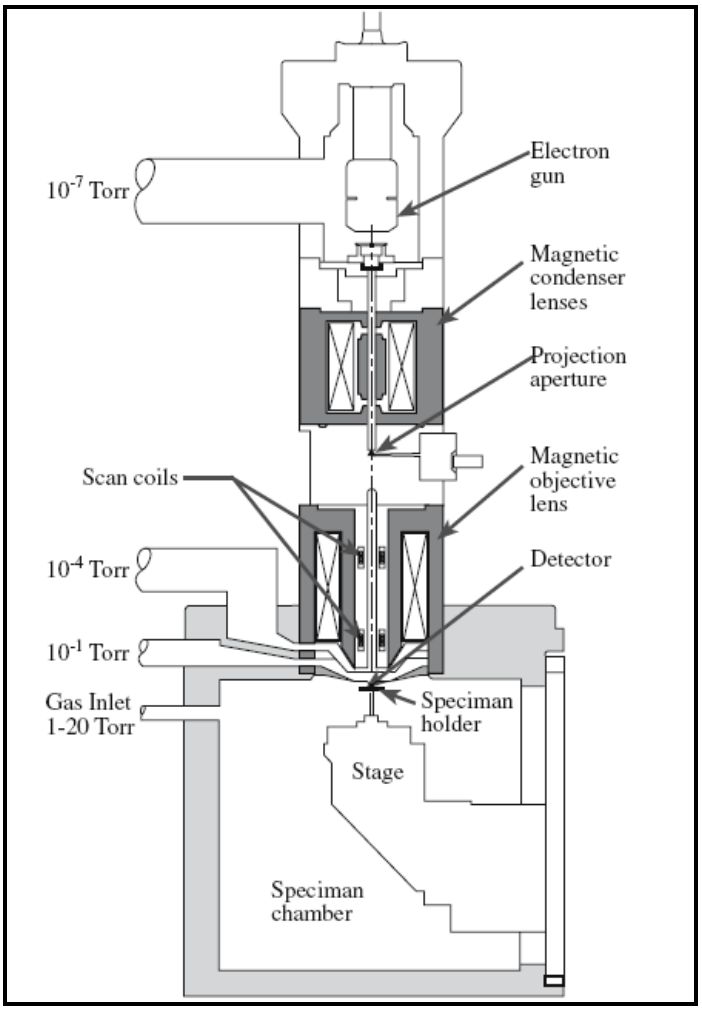

Figure II.6 Schematic of an SEM showing examples of pressures used.

SEs are low-energy electrons so they are very sensitive to surface topology. BSEs are higher-energy electrons and are sensitive to the atomic number of the scattering atom. Hence the intensity of the BSE signal depends on a combination of the average atomic number and density of the ceramic. As the kilovolts are reduced, the scattering volume becomes more localized close to the surface of the sample. The BSE electrons penetrate further into the sample and have further to come out after being scattered. Hence the BSE image can give excellent mass discrimination even at low voltages.

II.1.3.4 Imaging in Transmission Electron Microscopy (TEM)

The key requirement for using TEM is the requirement of the sample to be very thin (usually≤200 nm). Figure II.7 shows a state of-the-art TEM with a field emission source. So the technique is destructive and specimen preparation can be

time consuming. The benefits, however, are significant. Because of the large range of signals generated by the incident electron beam, a TEM allows full characterization of a sample at high resolution. The conventional imaging modes in a TEM are brightfield (BF) imaging and dark-field (DF) imaging. In BF imaging the image is formed using only the direct beam. An aperture (the objective aperture) is used to exclude all the diffracted electrons from contributing to the image. In DF imaging, the image is formed from one of the elastically scattered beams and the objective aperture blocks the direct beam and all the other scattered electrons.

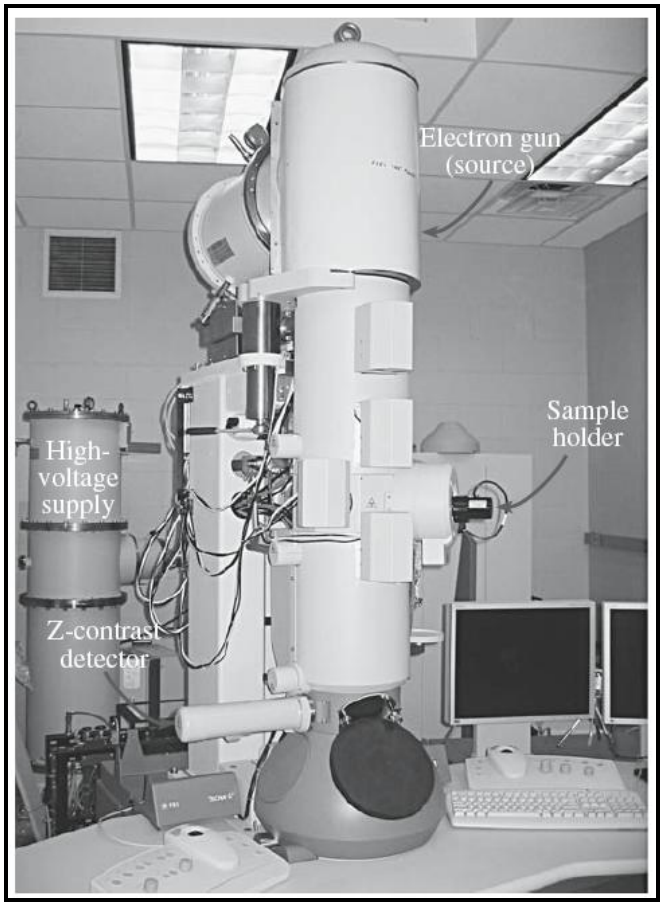

Figure II.7 A TEM with key features labeled.

The resolution of a TEM is determined by the energy of the electrons (controlled by the accelerating voltage), the thickness of the specimen, the distance between the sample and the objective lens, and the inherent quality of the lens (defined by its spherical aberration coefficient).

II.1.3.5 Energy Dispersive X-Ray Spectroscopy (EDS)

Energy Dispersive X-Ray Spectroscopy (EDS) is a chemical microanalysis technique used in conjunction with scanning electron microscopy (SEM). The EDS technique detects X-Rays emitted from the sample during bombardment by an electron beam to characterize the elemental composition of the analyzed volume. Features or phases as small as 1 μm or less can be analyzed.

When the sample is bombarded by the SEM's electron beam, electrons are ejected from the atoms comprising the sample's surface. The resulting electron vacancies are filled by electrons from a higher state, and an X-Ray is emitted to balance the energy difference between the two electrons' states. The X-Ray energy is characteristic of the element from which it was emitted.

The EDS X-Ray detector measures the relative abundance of emitted x-rays versus their energy. The detector is typically a lithium-drifted silicon, solid-state device. When an incident X-Ray strikes the detector, it creates a charge pulse that is proportional to the energy of the X-Ray. The charge pulse is converted to a voltage pulse (which remains proportional to the X-Ray energy) by a charge-sensitive preamplifier. The signal is then sent to a multichannel analyzer where the pulses are sorted by voltage. The energy, as determined from the voltage measurement, for each incident x-ray is sent to a computer for display and further data evaluation. The spectrum of X-Ray energy versus counts is evaluated to determine the elemental composition of the sampled volume [20].

II.1.3.6 Fourier Transform Infrared Spectroscopy (FTIR)

IR spectroscopy involves the scattering of light. In IR spectroscopy, the light is polychromatic and couples to vibrational modes in the solid through dipole moments, which are associated with the vibration. These vibrational modes cause a dip in the transmission spectra or a peak in the absorption spectra. The IR range is from 0.78 to 1000 μm (12,820 to 10 cm^{-1}). The region where most fundamental vibrational modes occur, which is the most useful for materials characterization, is between 2.5 and 25 μm (4000–400 cm^{-1}). This is sometimes called the mid-IR region. The light source is a heated ceramic (usually a conducting ceramic or a wire heater coated with ceramic) that emits a range of frequencies.

Infrared spectroscopy (IR spectroscopy) is the subset of spectroscopy that deals with the infrared region of the electromagnetic spectrum. It covers a range of

techniques, the most common being a form of absorption spectroscopy. As with all spectroscopic techniques, it can be used to identify compounds and investigate sample composition.

Fourier transform infrared (FTIR) spectroscopy is a measurement technique that allows one to record infrared spectra. The main advantages of FTIR are that it is much quicker because it measures all the frequencies simultaneously and it is more sensitive than dispersive IR spectrometers. The key component of an FTIR is the interferometer, which can be understood by considering the Michelson interferometer shown in Figure II.8.

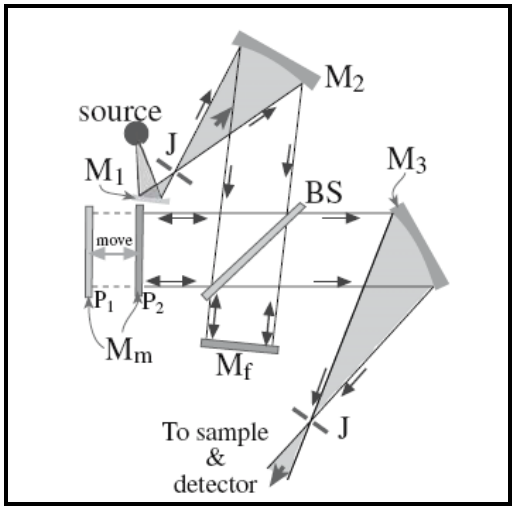

Figure II.8 Schematic of the arrangement of mirrors and ray paths in FTIR.

A parallel beam directed from the source is split at B_s so that 50% of the light is transmitted and reflected back by mirror M_F, while the rest is reflected at Bs and then again at M_M. The beams recombine at Bs. The recombined beam will show constructive or destructive interference depending on the difference in the path lengths B_s to M_F and B_s to M_M. As M_M is moved smoothly toward or away from B_s the detector sees a signal that alters in intensity. If the recombined beam from B_s is passed through a sample before reaching the detector sample absorptions will show up as gaps in the frequency distribution. The complex intensity distribution received by the detector is Fourier transformed by a computer to produce an absorption spectrum.

FTIR spectra are output in the form of plots of intensity (percent transmittance, %T, or absorbance, A) versus either energy (in J), frequency (in Hz), wavelength (in

μm), or wavenumber (in cm^{-1}). The use of wavenumber is preferred, but some of the standard reference sources of FTIR spectra use wavelength [11].

II.2 DIELECTRIC CERAMICS

Dielectric ceramics and substrates are electrical insulators with dielectric strength, dielectric constant and loss tangent values tailored for specific device or circuit applications. In capacitor applications, ceramics with a high dielectric constant are used to increase the charge that can be stored. In micro electronic circuits, low dielectric constant or low-k materials are sought to reduce inductive crosstalk and noise generation in the circuit. In high voltage insulator applications, high electrical resistivity (ohm-cm) and high dielectric strength (KV/meter) is required.

Parameters that are important to consider when specifying dielectric ceramics and substrates include dielectric strength, dielectric constant (relative permittivity), loss tangent (tan γ), electrical resistivity, and operating frequency.

Ceramic dielectrics covers a wide range of properties, from steatite with a relative permittivity (ε_r) of 6 to complex ferroelectric compositions with relative permittivities exceeding 20 000.

Class I dielectrics usually include low and medium-permittivity ceramics with dielectric loss less than 0.003. Medium-permittivity covers a ε_r range of 15–500 with stable temperature coefficients of permittivity that lie between +100 and 2000 MK^{-1}.

Class II/III dielectrics consist of high-permittivity ceramics based on ferroelectrics. They have ε_r values between 2000 and 20 000 and properties that vary more with temperature, field strength and frequency than Class I dielectrics. Their dielectric loss are generally below 0.03 but may exceed this level in some temperature ranges and in many cases become much higher when high a.c. fields are applied.

Class IV dielectrics contain a conductive phase that effectively reduces the thickness of dielectric in capacitors by at least an order of magnitude. Very simple structures such as small discs and tubes with two parallel electrodes can give capacitances of over 1 μF. Disadvantages are low working voltages, mostly between 2 and 25 V and high losses [21].

The low permittivity (ε_r) ceramics are used for millimeter-wave communication and also as substrates for microwave integrated circuits. The medium ε_r ceramics with permittivity in the range of 25 – 50 are used for satellite communications and in cell phone base stations. The high ε_r materials are used in mobile phones, where miniaturization of the device is very important. For millimeter-wave and substrate application, a temperature-stable low permittivity and high Q (low loss) materials are required for high-speed signal transmission with minimum attenuation [22].

II.2.1 Polarization Mechanisms

All materials contain electrically charged particles. At a minimum these are the electrons and protons that are part of the constituent atoms. Many ceramics also contain ions, which are charged. In a dielectric, charges have a limited mobility and they will move only when they have enough energy to overcome their inertia. When an insulator receives a charge, it retains that charge, confining it within the localized region in which it was introduced. However, a conductor allows charge to flow freely and redistribute itself within the material. The distinction between conductors and nonconductors (and it is not always a clear one) arises from the relative mobility of charge within the material. The terms "dielectric," "nonconductor," and "insulator" are often used interchangeably. However, we often specify dielectrics as materials that are not only electrically insulating but also have a high dielectric constant, κ.

Even though no charge is transferred when a dielectric is placed in an electric field there is a redistribution of charge, which occurs by the formation and movement of electric dipoles. There is an associated dipole moment, μ, having both magnitude and direction:

$$\mu = qd \qquad \text{(II.2)}$$

q: electronic charge (Coulomb),

d: the separation of the positive and negative ends of the dipole.

The dipole direction is, by convention, taken to point from the negative end to the positive end. When a dielectric material is placed in an electric field the induced

dipoles, and any permanent dipoles, become aligned. The material is now polarized and the polarization (or dipole moment per unit volume) is given by:

$$P = Nqd \tag{II.3}$$

where N is the number of dipoles.

There are four possible polarization mechanisms in a dielectric [11]:

- Electronic
- Ionic
- Dipolar (also called molecular or orientation)
- Interfacial (also called space charge)

These mechanisms are each illustrated in Figure II.9.

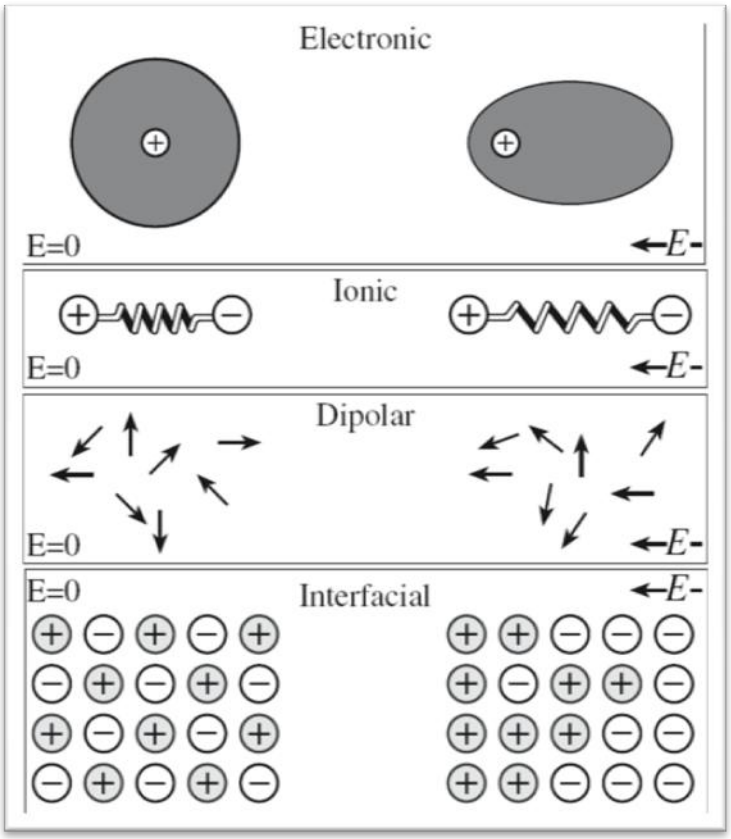

Figure II.9 Illustration of the different polarization mechanisms in a solid.

II.2.1.1 Electronic Polarization

When an electric field is applied to an atom, there is a displacement of the electrons relative to the nucleus. The electrons will concentrate on the side of the

nucleus near the positive end of the field. The atom acts as a temporarily induced dipole. This effect occurs in all materials (because all materials contain atoms), but the magnitude is small because d is very small. Typical displacements are ~1 am (attometer) giving $\mu \sim 1.6 \times 10^{-37}$ C·m. Electronic polarization is the only possible mechanism in pure materials that are covalently bonded and does not contain permanent dipoles (e.g., diamond and silicon).

II.2.1.2 Ionic Polarization

This occurs when an ionically bonded material is placed in an electric field; it is common in many ceramics (e.g., MgO, Al_2O_3, NaCl). The bonds between the ions are elastically deformed. Consequently the charge is minutely redistributed. Depending on the direction of the field, the cations and anions move either closer together or further apart. These temporarily induced dipoles cause polarization and may also change the overall dimensions of the material. The dipole moment is usually small because, once again, the displacements involved are very small. Typically the ion displacements are only 10–100 am.

II.2.1.3 Dipolar Polarization

This mechanism is generally common in ceramics because most of the permanent dipoles cannot be reoriented without destroying their crystal structure. The typical example is barium titanate. At room temperature the octahedrally coordinated Ti^{4+} ion is displaced slightly from its ideal symmetric position causing the crystal structure to become tetragonal and permanently polarized. When an alternating electric field is applied to a crystal of barium titanate, the Ti^{4+} ion moves back and forth between its two allowable positions to ensure that the polarization is aligned with the field.

II.2.1.4 Interfacial Polarization

A charge may develop at interfaces (such as grain or phase boundaries and free surfaces) normally as a result of the presence of impurities. The charge moves on the surface when the material is placed in an electric field. This type of polarization is not well understood, although it has considerable practical interest because most real materials and, in particular, many ceramics, are not pure.

The total P for the material is then the sum of all the individual contributions [11]:

$$P = P_{electronic} + P_{ionic} + P_{dipolar} + P_{interfacial} \quad \text{(II.4)}$$

II.2.1.5 Relating Polarization and Dielectric Constant

The dielectric constant is an important materials property and is a measure of the ability of an insulating material to store charge when subjected to an electric field; it is directly related to P. An equation can be developed to relate P and κ by beginning with a simple parallel plate capacitor. From electromagnetic theory it is known that the total charge per unit area of a capacitor plate, D_0, is proportional to the applied electric field ξ. The constant of proportionality is ε_0:

$$D_0 = \frac{Q}{A} = \varepsilon_0 \xi \quad \text{(II.5)}$$

If we now place a dielectric between the parallel plates we write:

$$D = \varepsilon \xi \quad \text{(II.6)}$$

D is also known as the dielectric displacement and represents the extra charge that can be stored because of the presence of the dielectric. So we can rewrite Equation II.6 as

$$D = \varepsilon_0 \xi + P \quad \text{(II.7)}$$

By substituting Equation II.6 into Equaiton II.7 we obtain

$$\varepsilon \xi = \varepsilon_0 \xi + P \quad \text{(II.8)}$$

By simple rearrangement we can write

$$P = (\kappa - 1)\varepsilon_0 \xi = \chi \varepsilon_0 \xi \quad \text{(II.9)}$$

where χ is a measure of the ratio of the bound charge/free charge (i.e., P/Q). For dielectrics that polarize easily κ will be large and, in turn, a large quantity of charge can be stored.

Table II.2 lists κ for a range of materials. Many ceramics and glasses have κ in the range of 4–10. Polarization is electronic only in covalent ceramics such as diamond and is a combination of electronic and ionic in materials such as MgO. Some ceramics, in particular $BaTiO_3$ and other titanates and zirconates, have very large κ due to their permanent dipole moments.

Table II.2 Dielectric constants of various ceramics [11].

Material	*κ at 1 MHz*	*Material*	*κ at 1 MHz*
Diamond	5.5–6.6	Al_2O_3	8.8
SiO_2	3.7–3.8	MgO	9.6
NaCl	5.9	$BaTiO_3$	3000
Mica	5.4–8.7	Pyrex glass	4.0–6.0
Soda-lime glass	7.0–7.6	TiO_2	14–110
Steatite (SiO_2 + MgO + Al_2O_3)	5.5–7.5	Forsterite ($2MgO \cdot SiO_2$)	6.2
Cordierite (SiO_2 +MgO + Al_2O_3)	4.5–5.4	Mullite	6.6
High-lead glass	19	Vycor glass	3.9

II.2.1.6 Frequency Dependence of Polarization

When a dielectric is placed in an alternating electric field the dipoles attempt to maintain alignment with the field. This process requires a finite time that is different for each polarization mechanism. At the relaxation frequency the dipoles will only just be able to reorient themselves in time with the applied field. At this frequency the dielectric is "lossy" and energy is lost in the form of heat. The dielectric loss is at a maximum when the frequency of the external field coincides with the relaxation frequency of a given polarization mechanism.

At frequencies above the relaxation frequency the dipoles will no longer be able to keep up with changes in the applied field and the contributing polarization mechanism becomes effectively "frozen" and no longer contributes. Figure II.10 shows the variation of polarization with frequency for a hypothetical material that exhibits all four of the polarization mechanisms.

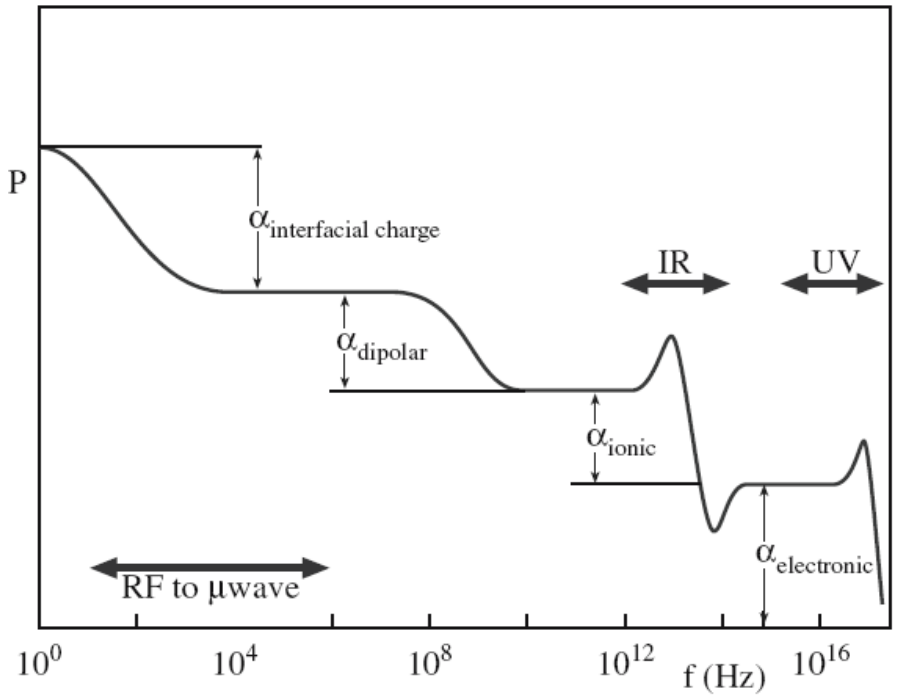

Figure II.10 Frequency dependence of polarization.

- At optical frequencies only electronic polarization is operative.
- Dipolar and ionic contributions are small at high frequencies because of the inertia of the molecules and ions. The peaks occurring at $\sim 10^{13}$ and $\sim 10^{15}$ Hz are due to resonance effects where the external field is alternating at the natural vibrational frequency of the bound ions or electrons, respectively [11].

II.2.2 Dielectric Properties

II.2.2.1 Permittivity (ε_r)

The relative permittivity (ε_r) of the material shows its energy storing capacity when a potential is applied across it. It is related to the macroscopic properties like polarization or capacitance. For circuit miniaturization, usually one employs a high ε_r material. A high ε_r facilitates circuit miniaturization because the wavelength inside the material is inversely proportional to the square root of its permittivity as given by the equation:

$$\lambda_d = \frac{\lambda_0}{\sqrt{\varepsilon_r}} \qquad \text{(II.10)}$$

$\varepsilon_{r:}$ relative permittivity

λ_d: wavelength in the dielectric

λ_0: wavelenght in air

The permittivity of a material determines the relative speed that an electrical signal can travel in that material. A low permittivity will result in a high signal propagation speed. When microwaves enter a dielectric material, they are slowed down by a factor roughly equal to the square root of the permittivity which implies that the wavelength decreases by the same amount and the frequency is unaffected as shown in Figure II.11.

By definition, the ε_r is related to the refractive index n by:

$$\varepsilon_r = n^2 \tag{II.11}$$

As permittivity is frequency dependent, it is very rare that the square of the refractive index measured at optical frequencies is the same as permittivity measured at microwaves [22]. This rule is applicable only if the same polarization processes are excited by both optical and microwave (or RF) frequencies, which is generally true only for elemental solid materials like diamond (ε_r = 5.68, n^2 = 5.85) or germanium (ε_r = 16, n^2 = 16.73) [23]. In other materials, this rule is not valid since dipolar polarization processes, which occur at lower frequencies, do not usually occur at higher optical frequencies. At microwave frequencies, ionic and electronic polarization mechanisms contribute predominantly to the net dipole moments and the permittivity as depicted in Figure II.12.

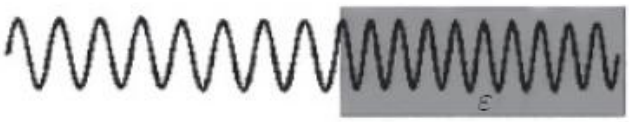

Figure II.11 The wavelength is reduced by a factor of $\varepsilon^{1/2}$ when the wave enters the dielectric.

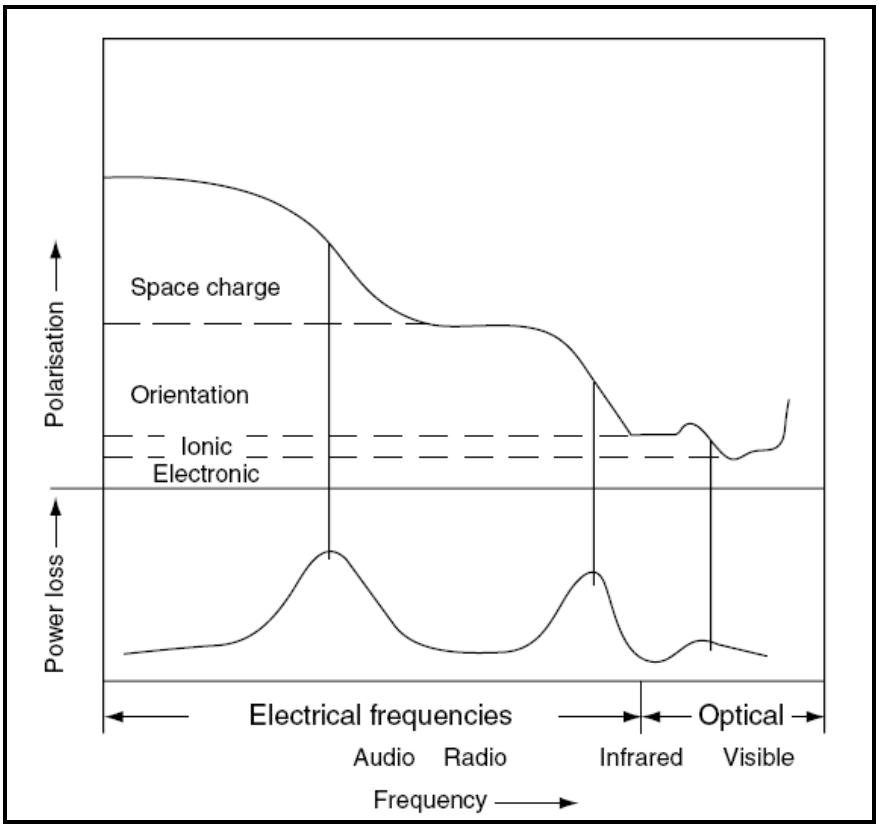

Figure II.12 Frequency dependence of polarization processes and peak power losses.

The permittivity of the material at low frequencies is measured by making a parallel plate capacitor but at high frequencies it is often measured by the method developed by Hakki and Coleman [24] and modified by Courtney [25], in which a cylindrical disc of material to be measured is inserted between two mathematically infinite conducting plates.

II.2.2.2 Dielectric Losses (tan γ) or Quality Factor (Q)

The dielectric loss tangent (tan γ) of a material denotes quantitatively dissipation of the electrical energy due to different physical processes such as electrical conduction, dielectric relaxation, dielectric resonance and loss from non-linear processes [22]. Origin of dielectric losses can also be considered as being related to delay between the electric field and the electric displacement vectors [26]. The total dielectric loss is the sum of intrinsic and extrinsic losses. Intrinsic dielectric losses are the losses in the perfect crystals, which depend on the crystal structure and can be described by the interaction of the phonon system with the AC electric field. Gurevich and Tagantsev developed a complete theory of intrinsic dielectric losses. The AC electric field alters the equilibrium of the phonon system

and the subsequent relaxation is associated with energy dissipation [27]. The phonon frequency is much higher than the microwave frequency. Hence the low frequency dielectric relaxation in the ideal lattice should be of a harmonic origin. As a result, energy of the field dissipates heat and the sample gets heated up. Gurevich and Tagantsev have reviewed [27] the theory of intrinsic losses. The intrinsic dielectric losses depend on the crystal symmetry, AC field frequency and temperature. These intrinsic losses fix the lower limit of losses in defect-free single crystals or ideal pure materials. Extrinsic losses are associated with imperfections in the crystal lattice such as impurities, microstructural defects, grain boundaries, porosity, microcracks, order–disorder, random crystallite orientation, dislocations, vacancies, dopant atoms etc. The extrinsic losses are caused by lattice defects and therefore can be in principle eliminated or reduced to the minimum by proper material processing. The losses due to different types of defects show different frequency and temperature dependence. The crystals belonging to different symmetry groups have very different temperature and frequency dependences of dielectric loss [27]. Manufacturers of dielectric ceramics often use the name ‘‘quality factor’’ for the reciprocal of the tan γ. One should carefully distinguish this quantity from the Q-factor of a resonator, which is defined as

$$Q = 2\Pi \frac{\text{maximum energy stored per cycle}}{\text{average energy dissipated per cycle}} \qquad \text{(II.12)}$$

The term ‘‘quality factor’’ is more commonly associated with microwave resonators. Quality factor, or Q, is a measure of the power loss of a microwave system. For the microwave resonator, losses can be of four types: (a) dielectric, (b) conduction, (c) radiation and (d) external [28].

II.2.2.3 Temperature Coefficient of Resonant Frequency (τ_f)

The temperature coefficient of resonant frequency τ_f is the parameter which indicates the thermal stability of the resonator. The τ_f indicates how much the resonant frequency drifts with changing temperature. The electronic device with microwave resonators requires τ_f values as close to zero as possible. Microwave circuits will normally have some low characteristics τ_f, so the resonator components which go into them are required to compensate for the inherent drift. For this reason, the τ_f values of resonators required are typically non-zero but with some low finite

value [22]. The origin of τ_f is related to linear expansion coefficient α_L which affects the resonator dimensions and its dielectric constant variation with temperature [29]. Mathematically the relationship is:

$$\tau_f = -\alpha_L - \frac{\tau_\varepsilon}{2} \qquad \text{(II.13)}$$

τ_ε: temperature coefficient of the permittivity

α_L: linear thermal expansion coefficient of the dielectric material

For an ideal resonator the temperature coefficient of resonant frequency (τ_f) should be near to zero. Hence from Equation (II.13) for a zero τ_f, the τ_ε should have twice the value of α_L and should be negative. Since resonators are used in communication systems, temperature stability is an important factor and should be close to zero. For most of the electronic ceramic materials, α_L is about +10 ppm/°C indicating the significant influence of τ_ε on τ_f [22].

II.3 MICROWAVE DIELECTRIC CERAMICS

Microwave dielectric materials play a key role in global society with a wide range of applications from terrestrial and satellite communication including software radio, Global Positioning System (GPS), and Direct Broadcast Satellite TV (DBS TV) to environmental monitoring via satellites. Wireless communication technology demands materials, which have their own specialized requirements and functions. New microwave materials and components with improved properties and new designs are required to meet the demands of the current and future systems. Mobile phone and satellite communication systems that use microwaves as the carrier have been one of the biggest area where intensive research and development studies have been made in order to decrease the size of the devices. This revolution is apparent on a daily basis in the ever-increasing number of cell phone users. The constant need for miniaturization provides a continuing driving force for the discovery and development of increasingly sophisticated materials to perform the same or improved function with decreased size and weight. Dielectric oxide ceramics have revolutionized the microwave wireless communication industry by reducing the size and cost of filter, oscillator and antenna components used in various applications ranging from cellular phones to global positioning systems [22].

Most of the microwave-based device systems are located in the frequency range of 300 MHz – 300 GHz (Figure II.13).

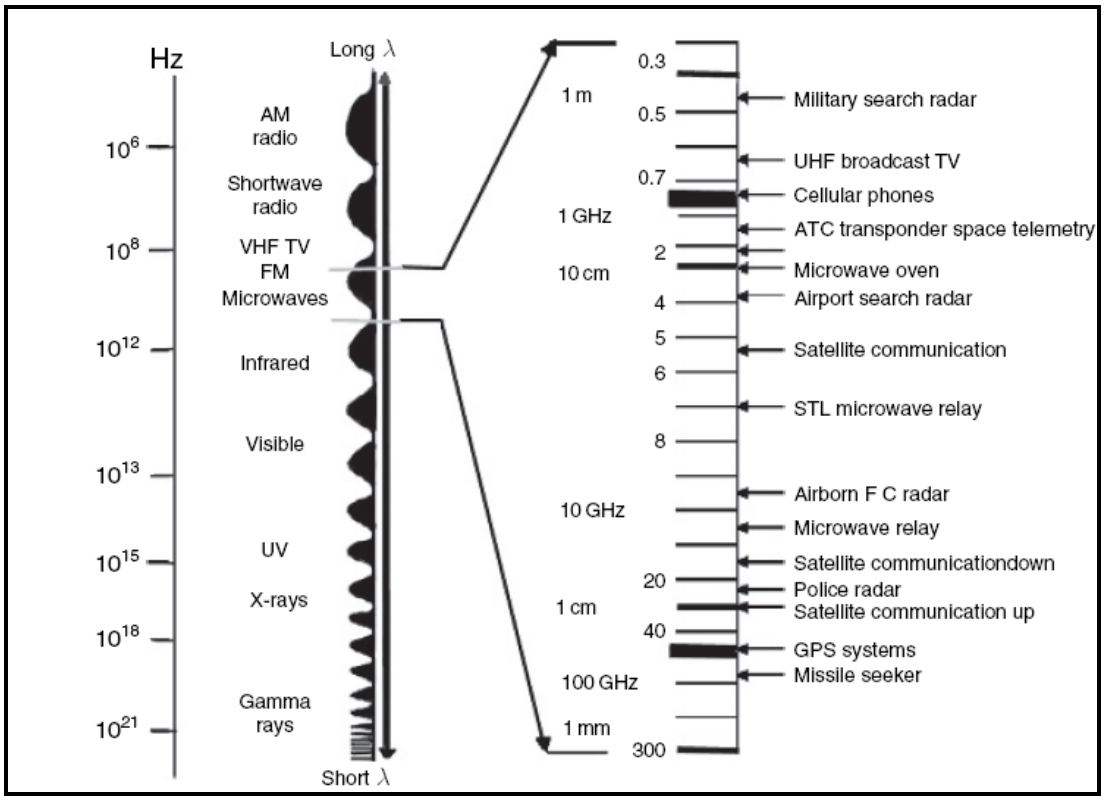

Figure II.13 Microwave spectrum and applications.

Microwave dielectric materials are required to have high dielectric constant (ε_r>30), low dielectric loss, good temperature stability of frequency in a wide spectral range and good mechanical and thermal stability as they are investigated in terms of electrical properties [21]. Beside satellite systems and mobile communication, microwave dielectric materials are used in multilayer ceramic capacitors and various kinds of detectors such as thermal, pressure, vibration and radiation.

II.3.1 ABO_3 Type Perovskites

The perovskite family of materials is of considerable technological importance, particularly with regard to physical and electrical properties such as pyro and piezo electricity, linear and non-linear electro-optic effects, dielectric and superconducting properties. Many of these properties are gross effects varying considerably from one perovskite to another, yet the differences in the crystal structures are hardly apparent.

Compounds having the ideal perovskite structure can be represented by the general formula ABX_3 (X=O, F) where A is a large metal cation close-packed in layers with oxygen ions and B is a smaller metal ion situated in an octahedrally coordinated hole between the close-packed layers. ABF_3 materials in general have relatively high dielectric loss factor in contrary to ABO_3 type materials [22].

The perovskite structure is one of the most extensively studied structures in materials science. German chemist and mineralogist Gustav Rose discovered the mineral $CaTiO_3$ in 1839. Rose named $CaTiO_3$ after Lev Alexeievitch Perovsky, a Russian military official and dignitary [30]. The atomic arrangement for ABO_3 perovskite structure was first found for the mineral perovskite $CaTiO_3$. It was earlier thought that the $CaTiO_3$ unit cell could be represented by Ca (A) ions at the corners of a cube with Ti (B) ions at the body center and oxygen ions at the center of the faces as shown in Figure II.14.

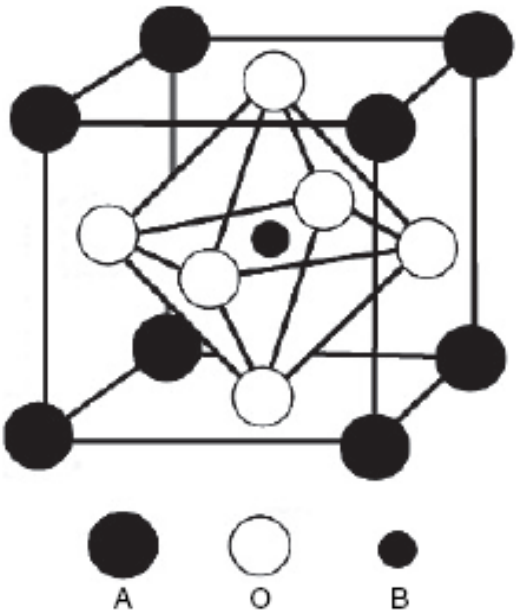

Figure II.14 Ideal perovskite structure.

The ideal perovskite structure having cubic symmetry with one ABO_3 formula per unit cell is shown in Figure II.14 [22]. Many perovskite materials have symmetry different from cubic at room temperature, but transform to cubic symmetry at high temperatures. The low temperature (low symmetry) structure is called hettotype and the high temperature cubic structure is called aristotype [31]. Perovskites having the ideal structure adopt the cubic space group Pm3m.

The perovskite structure is viable to wide departures in compositions from the ideal formula ABO_3. Isomorphous substitutions at A or B sites, and cationic and anionic deficiencies can achieve these variations. These can be represented as $A_{1-x}A'_xBO_3$ and $AB_{1-x}B'_xO_3$. Frequently, the composition changes are accompanied by structural changes both of which have profound effects on the electrical and magnetic properties of the material. Non-ferroelectric perovskite ceramics with high permittivity, low τ_f and low loss represent one of the most important material families for applications in wireless communication [22].

One interesting feature of the perovskites is that they can accommodate more than one aliovalent elements for both A and B sites and such compositions which can be typically represented as $A(B'_xB''_y)O_3$ and termed as complex perovskites. The B' and B'' are two elements in different oxidation states and x + y= 1. Roy [32] has studied the possible multiple substitution in perovskites.

The complex perovskite type compounds $A(B'_xB''_y)O_3$ can be divided into:

1. $A(B'_{2/3}B''_{1/3})O_3$ which contain twice as much lower valence state element as higher valence state element.

2. $A(B'_{1/3}B''_{2/3})O_3$ which contain twice as much of the higher valence state element as the lower valence state.

3. $A(B'_{1/2}B''_{1/2})O_3$, contain the B elements in equal amounts.

4. Oxygen deficient phases $A(B'_xB''_y)O_{3-\delta}$.

5. Hexagonal perovskites of the type $A_nB_{n-1}O_{3n}$ and related compounds [22].

II.3.2 $A(B'_{1/3}B''_{2/3})O_3$ Complex Perovskites

The $A(B'_{1/3}B''_{2/3})O_3$ perovskites are the most widely studied family of materials in microwave ceramics. They have gained a giant importance for the last 20 years after the discovery of $Ba(Zn_{1/3}Ta_{2/3})O_3$ ceramics. The group of ceramics such as $Ba(Zn_{1/3}Ta_{2/3})O_3$, $Ba(Mg_{1/3}Ta_{2/3})O_3$ and $Ba(Mn_{1/3}Ta_{2/3})O_3$ have excellent microwave dielectric properties [4, 5]. A broad range of chemical substitutions such as Ba, Sr, Ca, at A site; Mg, Zn, Ni, Co, Sr, Ca, Mn, Cd at B' site and Nb and Ta at B'' site are possible and the substitutions enable the tailoring of the dielectric properties. $Ba(Mg_{1/3}Ta_{2/3})O_3$ (BMT), $Ba(Zn_{1/3}Ta_{2/3})O_3$ (BZT) and $Ba[(Zn,Co)_{1/3}Nb_{2/3}]O_3$ (BZCN) are the most widely studied materials in this family and are commercially produced for applications in wireless communication. A large number of compounds with niobium or tantalum as the B'' ions in the

$A(B'_{1/3}B''_{2/3})O_3$ complex perovskite were reported by Roy [33] and Galasso and co-workers [34]. These oxides have twice the B'' ions as the B' ions. It was believed that $A(B'_{1/3}B''_{2/3})O_3$ has a cubic perovskite cell with three layers of BaO_3, one layer of B^{2+} and two layers of B^{5+} in the unit cell. Galasso and co-workers observed extra weak reflections on the X-ray diffraction patterns of some of these complex perovskites. Later, Galasso et al. found [35] that one of the compound $Ba(Sr_{1/3}Ta_{2/3})O_3$ has an ordered structure in which Sr and Ta occupy ordered positions which account for the extra reflections. Galasso reported [36] that the ordered $Ba(Sr_{1/3}Ta_{2/3})O_3$ has a hexagonal unit cell whose c-axis is equivalent to the <111> direction of the disordered cubic perovskite cell. It was found [36] that many of the $A(B'_{1/3}B''_{2/3})O_3$ compounds show ordered perovskite structure. It was also reported [37] that 1:2 ordering in the B site for compounds of general formula $A(B'_{1/3}B''_{2/3})O_3$ is a strong function of radius mismatch between B' and B'' ions. Galasso and Pyle observed [37] that the ordering increased with increasing size difference between the B^{2+} and the B^{5+} ions. It was found [36] that the ordering increased when the samples were annealed and was attributed to the existence of small ordered domains, which grew on annealing at high temperatures.

In 1977, Kawashima and co-workers reported [38] for the first time useful microwave dielectric resonator materials in the $Ba(B'_{1/3}B''_{2/3})O_3$ system. They reported $Ba(Zn_{1/3}Nb_{2/3})O_3$ (BZN) with ε_r = 41, Q= 5600, τ_f = +28 ppm/ºC and $Ba(Zn_{1/3}Ta_{2/3})O_3$ [BZT] with ε_r = 30, τ_f = 0±0.5 ppm/ºC and Q = 6500. Since then several papers appeared in the literature reporting microwave dielectric properties of several $A(B'_{1/3}B''_{2/3})O_3$ complex perovskites, some of which are given in Table II.3 [22].

Table II.3 Microwave dielectric properties of $A(B'_{1/3}B''_{2/3})O_3$ ceramics.

Composition	Tolerance factor	Sintering temperature (°C)	ε_r	Qf (GHz)	τ_f (ppm/°C)
$Ba(Mg_{1/3-x}Nb_{2/3})O_{3-\delta}$ $(x = 0.02)$	1.037	1450	32	96 000	30
$Ba(Ni_{1/3}Nb_{2/3})O_3$	1.035	1400	31	48 000	–18
$Ba(Ni_{1/3}Ta_{2/3})O_3$	1.035	1500	23	49 700	–18
$Ba(Mg_{1/3}Ta_{2/3})O_3$	1.029	1640	24	430 000	8
$Ba(Mg_{1/3}Nb_{2/3})O_3$	1.029	1350	31	46 000	18
$Ba(Zn_{1/3}Nb_{2/3})O_3$	1.027	1390	41	87 000	30
$Ba(Zn_{1/3}Ta_{2/3})O_3$	1.027	1350/120 h	28	168 000	0.5
$Ba(Co_{1/3}Nb_{2/3})O_3$	1.026	1400	32	78 000	–12
$Ba(Co_{1/3}Ta_{2/3})O_3$	1.026	1500	25	71 400	–16
$Ba(Mn_{1/3}Ta_{2/3})O_3$	1.012	1600/air	27	15 500	45
$Ba(Mn_{1/3}Ta_{2/3})O_3$	1.012	1600/N_2	27	104 000	45

II.4 $Ba(Zn_{1/3}Nb_{2/3})O_3$ (BZN) COMPLEX PEROVSKITE CERAMIC

Improvement of cheaper materials that have similar properties with $Ba(Zn_{1/3}Ta_{2/3})O_3$ microwave dielectric ceramics has become important since Ta_2O_5 is an expensive oxide. As compared with Ta_2O_5, Nb_2O_5 has the same crystal structure, similar ionic radius (0.64 Å) and electronic structure. The most importantly Nb_2O_5 is rather cheaper than Ta_2O_5. In 1977, Kawashima et al. reported [38] $Ba(Zn_{1/3}Nb_{2/3})O_3$ (BZN) as a low loss microwave dielectric material. Since then several authors investigated [39] the microwave dielectric properties of BZN.

II.4.1 Preparation of $Ba(Zn_{1/3}Nb_{2/3})O_3$ (BZN) by Solid State Route

BZN is commonly prepared by the conventional solid-state ceramic route by ball milling the stoichiometric amounts of raw materials ($BaCO_3$, ZnO, Nb_2O_5) and calcining in the temperature range 1100–1200 ºC followed by sintering in the temperature range 1400–1500 ºC. It has been reported [39] that the sintering temperature of BZN can be lowered by the addition of additives such as CuO, Sb_2O_3, B_2O_3, B_2O_3+LiF, $Ba_3W_2O_9$. Roulland and coworkers reported [40] that BZN can be sintered at about 1000 ºC by the addition of 10 mol% B_2O_3+5 mol% LiF. A slight

non-stoichiometry at A site (~1%) can further lower sintering temperature to about 900 ºC [41] enabling silver co-sintering applications. Secondary phases of $Ba_5Nb_4O_{15}$, $BaNb_2O_6$, etc. are often found in the sintered BZN ceramics. Liou et al. [42] prepared $Ba_xSr_{1-x}(Zn_{1/3}Nb_{2/3})O_3$ by a reaction sintering process with 3 wt% CuO without the calcination process at 1450 ºC. However, secondary phases of $ZnNb_2O_6$ and $(Cu_2Zn)Nb_2O_8$ were found in the sintered ceramics.

Kolodiazhyni from a study using ESR, positron annihilation spectroscopy and dielectric spectroscopy reported [43] that $Ba(B'_{1/3}B''_{2/3})O_3$ ceramics contain substantial amount of lattice vacancy defects and some of them contain unpaired electron spin. The BZN when prepared at high temperatures has a disordered cubic structure with lattice parameter a = 4.09Å [44]. BZN undergoes a transition from a 1:2 ordered structure to a disordered B site arrangement at about 1375 ºC [45]. The lower thermal stability means that BZN needs to be annealed at temperatures lower than 1375 ºC to increase the ordering and thereby increase the quality factor.

II.4.2 Preparation of $Ba(Zn_{1/3}Nb_{2/3})O_3$ (BZN) by Chemical Methods

BZN perovskite ceramic is also prepared by the chemical methods. Because conventional solid state route requires high calcination and sintering temperatures, gives larger particle sizes, high degree of agglomeration and lower homogeneity level which may affect the microwave dielectric properties negatively. However, chemical methods use high purity powders and the homogeneity attained is at atomic or molecular level. In addition, employing the chemical methods nano powders can be produced which may decrease the sintering temperature and increase the desired properties. Nevertheless, limited number of chemical methods has been applied to produce BZN ceramics, although various chemical methods were applied to produce other identical complex perovskites. For example; $Ba(Zn_{1/3}Ta_{2/3})O_3$ nanopowders were synthesized by citrate polymer pyrolysis [46]. But the sintering properties were very poor. Single phase $Ba(Zn_{1/3}Ta_{2/3})O_3$ were also produced using sol-gel method at low temperatures of 600 °C which gave well sinterable perovskite ceramic between 1500-1600 °C [47, 48]. $Ba(Mg_{1/3}Ta_{2/3})O_3$ ceramic prepared by coprecipitation and hydrolysis of alkoxides gave secondary phases after sintering but they exhibited larger Q×f (880,000) than mixed oxide derived material (556,000) [49]. $Ba(Mg_{1/3}Ta_{2/3})O_3$ ceramic powders were successfully synthesized by sol-gel method using acetate salts with a particle size of 100 nm [50]. The microwave

dielectric properties of $Ba(Zn_{1/3}Ta_{2/3})O_3$ ceramic sintered at 1400°C for 2h were at acceptable level [50].

Some of the chemical methods applied in the production of BZN ceramics are given below: Liang et al. [51] prepared BZN powder by a spray pyrolysis technique and the ceramic sintered at 1250 ºC showed presence of $Ba_5Nb_4O_{15}$ secondary phase. The powders obtained by the wet chemical methods have small particle size and hence ZnO can escape easily which led to the formation of $Ba_5Nb_4O_{15}$ and $BaNb_2O_6$ secondary phases. In a very recent study, a simple coprecipitation technique was successfully applied for the preparation of pure, nanosized, single phase $Ba(Zn_{1/3}Nb_{2/3})O_3$ microwave dielectric ceramic by Mergen and Sert [52]. Single phase $Ba(Zn_{1/3}Nb_{2/3})O_3$ ceramic was produced at 900 °C. TEM investigation of coprecipitated powders indicated that the particles had nearly spherical morphology with particle size ranging between 90-120 nm within large agglomerated clusters of hundred nanometers. BZN ceramics sintered at 1250 °C had high density (~95% of relative density) and fine grain size (<1 μm). BZN ceramics produced from coprecipitated powders had a dielectric constant of between 38-40 with dielectric losses lower than 3×10^{-3} at frequency ranges of 1 kHz-2 MHz between 20-200°C.

II.4.3 Dielectric Properties

BZN ceramic has a high dielectric constant (ε_r=40), low dielectric loss or Q_f of about 80000 GHz and high resistivity [38]. These electrical properties make $Ba(Zn_{1/3}Nb_{2/3})O_3$ dielectric ceramic a popular material in the communication industry and also increase the usage potential in applications such as capacitors and high frequency resonators. However, the temperature coefficient of resonant frequency of $Ba(Zn_{1/3}Nb_{2/3})O_3$ ceramic is high (τ_f=30 ppm/K) which restricts the use of these ceramics in microwave applications.

Various methods have been applied to improve the properties of $Ba(Zn_{1/3}Nb_{2/3})O_3$ ceramics such as doping with different elements like Ti [9] or making composite of $Ba(Zn_{1/3}Nb_{2/3})O_3$ ceramics with other $Ba(B'_{1/3}B''_{2/3})O_3$ microwave dielectric ceramics (B'=Mg, Zn, Ni; B''=Ta, Nb) like $Ba(Zn_{1/3}Nb_{2/3})O_3$-$Ba(Ni_{1/3}Nb_{2/3})O_3$ [10]. $0.35(Ba(Ni_{1/3}Nb_{2/3})O_3)–0.65(Ba(Zn_{1/3}Nb_{2/3})O_3)$ composite microwave dielectric material which was sintered at 1450 °C for 4 h and annealed for at 1300 °C for 72 h exhibited good dielectric properties: temperature coefficient of

resonant frequency (τ_f) of +0.6 ppm $°C^{-1}$, relative permittivity of 35 and quality factor in excess of 25,000 GHz [10].

Noh et al. [53] sintered BZN over a range of temperatures and concluded that the grain size and the density were more important in controlling the quality factor. They reported that volatility of ZnO and the formation of secondary phases degrade the quality factor [53]. However, Wu and Davies [54] found that BZN when sintered in ZnO-rich environment severely degraded the quality factor. Chemical analysis showed that the degradation of the properties were due to the uptake of ZnO to form non-stoichiometric BZN from the muffling agent. This is supported by the fact that addition of ZnO to BZN considerably reduces the quality factor [54]. Slow cooling of the ceramic after sintering through the order–disorder region greatly improves Q_f [55]. The high Q_f is obtained by annealing the sintered samples below the order–disorder transition temperature.

BZN has a relatively high τ_f of about 30 ppm/ºC which limits its use in practical applications. Hence several attempts were made to lower the τ_f of BZN by adding dopants such as B_2O_3, Sb_2O_3+B_2O_3, and by forming solid solution with $Ba(Mg_{1/3}Nb_{2/3})O_3$ (BMN), $Ba(Co_{1/3}Nb_{2/3})O_3$ (BCN), $BaSnO_3$, $Ba(Ni_{1/3}Nb_{2/3})O_3$ (BNN), $Ca(Zn_{1/3}Nb_{2/3})O3$ (CZN), $Sr(Zn_{1/3}Nb_{2/3})O_3$ (SZN), and $Ba(Ga_{1/2}Ta_{1/2})O_3$ (BGT) [56]. The BCN, BNN, SZN, and CZN are having negative τ_fs. Hence it is possible to compensate for the large positive τ_f of BZN by making a solid solution of BZN with BCN, SZN, BNN, and BGT. The BZN has a disordered cubic structure when prepared above 1375 °C. $Sr(Zn_{1/3}Nb_{2/3})O_3$ (SZN) is a hexagonally ordered perovskites with a=5.66 Å and c=6.95 Å [57] with ε_r=40, Q_f =20000 GHz and τ_f=-38 ppm/°C. Several authors tailored [58] the τ_f of BZN by forming a solid solution with SZN and obtained a nearly temperature compensated ceramics although the quality factor was reduced. The ε_r varied non-linearly with x with the maximum of 46 at x=0.6 (0.6BZN–0.4SZN). A τ_f value close to zero was obtained for 0.3BZN–0.7SZN with ε_r=40 with Q_f of 30500 GHz. It was reported [59] that in $Ba_xSr_{1-x}(ZnNb)O_3$ (BSZN) the substitution of Sr for Ba monotonously change the τ_f and ε_r and an anomaly existed at about x=0.5. Reaney and co-workers found [60] a strong correlation between tolerance factor and τ_ε and the BZN–SZN solid solution undergoes a structural transition involving octahedral tilting. The octahedral tilt transitions lead to doubling of the unit cell and appearance of superstructure reflections [61].

CHAPTER III

THE STUDY

III.1 PRODUCTION OF $Ba(Zn_{1/3}Nb_{2/3})O_3$ CERAMIC POWDERS BY CITRATE GEL METHOD

$Ba(Zn_{1/3}Nb_{2/3})O_3$ perovskite ceramic powders were synthesized by citrate gel method. This method is also known as Pechini method or modified sol-gel method in literature. In this method, barium nitrate [$Ba(NO_3)_2$] (99%, Merck), zinc acetate [$Zn(OOCCH_3)_2{\cdot}2H_2O$] (98.0–101.0%, Alfa Aesar) and niobium oxide [Nb_2O_5] (99.9%, Alfa Aesar) were used as starting materials. The steps of citrate gel method that is a chemical process to produce nanoscale powders, were followed according to the flowchart to produce $Ba(Zn_{1/3}Nb_{2/3})O_3$ ceramic powders (Figure III.2). Firstly, stoichiometric amounts of niobium oxide, Nb_2O_5, were dissolved in minimum amount of hydrofluoric acid [HF] (38–40%, Merck) to form NbF_5 solution of 0.3 M by heating in a hot water bath for 24 h. Then, 0.3 M NbF_5 solution was precipitated as niobium hydroxide by using 2N NaOH (97%, Merck) solution. The pH was maintained around 11 to ensure completion of the reaction for $Nb(OH)_5$ powder precipitation. Determination of pH value which causes complete precipitation of $Nb(OH)_5$ powders was fulfilled by performing several titration experiments on NbF_5 solution with the addition of 1 M NaOH solution (Figure III.1). Niobium cations started to precipitate approximately when pH=6.20 and precipitation reaction continued to occur till the pH value came close to 12. Figure III.1 indicates that pH value of over 11 is enough to precipitate all the Nb cations within the solution.

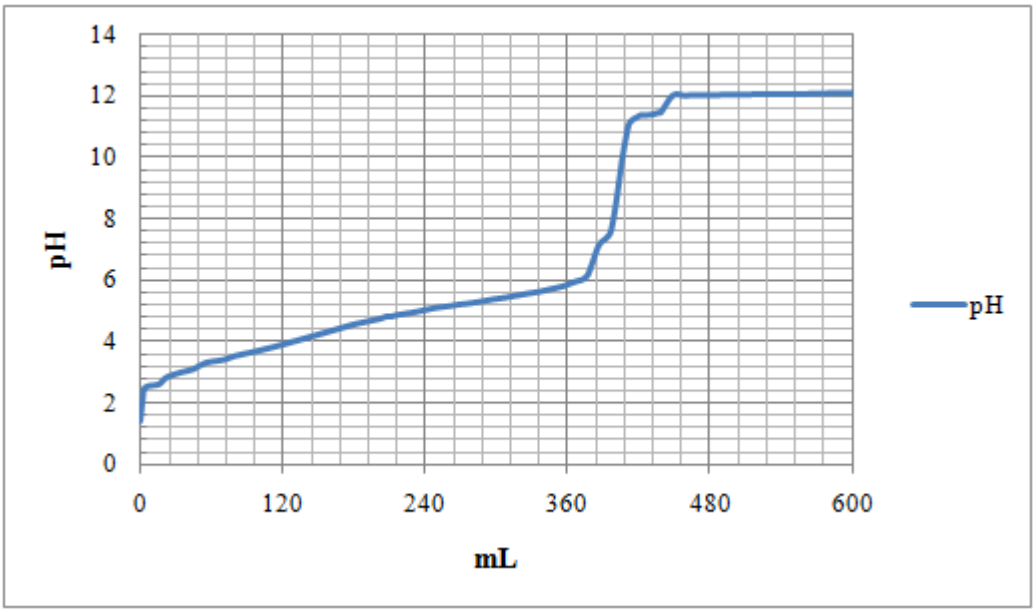

Figure III.1 Titration curve for the Nb cations within solution to form $Nb(OH)_5$ precipitates.

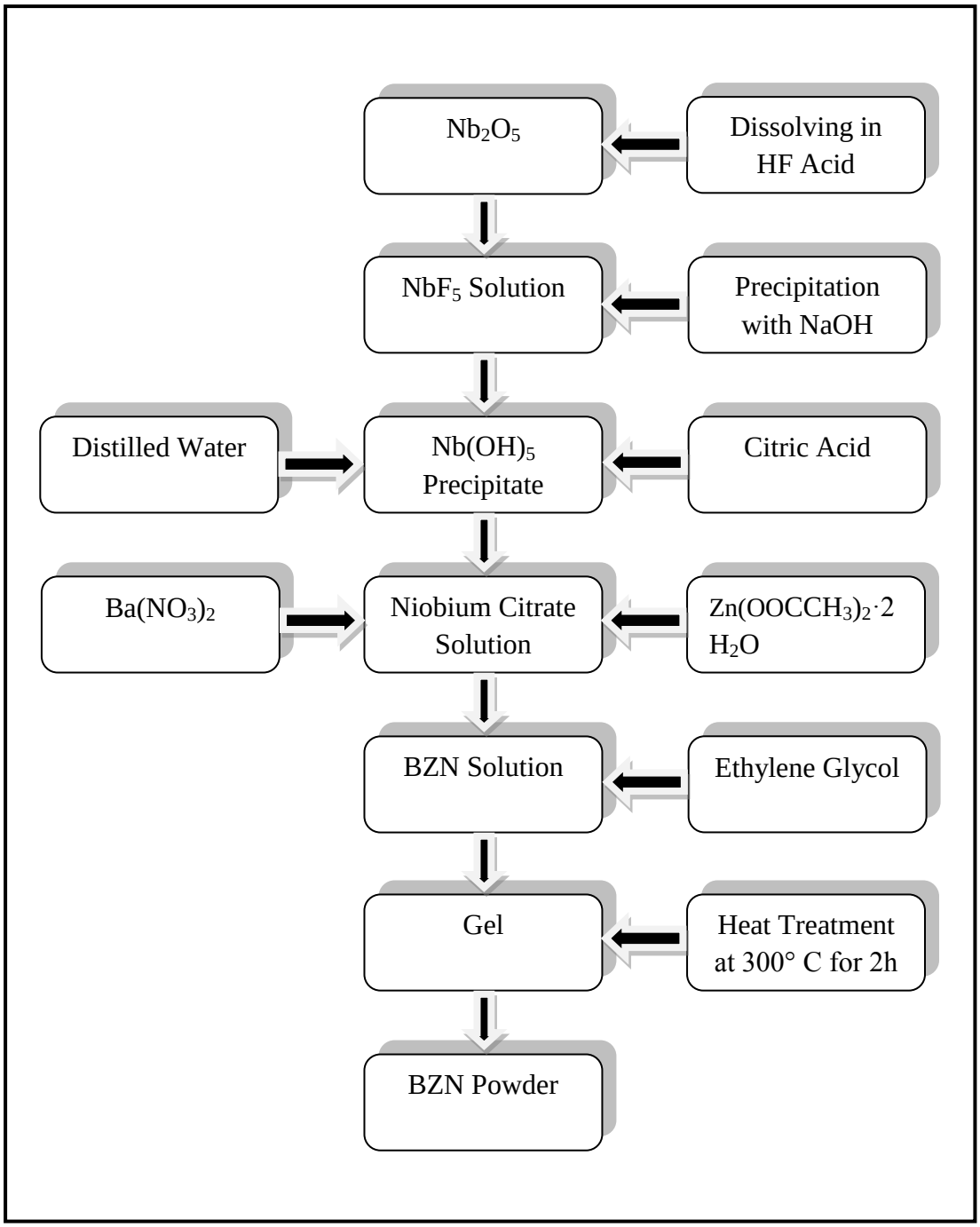

Figure III.2 Flowchart to produce $Ba(Zn_{1/3}Nb_{2/3})O_3$ perovskite ceramic powder by citrate gel method.

After complete precipitation of $Nb(OH)_5$ powders, they were filtered and washed with 5% distilled water-ammonia solution (%25, Merck). Fresh niobium hydroxide precipitates were dissolved in citric acid [$C_6H_8O_7 \cdot H_2O$] (99.5–100.5%, Merck) solution. Dissolution of $Nb(OH)_5$ precipitates in citric acid solution is a critical step since dissolution of $Nb(OH)_5$ is rather difficult. Therefore, it is

important that $Nb(OH)_5$ precipitates should be dissolved within the citric acid solution just after precipitation freshly. In addition, weak citric acid solution should be used in dissolution process to dissolve the $Nb(OH)_5$.

After dissolving $Nb(OH)_5$ precipitates in weak citric acid solution, stoichiometric amounts of barium nitrate and zinc acetate were added into niobium citrate solution. After complete dissolution of barium nitrate and zinc acetate, ethylene glycol [$HOCH_2CH_2OH$] (99%, Merck) was added to this solution with an amount of citric acid/ethylene glycol weight ratio as 60:40. The solution was kept at 80 °C to form a gel. After heat treatment at 300 °C for 2 h, the gel converted into a black porous powder indicating that charring occurred. The resin was lightly ground into a powder using an agate mortar. The black powder was calcined at different temperatures between 400–1200 °C for 4h to monitor the phase development and finally to produce $Ba(Zn_{1/3}Nb_{2/3})O_3$ ceramic powders by decomposition at high temperatures.

In order to investigate the effect of citric acid on the phase formation of $Ba(Zn_{1/3}Nb_{2/3})O_3$ and particle size, citric acid/total metal cations (Ba+Zn+Nb) mol ratio (C/M) was varied between 5.0, 2.0, 1.0 and 0.5 and the samples named as BZN-1, BZN-2, BZN-3, BZN-4, respectively.

III.2 CHARACTERIZATION OF $Ba(Zn_{1/3}Nb_{2/3})O_3$ CERAMIC POWDERS SYNTHESIZED BY CITRATE GEL METHOD

$Ba(Zn_{1/3}Nb_{2/3})O_3$ (BZN) ceramic powders, synthesized with different citric acid mol ratios to metal cations in $Ba(Zn_{1/3}Nb_{2/3})O_3$ system, were characterized by using Thermogravimetric and Differential Thermal Analysis (TG and DTA, NETZSCH STA 409C/CD), X-ray Diffractometer (Rigaku XRD, CuKα radiation), Fourier Transform Infrared Spectrum (FT-IR) Analysis, Scanning Electron Microscopy (SEM, JSM 5910LV) and Transmission Electron Microscopy (TEM, Tecnai G² F20 S-TWIN 200 kV).

III.2.1 Thermogravimetric and Differential Thermal Analysis

The thermogravimetric and differential thermal analysis (TG and DTA) of the gel synthesized by citrate gel method with different citric acid/metal cations mol ratios and heat treated at 300 °C for 2 hours, were carried out under static air with a heating rate of 10 $Kmin^{-1}$ from 25 °C to 1000 °C (NETZSCH STA 409C/CD) to

detect the thermal behavior of $Ba(Zn_{1/3}Nb_{2/3})O_3$ powders before calcination processes.

III.2.2 X-Ray Diffraction (XRD) Analysis

$Ba(Zn_{1/3}Nb_{2/3})O_3$ (BZN) ceramic powders synthesized with different citric acid/metal cations mol ratios and calcined at various temperatures between 400 and 1200 °C for 4h were investigated by X-ray diffractometer (Rigaku) (Figure III.3) with Cu Kα radiation in the range of 2θ: 20–80° with a scan rate of $2°min^{-1}$ to determine the phase development and effect of citric acid on phase formation.

Figure III.3 X-Ray Diffractometer, Rigaku.

III.2.3 Fourier Transform Infrared (FT-IR) Spectrum Analysis

Fourier transform infrared spectrum of the charred gel with a mol ratio of citric acid/metal cations as 2 (BZN-2), calcined at 300 °C for 2 hours and then heat treated at temperatures between 400 and 1200 °C for 4 hours, was recorded with a FT-IR

spectrometer (Nicolet 6700) in the range of 400–4000 cm^{-1} to investigate the organic residuals and phase formations in BZN structure.

III.2.4 Transmission Electron Microscopy (TEM) and Scanning Electron Microscopy (SEM)

The shape, size and morphology of the powders and the degree of agglomeration of the BZN powders, heat treated at 1000 °C for 4 hours, were investigated by transmission electron microscopy (TEM, Tecnai G² F20 S-TWIN 200 kV) and scanning electron microscopy (SEM, JSM 5910LV) (Figure III.4). In addition, effect of citric acid content on the size and shape of the particles and on the degree of agglomeration of powders were also investigated by SEM and TEM using BZN powders produced at various citric acid/metal cation mol ratios.

Figure III.4 Scanning Electron Microscope (SEM, JSM 5910LV).

In addition to SEM and TEM investigations for particle size and morphology, X-ray Diffractometer (Rigaku XRD, CuKα radiation) and also Energy Dispersive X-Ray Spectroscopy (EDS) that is integrated to SEM (Figure III.4) were used for the assessment of crystallite size and morphology of $Ba(Zn_{1/3}Nb_{2/3})O_3$ powders synthesized by citrate gel method with different citric acid/metal cations mol ratios.

The crystallite size of $Ba(Zn_{1/3}Nb_{2/3})O_3$ powders heat treated at different temperatures was calculated by using XRD analysis results in Scherrer equation:

$$D = \frac{k\lambda}{B\cos\theta} \quad \text{(III.1)}$$

λ: wavelength of the X-ray radiation (1.5406Å for Cu Kα),

k: a constant taken as 0.9,

θ: diffraction angle,

B: full-width at half-maximum (FWHM).

III.3 PRODUCTION AND CHARACTERIZATION OF $Ba(Zn_{1/3}Nb_{2/3})O_3$ PEROVSKITE CERAMICS

BZN ceramics were produced from BZN powders synthesized by citrate gel method at optimum conditions and calcined in a tightly closed alumina crucible at 1000 °C for 4 hours. Calcined BZN powders were ground in an agate mortar in alcohol and then ceramic pellets, which were 10 mm in diameter and 1-2 mm in thickness, were produced. The pellets were sintered between 1250-1400 °C for 4 hours. Sintering process was accomplished in tightly closed crucibles by embedding ceramic pellets into their own BZN powder to prevent evaporation of ZnO from BZN system since ZnO has a high evaporation rate at high temperatures (>1200 °C) [62].

Fabricated BZN pellets were characterized using several techniques. The densities of BZN ceramics sintered between 1250-1400 °C for 4 hours were measured by means of Archimedes' method. In this method, first of all, dry samples were weighed (W_D), and then the samples were boiled in distilled water for 5 minutes. After cooling the specimens in water for 5 minutes, their weights were measured in distilled water after suspension (W_S). Finally, removing the specimens from water, wet weights were measured in air (W_w). The bulk densities were found using the below equation:

$$\rho_B = \frac{W_D}{V} = \frac{W_D}{W_D - W_S} \quad \text{(III.2)}$$

Relative densities of BZN perovskite ceramic samples were calculated by using theoretical density of BZN ceramic. Theoretical density of $Ba(Zn_{1/3}Nb_{2/3})O_3$ ceramic is 6.516 g/cm^3 [63].

X-ray diffractometer is used to examine the BZN ceramics to check whether single phase BZN is obtained. Microstructure of dense BZN ceramics sintered at 1300°C for 4 hours, was investigated using scanning electron microscopy (SEM, JSM 5910LV) equipped with Energy Dispersive X-Ray Spectroscopy (EDS, Oxford-Inca-7274) which is used for compositional analysis of the phases.

Dielectric properties of BZN perovskite ceramics sintered at 1300 °C for 4h were measured, before which they were coated with gold. Coating process was performed by using Boc Edwards Auto 500 System (Figure III.5).

Figure III.5 Silver or gold coating system (Boc Edwards Auto 500).

In coating process, firstly BZN ceramic pellets were placed into a mask which was 5 mm in diameter. Then, those ceramic pellets inside the mask were put into Boc Edwards Auto 500 coating device and coated by pure gold. After coating, contacts to both two surfaces of coated BZN ceramic pellets were applied with silver wires with 50 ohm resistance by using silver paste. Then, those pellets stick onto a 3 cm^2 glass substrate were placed into vacuum chamber under pressures of around 10^{-2}-10^{-4} bar.

Dielectric measurements were performed at various temperatures between 25-200 °C and at different frequencies between 1 kHz-2 MHz by using Agilent E4980A

Precision LCR Meter (Figure III.6). Dielectric constant and dielectric loss values of BZN perovskite ceramics were obtained as a function of frequency and temperature.

Figure III.6 Dielectric properties measurement device (Agilent E4980A Precision LCR Meter).

CHAPTER IV

RESULTS AND DISCUSSION

IV.1 EFFECT OF CITRIC ACID CONTENT ON THE PHASE FORMATION

It is known in literature that different citric acid ratios affect phase formation, particle size and morphology of powders in citrate gel method [64, 65, 66]. In this scope, $Ba(Zn_{1/3}Nb_{2/3})O_3$ (BZN) powders, synthesized by citrate gel method with different citric acid/metal cations mol ratios were characterized by differential thermal and thermogravimetric analysis and XRD to reveal the phase development during single phase BZN formation.

IV.1.1 BZN-1 (Citric Acid / Metal Cations: 5)

BZN powders, which were synthesized by citrate gel method with citric acid/metal cations mol ratios of 5 (CA/MC: 5) were named as BZN-1. Thermal behavior of BZN-1 powders was investigated with thermogravimetric and differential thermal analysis (TG-DTA) using powder heat treated at 300 °C for 2 hours, and the results are given in Figure IV.1. As it is seen from TG curve, a total weight loss of 39% occurred in the system between temperatures as 20-1000 °C. This 39% total weight loss is composed of weight losses of approximately 22% between 350-450 °C and 17% between 450-1000 °C. Endothermic peak at 345 °C is formed due to decomposition of citrate (or decomposition of weakly bonded organics in the citrate structure) and the other organics in the system. The second weight loss of 17% in the system was due to the combustion of carbon that arises as a result of the decomposition of organics in the system. This weight loss matches with exothermic peaks at 540 °C and 680 °C. The second weight loss was also due to the decomposition of residual organics in the system, probably decomposition of barium carbonate ($BaCO_3$) and evaporation of zinc oxide (ZnO) since there were $BaCO_3$

peaks at 800 °C and 900 °C in XRD. The decomposition of barium carbonate and evaporation of ZnO are related with the endothermic peaks at 870 °C and 945 °C.

The phase formation in powder with different CA/MC ratios charred at 300 °C for 2h and heat treated between 300-1200 °C for 4h was studied by XRD (Figure IV.2). The powder was amorphous at 300 and 400 °C, although $BaCO_3$ peaks were seen at 400 °C. Barium carbonate phase formation in the structure was caused by the reaction of Ba^{2+} ions with CO_2 and CO gases which emerged due to the decomposition of citric acid [67]. Mali and Ataie (2005) indicated in a study of investigation the structure of nano $BaFe_{12}O_{19}$ crystals produced by sol-gel combustion method that the reaction of reactive Ba^{2+} ions with CO_2 and CO gases which emerge by decomposition of citric acid causes the formation of $BaCO_3$ phase. The first BZN peaks started to form at 500 °C and their intensities increased with increasing temperature. However, the powder was also mostly amorphous at 500 °C possibly due to high citric acid content. At 600 °C, the content of $BaCO_3$ and ZnO phases decreased sharply which indicated that BZN phase directly formed from reaction of $BaCO_3$ with other oxides. As the heat treatment temperature increased the amount of $BaCO_3$ and ZnO decreased giving eventually nearly single phase BZN at 1000 °C. However, above 1000 °C an unknown phase formed and its amount increased with increasing temperature. This could be due to evaporation of ZnO which led to formation of nonstoichimetric phases since ZnO has a high volatility at high temperatures (>1200 °C) [62, 63, 68]. Although Nb_2O_5 was not detected in the XRD possibly due to amorphous nature of XRD pattern, it can be concluded that, the formation of BZN occurs via a direct reaction of $BaCO_3$, ZnO and Nb_2O_5:

$$BaCO_3 + ZnO + Nb_2O_5 \xrightarrow{>600°C} Ba(Zn_{1/3}Nb_{2/3})O_3 \qquad \text{(IV.1)}$$

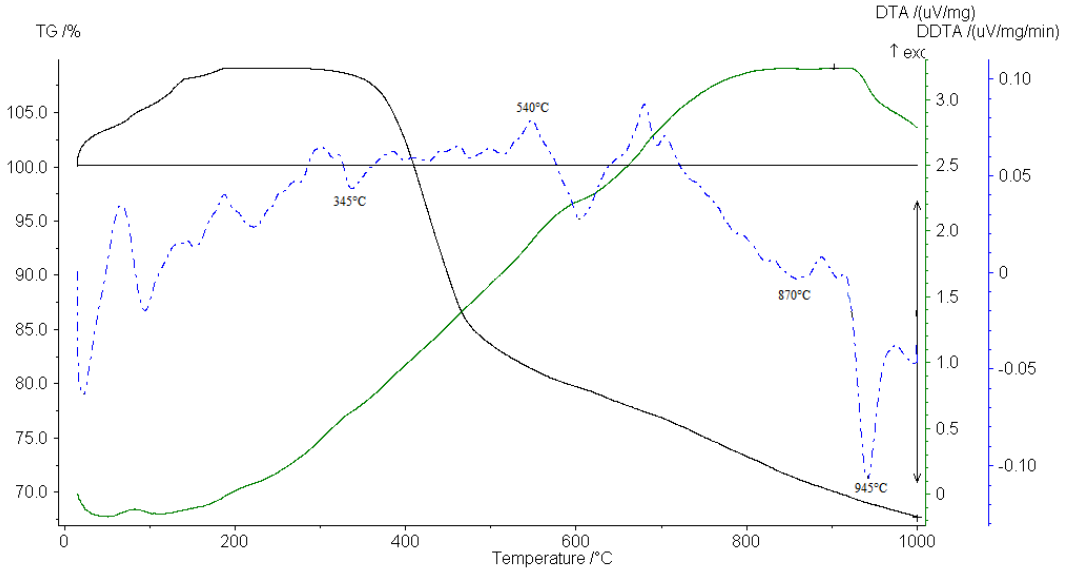

Figure IV.1 TG-DTA curves of BZN-1 sample (CA/MC:5).

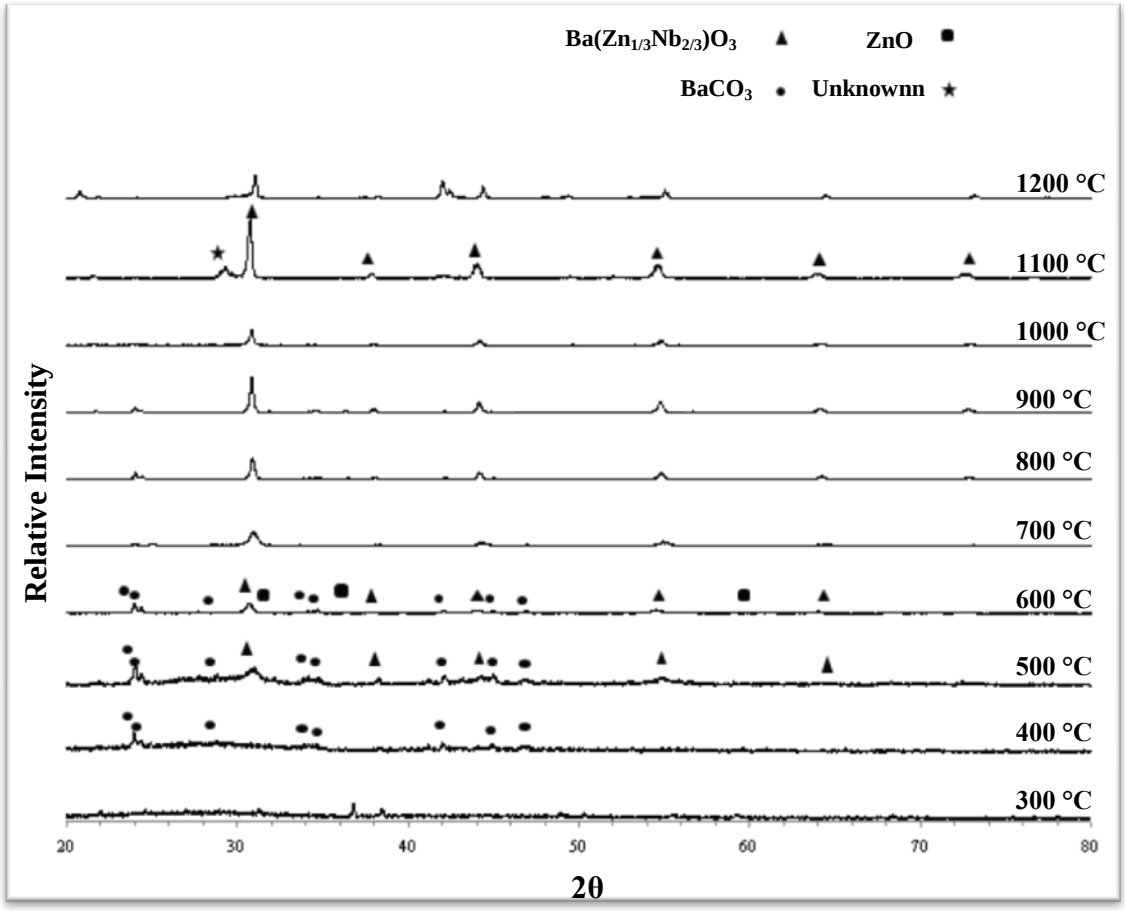

Figure IV.2 XRD patterns of BZN-1 samples (CA/MC: 5) synthesized by citrate gel method and calcined at various temperatures for 4h after heat treatment at 300 °C for 2h.

In Figure IV.3, scanning electron microscopy images of BZN-1 powders with CA/MC ratio of 5 which were calcined at 1100 °C for 4 h are given. BZN-1 powders are in nano scale although they contain agglomeration. Particle size of powder changed from 55 nm to115 nm with a homogenous size distribution. The particles had near spherical shape.

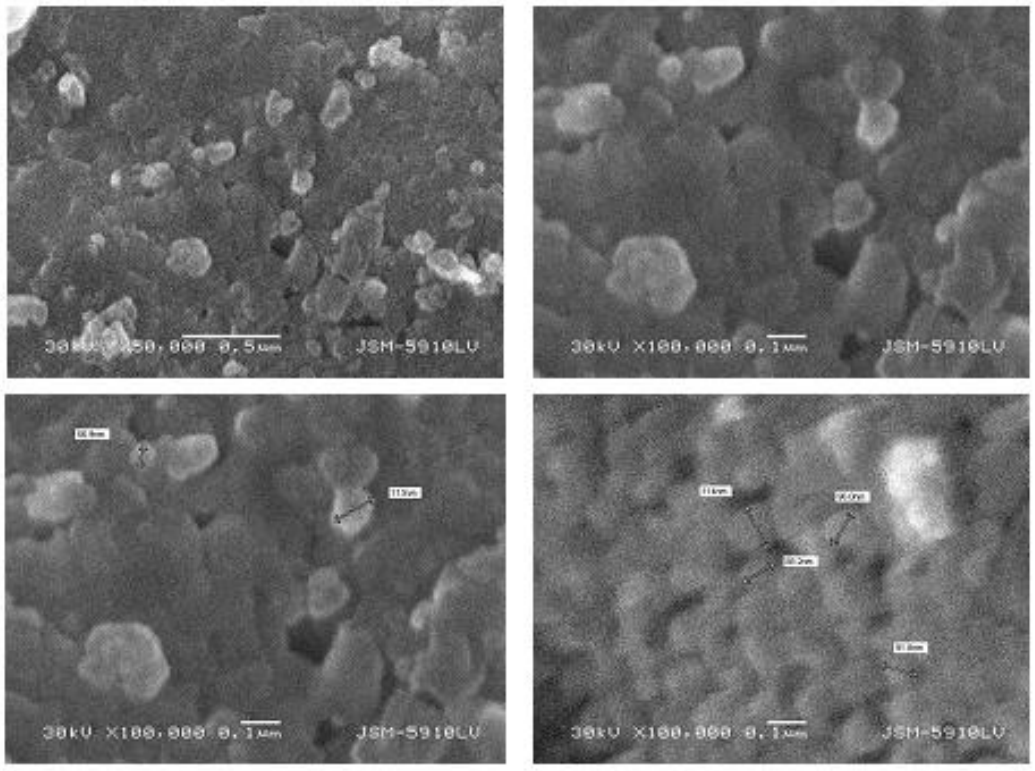

Figure IV.3 SEM images of BZN-1 sample (CA/MC:5) that was synthesized by citrate gel method, heat treated at 300 °C for 2 hours and calcined at 1100 °C for 4 hours.

Transmission electron microscopy (TEM) investigations showed that BZN-1 powders contained high degree of agglomeration and they had a particle size distribution of 75-150 nm (Figure IV.4). Morphology of BZN-1 powders was close to be spherical. However, investigation of powders with transmission electron microscopy could not be performed in detail since powders were decomposed by radiation as a result of the interaction of BZN-1 powders with electron beam at high magnifications. In transmission electron microscopy studies, the interaction between electron beam and sample causes different kinds of radiation damages depending on sample and running conditions of microscope. In this reaction between specimen

and electron beam, two main radiation damage mechanisms exist: a) knock-on displacement: occurs as a result of the reaction between electron beam and nucleus of sample atoms, b) radiation or ionization: occurred as a result of the reaction between electron beam and electrons of sample atoms. Besides microstructure changes, the reaction between electron beam and sample may also increase the defective structure of material without any change in microstructure [69, 70]. Some microstructural changes occurred in BZN-1 samples preventing the use of high magnification during the study to investigate samples under electron beam for sufficient time and also to take images of samples.

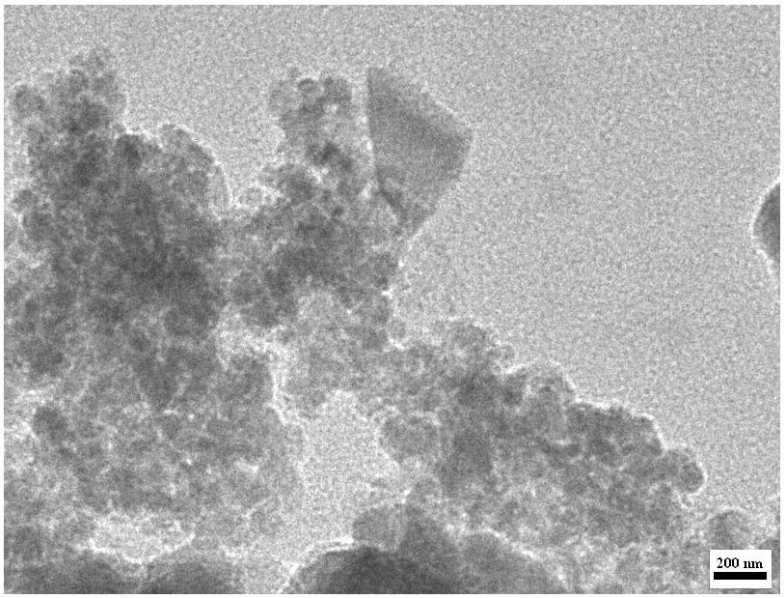

Figure IV.4 TEM image of BZN-1 sample (CA/MC:5) that was synthesized by citrate gel method, heat treated at 300 °C for 2 hours and calcined at 1100 °C for 4 hours.

IV.1.2 BZN-2 (Citric Acid / Metal Cations: 2)

TG-DTA curves of BZN-2 powders, which were synthesized by citrate gel method with citric acid/metal cations mol ratio of 2 (CA/MC: 2) and heat treated at 300 °C for 2 hours, are given in Figure IV.5. Thermogravimetric analysis showed that weight loss occurred in 3 main steps: 40-335 °C, 335-700 °C and 700-1000 °C. The weight loss of 4% between 40-335 °C was probably caused by the evaporation of water adsorbed by the powder surface which gave endothermic peaks at 40 °C and 110 °C in the DTA. The rest of the 4% total weight loss was related to the

endothermic peaks observed at 235 °C and 330 °C in DTA curve and it was due to the decomposition of weakly bonded organics in the citrate structure. The second weight loss in the system between 335-700 °C was around 20% which was due to the combustion of carbon that arised as a result of the decomposition of organics in the system. This weight loss matches with exothermic peaks at 510 °C and 625 °C. Two endothermic peaks at 748 °C and 845 °C were observed in the last weight loss step occurred between 700-1000 °C. These peaks are formed probably due to the decomposition of the $BaCO_3$ and remaining organics, and also possibly due to the evaporation of ZnO in the system.

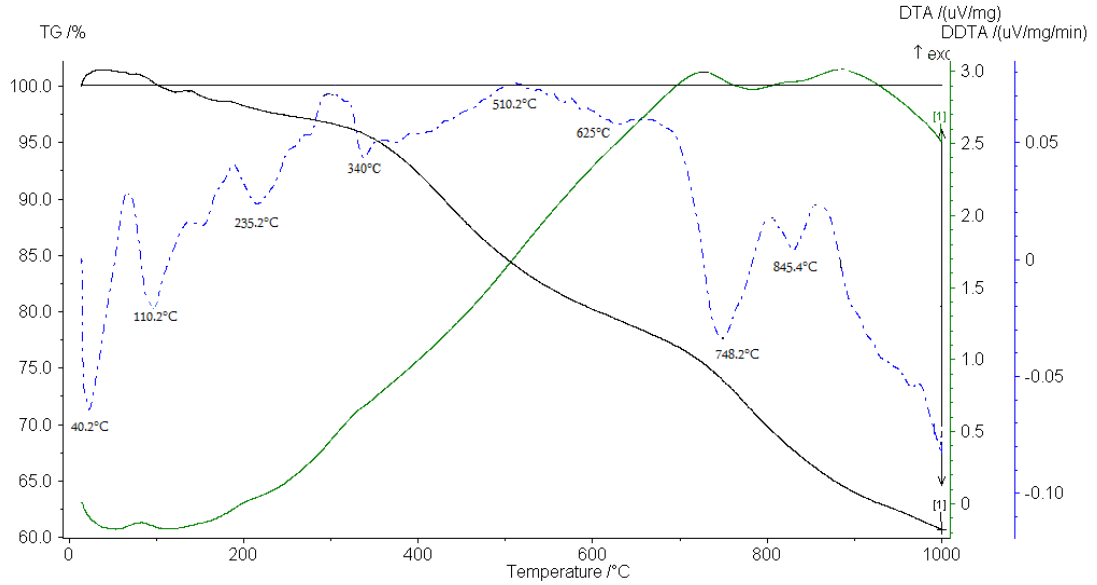

Figure IV.5 TG-DTA curves of BZN-2 sample (CA/MC:2).

The phase formation of BZN-2 powders starting from the gel charred at 300 °C for 2 h was studied by means of XRD (Figure IV.6). The powders at 300 °C were almost amorphous. Heat treatment at 400 °C caused the formation of $BaCO_3$ phase peaks in significant amounts. $BaCO_3$ is formed due to the reaction between reactive Ba^{2+} ions in the system and CO and CO_2 gases emerged as a result of the citric acid decomposition [13]. Small amounts of ZnO phase are determined as a secondary phase apart from $BaCO_3$ at 400 °C. BZN-2 powders have higher ratios of crystalline structure than BZN-1 powders at 400 °C. This could be due to the high amount of citric acid in BZN-1 powder leading to amorphous structures in the system. $Ba(Zn_{1/3}Nb_{2/3})O_3$ phase started to form at 500 °C first and the intensity of BZN peaks

increased with increasing heat treatment temperature. $BaCO_3$ phase content also increased at 500 °C compared to the 400 °C. However, $BaCO_3$ phase content suddenly decreased at 600 °C which indicates that BZN phase is directly formed as a result of the reaction of $BaCO_3$ phase with the other oxides in the system. While increasing temperature lowered the amount of secondary phases in the system, BZN phase amount increased and single phase $Ba(Zn_{1/3}Nb_{2/3})O_3$ phase formed at 1100 °C without any secondary phases in the system. In addition, increasing calcination temperature did not cause the transformation of BZN phase to any other phases even at 1200 °C, as it occurred in BZN-1 powder (citric acid/metal cations : 5), and single phase perovskite structure was observed to be stable at high temperatures.

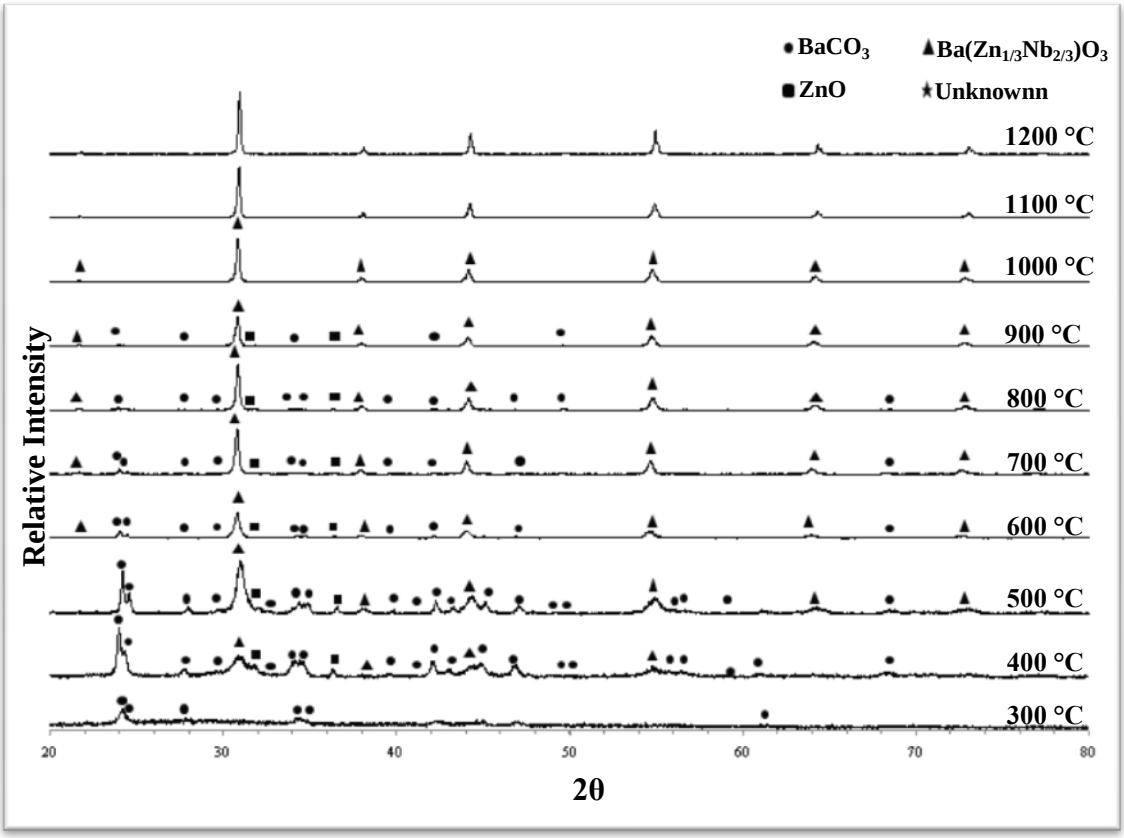

Figure IV.6 XRD patterns of BZN-2 sample (CA/MC: 2) that was synthesized by citrate gel method, heat treated at 300 °C for 2 hours and calcined at various temperatures for 4 hours.

The FT-IR spectrum of the gel heat treated at 300 °C for 2 hours indicated mainly a broad band at 1610 cm^{-1} which was assigned to the carboxyl groups of citric acid (Figure IV.7). XRD analysis also indicated an amorphous nature at this

temperature. However, higher amounts of bands formed in powder heat treated at 400 °C. Bands at 1440 and 860 cm^{-1} decreased in intensity with temperature increase, but the bands at 1760, 1090 and 700 cm^{-1} disappeared at lower temperatures of around 600 °C. These bands occurred due to $BaCO_3$ presence in the material [71]. But the bands at 1440 and 860 cm^{-1} disappeared at higher temperatures of 1100 °C which indicated that the carbonates were present in the material up to 1100 °C. However, although XRD indicated $BaCO_3$ peaks at 800 °C, they were not observed at 900 °C possibly due to their low content. Bands at 680 and 600 cm^{-1} got well defined at higher temperatures. These bands can be attributed to metal-oxygen stretching vibration of $Ba(Zn_{1/3}Nb_{2/3})O_3$. An absorption band below 800 cm^{-1} is the characteristic of metal oxides [72]. These bands were broader at lower temperatures indicating amorphous species.

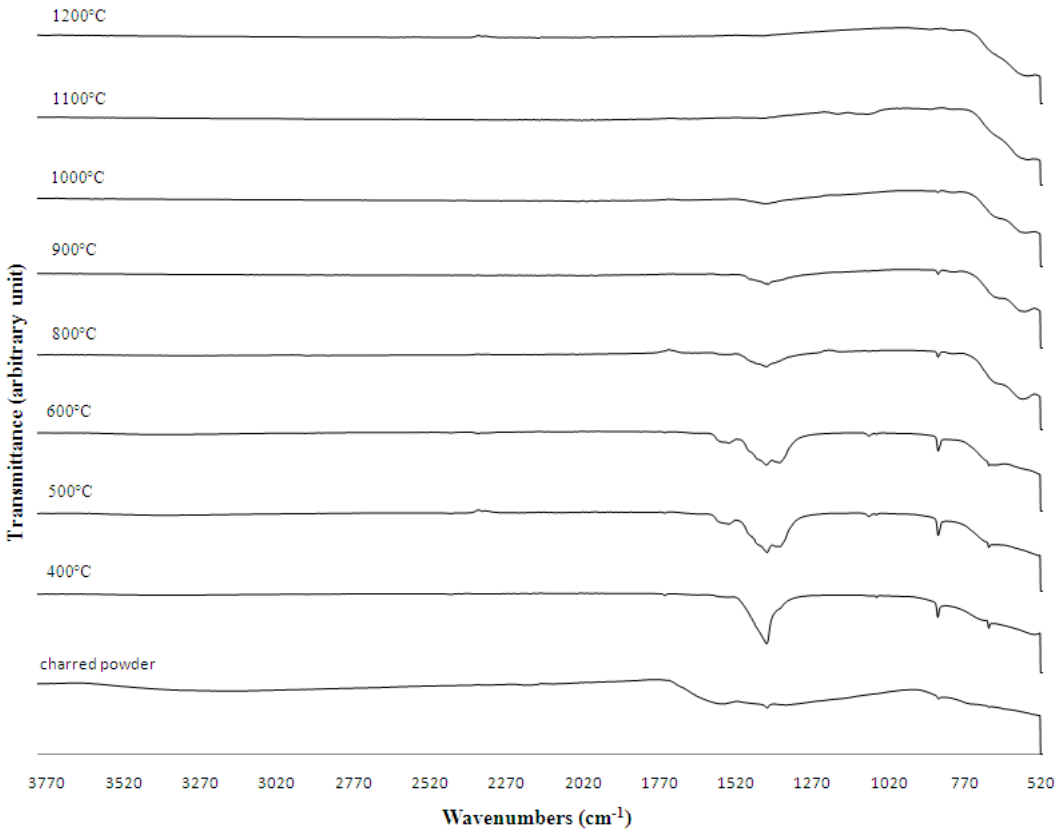

Figure IV.7 FT-IR spectrum of BZN-2 sample (CA/MC:2) that was synthesized by citrate gel method, heat treated at 300 °C for 2 hours and calcined at various temperatures for 4 hours.

Scanning electron microscopy images of BZN-2 powder that was calcined at 1100 °C are given in Figure IV.8. SEM images showed that BZN powders were in nanoscale although they contained agglomerations. Particle size of powders changed approximately between 70-100 nm with partial homogeneous size distribution. On the other hand, transmission electron microscopy (TEM) images of BZN-2 powders which were calcined at 1100 °C revealed that particle size of powder changed between 60-150 nm with some agglomerations (Figure IV.9). As the same with BZN-1 powders, BZN-2 powders could not be investigated properly by TEM due to the reaction of powders with electron beam.

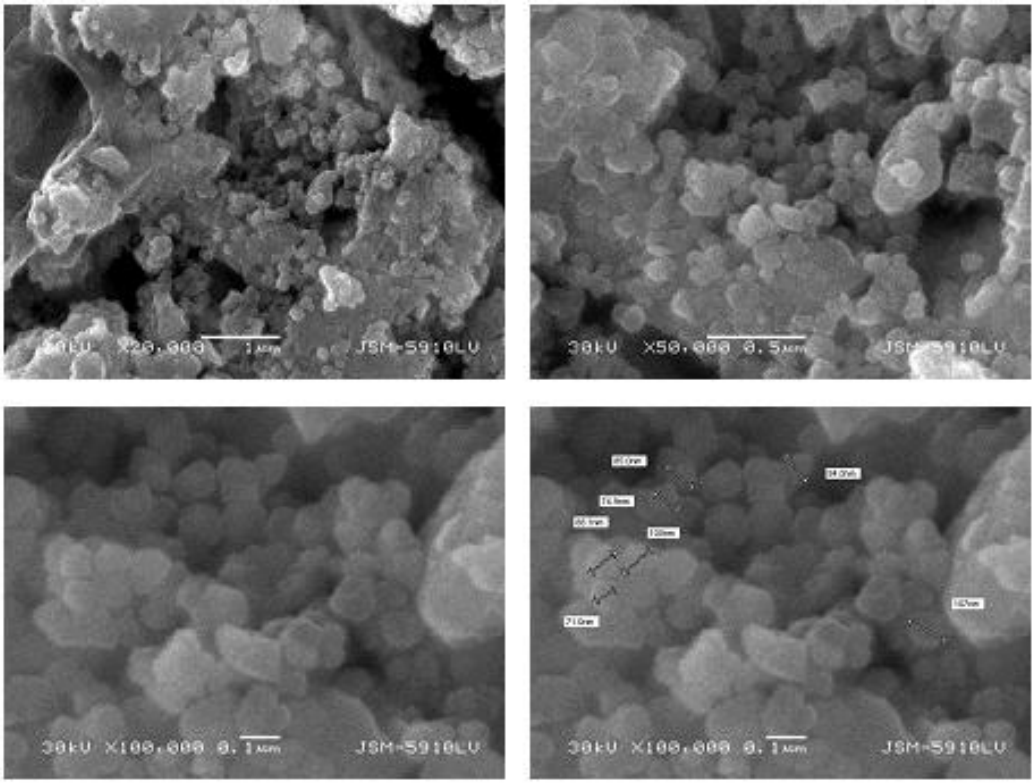

Figure IV.8 SEM images of BZN-2 sample (CA/MC:2) that was synthesized by citrate gel method, heat treated at 300 °C for 2 hours and calcined at 1100 °C for 4 hours.

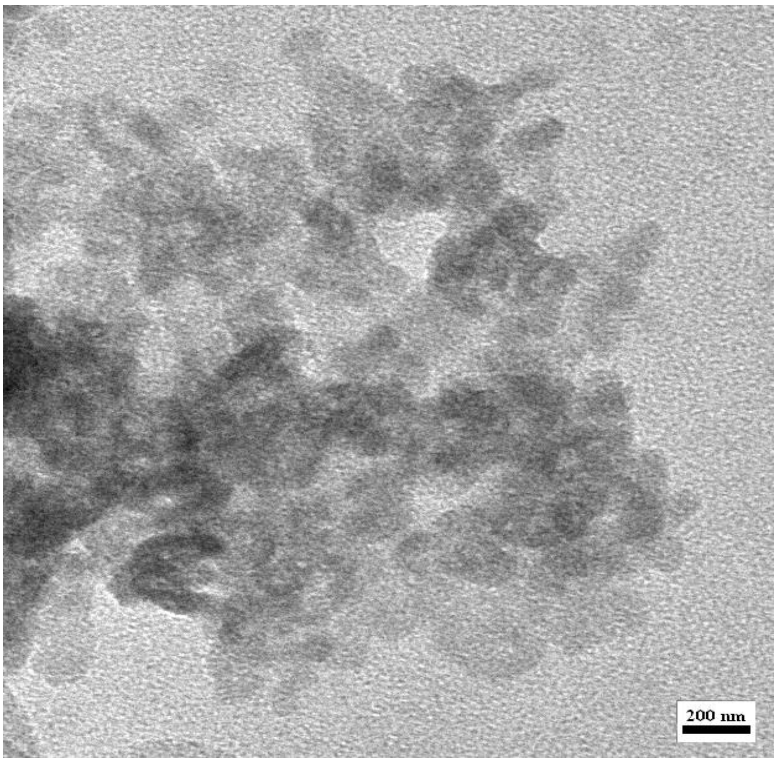

Figure IV.9 TEM image of BZN-2 sample (CA/MC:2) that was synthesized by citrate gel method, heat treated at 300 °C for 2 hours and calcined at 1100 °C for 4 hours.

IV.1.3 BZN-3 (Citric Acid / Metal Cation: 1)

BZN-3 powders that were synthesized by citrate gel method with citric acid/metal cations mol ratio of 1 (CA/MC: 1) were heat treated at 300 °C for 2 hours and then they were analyzed by TG-DTA to track the thermal behavior of powders (Figure IV.10). TG curve showed that a total weight loss of 36% occurred in the system up to 1000 °C. 36% weight loss was composed of two steps which were occurred in the temperature ranges of 360-470 °C, 470-1000 °C subsequently. In the first step of 18%, weight loss occurred due to the decomposition of the organics in the system. Endothermic peak approximately at 330 °C and subsequent exothermic peak at 465 °C were due to the decomposition of organics and so combustion of carbon that came out as a result of decomposition process. In the second step of 18%, it was thought that the decomposition of residual organics and combustion of carbon continued in this step. But the weight loss in this step was also thought to be probably due to decomposition of $BaCO_3$ and also evaporation of ZnO. Endothermic peaks at 605 °C, 845 °C and 875 °C formed due to these decomposition and evaporation processes.

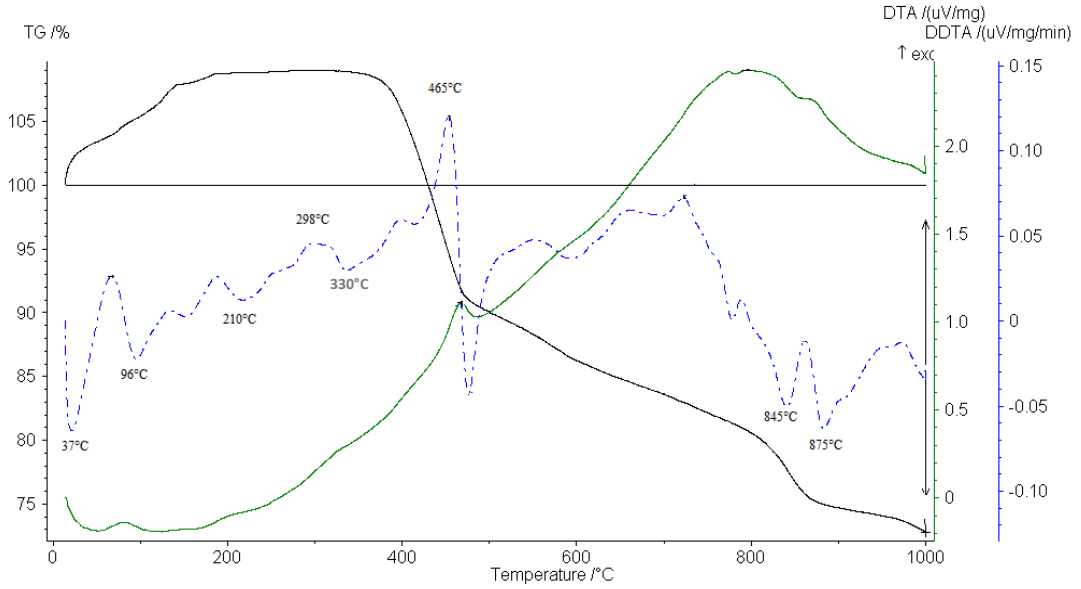

Figure IV.10 DTA and TG curves of BZN-3 sample (CA/MC: 1).

BZN-3 powders that were heat treated at 300 °C for 2 hours and then heat treated at temperatures between 400-1200 °C for 4 hours were investigated by XRD to reveal phase formation in the system with increasing heat treatment temperature (Figure IV.11). BZN-3 powders were almost completely amorphous at 300 °C with barium carbonate peaks. BZN phase started to form at 400 °C contrary to BZN-1 and BZN-2 powders. However, considerable amounts of $BaCO_3$ and ZnO phases existed at 400 °C beside BZN phase. The amount of BZN phase increased at 500 °C, while the content of ZnO phase decreased. But, $BaCO_3$ phase was still in considerable amounts at 500 °C. Increasing heat treatment temperature caused a sharp decrease in $BaCO_3$ and ZnO phase amounts at 600 °C proving that BZN phase formation was caused by the reaction of $BaCO_3$ with ZnO and also with the other oxides in the system. At 1000 °C, single phase BZN perovskite structure was obtained. In addition, at higher temperatures above 1000 °C, it was seen that BZN phase still existed without any phase decomposition as in BZN-1 powder.

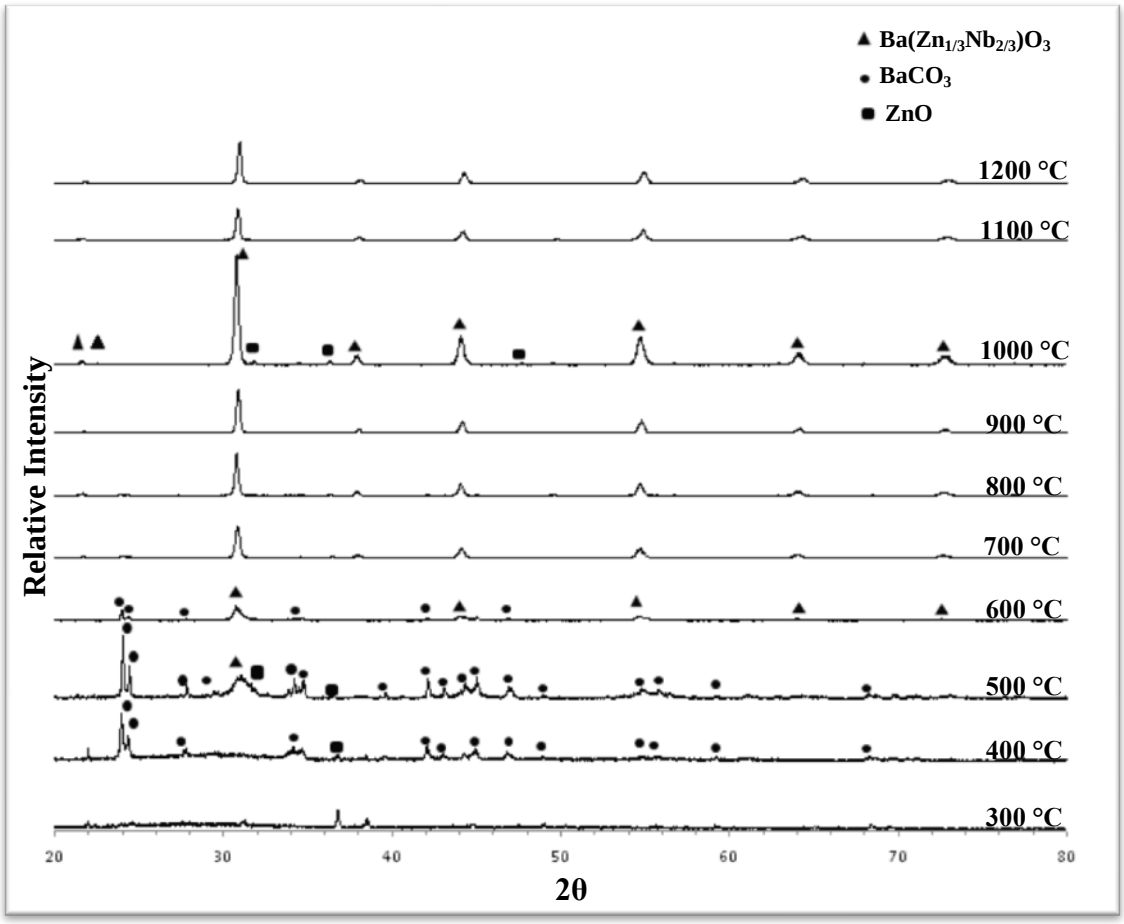

Figure IV.11 XRD patterns of BZN-3 sample (CA/MC: 1) that was synthesized by citrate gel method, heat treated at 300 °C for 2 hours and calcined at various temperatures for 4 hours.

In Figure IV.12, SEM images of BZN-3 powders that were calcined at 1100 °C are given. It can be clearly seen from the images that BZN powders were in nanoscale but they contained some agglomeration. Particle sizes varied between 75-100 nm. In addition, TEM images in Figure IV.13 showed that particle size of BZN powders was in the range of 55 to 150 nm with a spherical morphology. BZN-3 powders were also agglomerated but its degree was lower than BZN-1 and BZN-2.

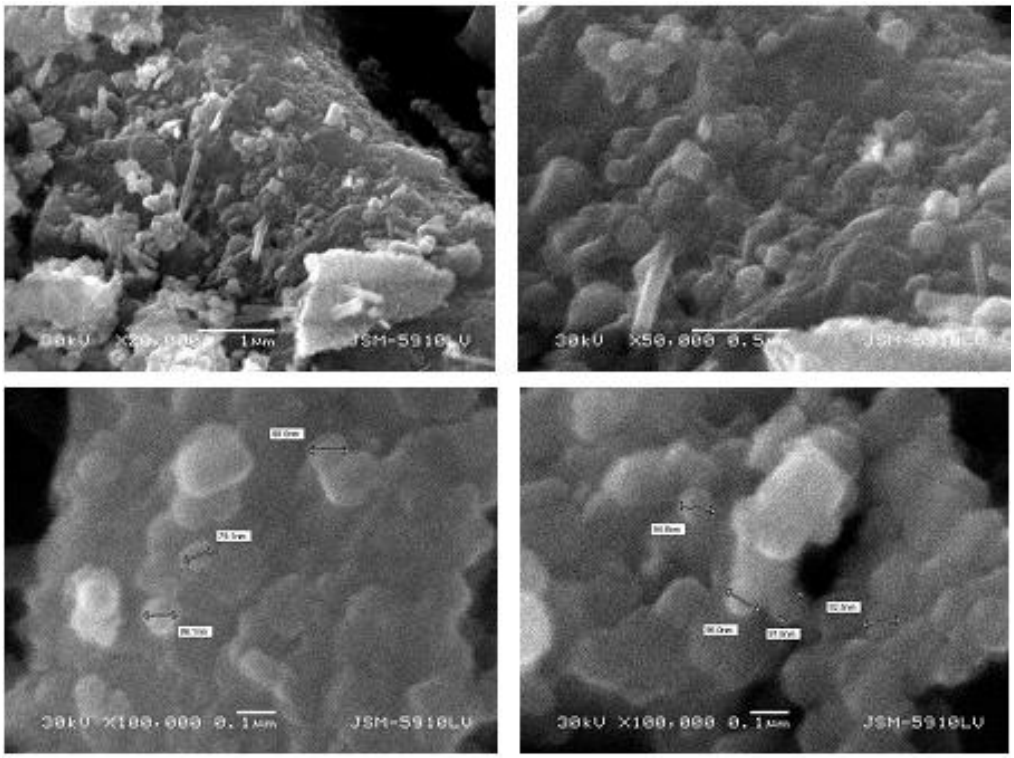

Figure IV.12 SEM images of BZN-3 sample (CA/MC: 1) that was synthesized by citrate gel method, heat treated at 300 °C for 2 hours and calcined at 1100 °C for 4 hours.

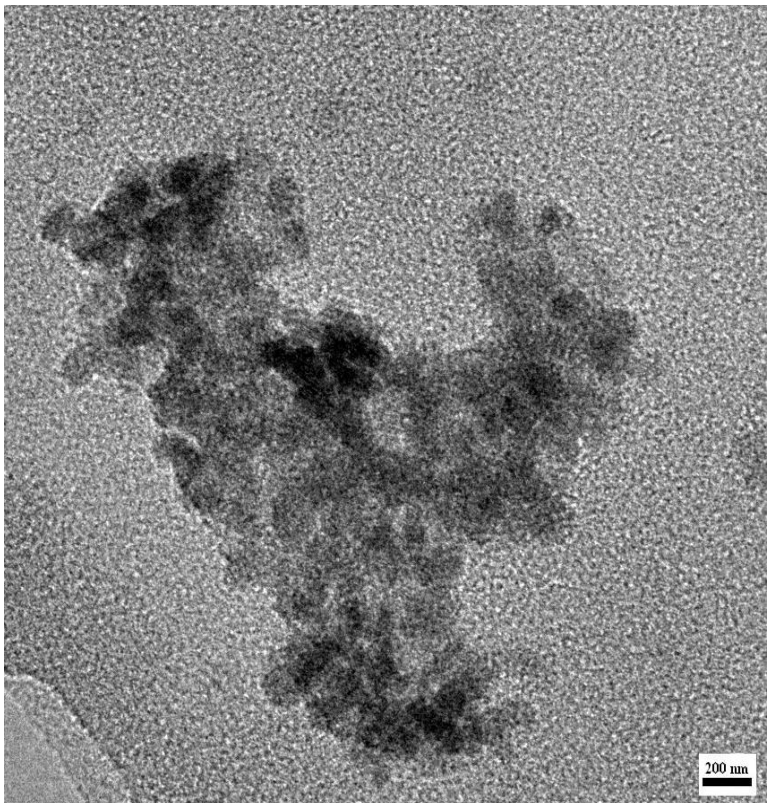

Figure IV.13 TEM image of BZN-3 sample (CA/MC: 1) that was synthesized by citrate gel method, heat treated at 300 °C for 2 hours and calcined at 1100 °C for 4 hours.

IV.I.4 BZN-4 (Citric Acid / Metal Cation: 0.5)

Thermal behavior of BZN-4 powders that were synthesized by citrate gel method with citric acid/metal cations mol ratio of 0.5 was investigated using TG-DTA (Figure IV.14). Investigation of thermogravimetric curve revealed that total weight loss up to 1000 °C was composed of 2 steps. Weight loss of 15% that occurred at temperatures between 340 °C and 450 °C was due to the decomposition of citrates and the other organics in the system. Exothermic peak at 440 °C was due to the combustion of carbon that came out as a result of decomposition of citrates and organics. 29% weight loss at 450-1000 °C was due to the decomposition of residual organics and combustion of released carbon and also due to decomposition of $BaCO_3$ and probably due to the evaporation ZnO. As a result of these decompositions and evaporation, three endothermic peaks at 560 °C, 750 °C and 845 °C formed in DDTA curve.

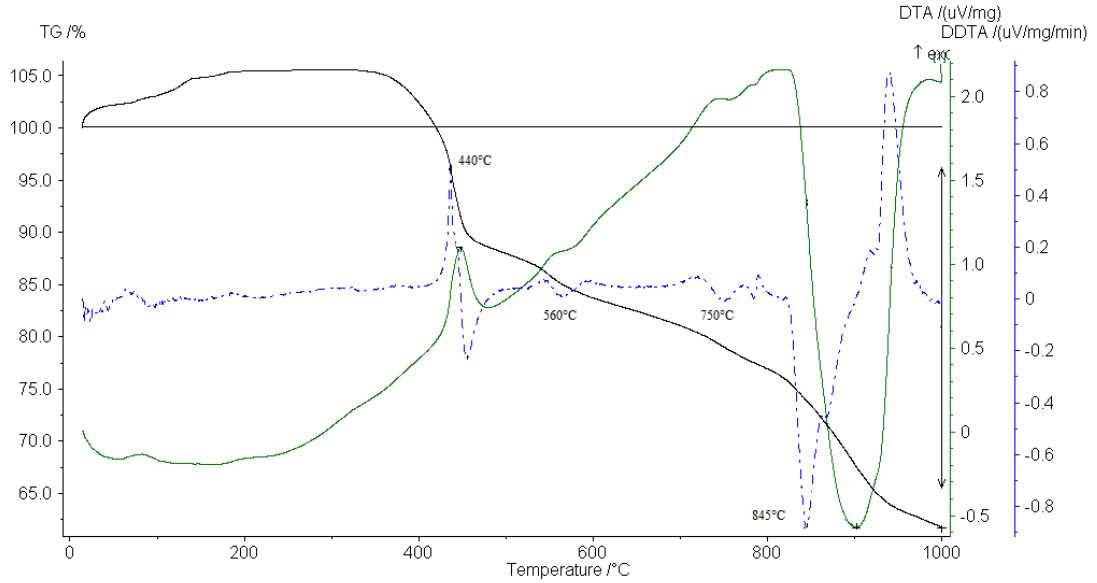

Figure IV.14 DTA and TG curves of BZN-4 sample (CA/MC: 0.5).

BZN-4 powders synthesized by citrate gel method using minimum amount of citric acid compared to the other BZN samples were heat treated at temperatures between 400-1200 °C for 4 hours after heat treatment at 300 °C for 2 hours and then, they were analyzed by XRD to investigate the phase formation in BZN structure (Figure IV.15). BZN-4 powder had almost completely amorphous structure with low amount of $BaCO_3$ at 300 °C as in the other powders (BZN-1, BZN-2 and BZN-3). But the reaction mechanism of BZN-4 powders was different from the others that $Ba_4Nb_{14}O_{23}$ phase (JCPDS Card No: 47-276) started to form at 400 °C together with $BaCO_3$ and ZnO whose amounts increased at 500 °C. The first BZN phase appeared at 600 °C where all $Ba_4Nb_{14}O_{23}$ converted to BZN and $BaCO_3$ and ZnO contents decreased to very low levels. The formation mechanism of BZN at low citric acid contents could be written as:

$$Ba_4Nb_{12}O_{23} + BaCO_3 + ZnO \xrightarrow{>500^{o}C} Ba(Zn_{1/3}Nb_{2/3})O_3 \qquad \text{(IV.2)}$$

Single phase BZN was obtained at 1100 °C since there was a small amount of $BaCO_3$ at 1000 °C. BZN phase was stable at 1200 °C and no decomposition occurred. These results indicate that low citric acid contents not only retarted the formation of BZN phase also increased the single phase BZN formation temperature.

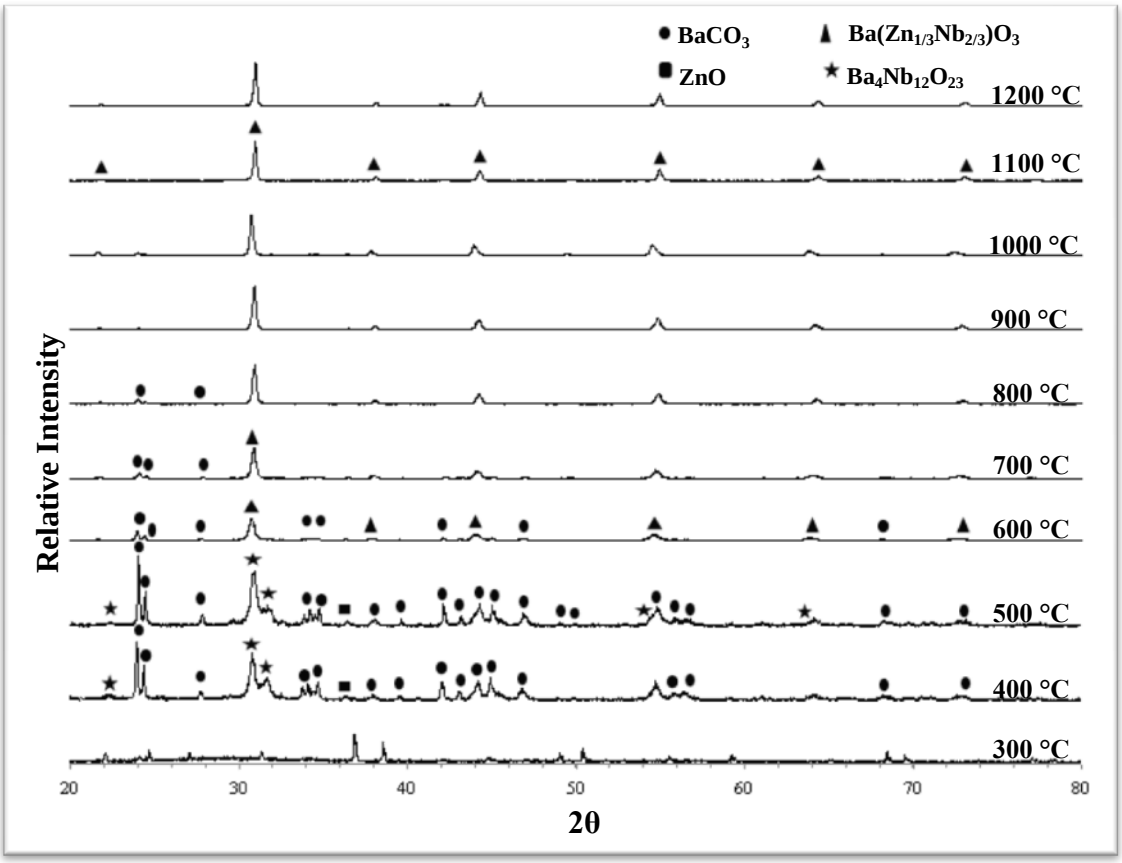

Figure IV.15 XRD patterns of BZN-4 sample (CA/MC: 0.5) that was synthesized by citrate gel method, heat treated at 300 °C for 2 hours and calcined at various temperatures for 4 hours.

SEM investigations of BZN-4 powders calcined at 1100 °C for 4h revealed identical results with the other BZN powders (Figure IV.16). BZN powders were in nanoscale with some agglomeration. Particle sizes were in the range of 60-130 nm with a partial homogeneous size distribution. TEM investigations of BZN-4 powder that were calcined at 1100 °C showed that particle sizes varied between 150-200 nm with a morphology of almost in spherical shape (Figure IV.17). In addition, SEM and TEM results indicated higher degree of agglomeration revealing that lower citric acid contents increased the agglomeration.

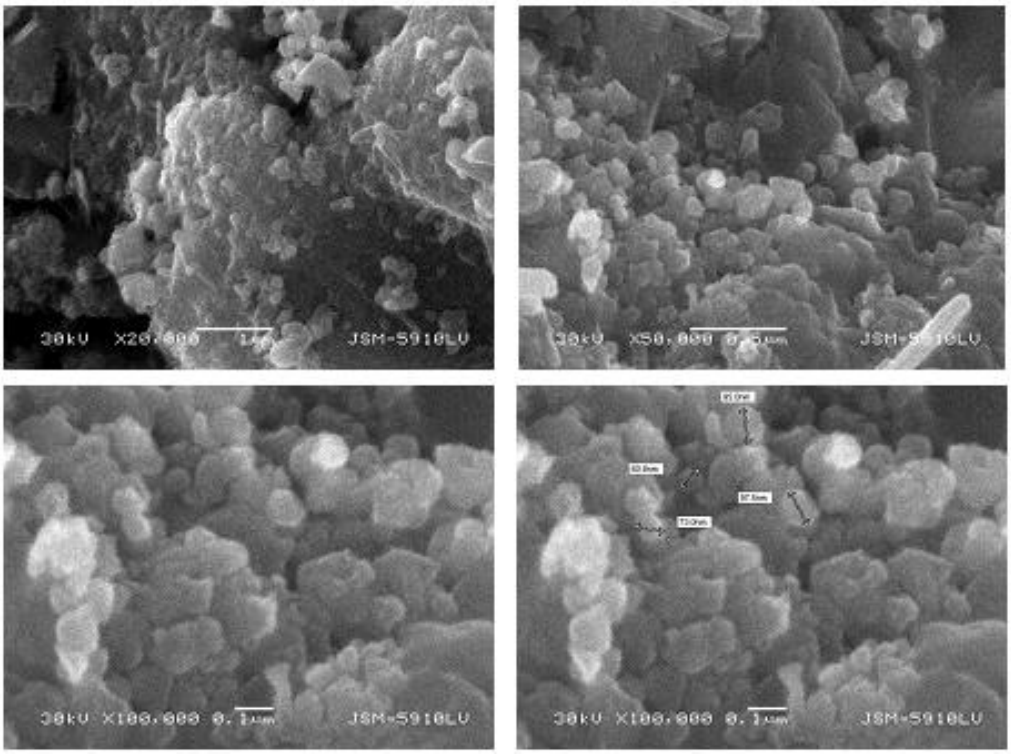

Figure IV.16 SEM images of BZN-4 sample (CA/MC: 0.5) that was synthesized by citrate gel method, heat treated at 300 °C for 2 hours and calcined at 1100 °C for 4 hours.

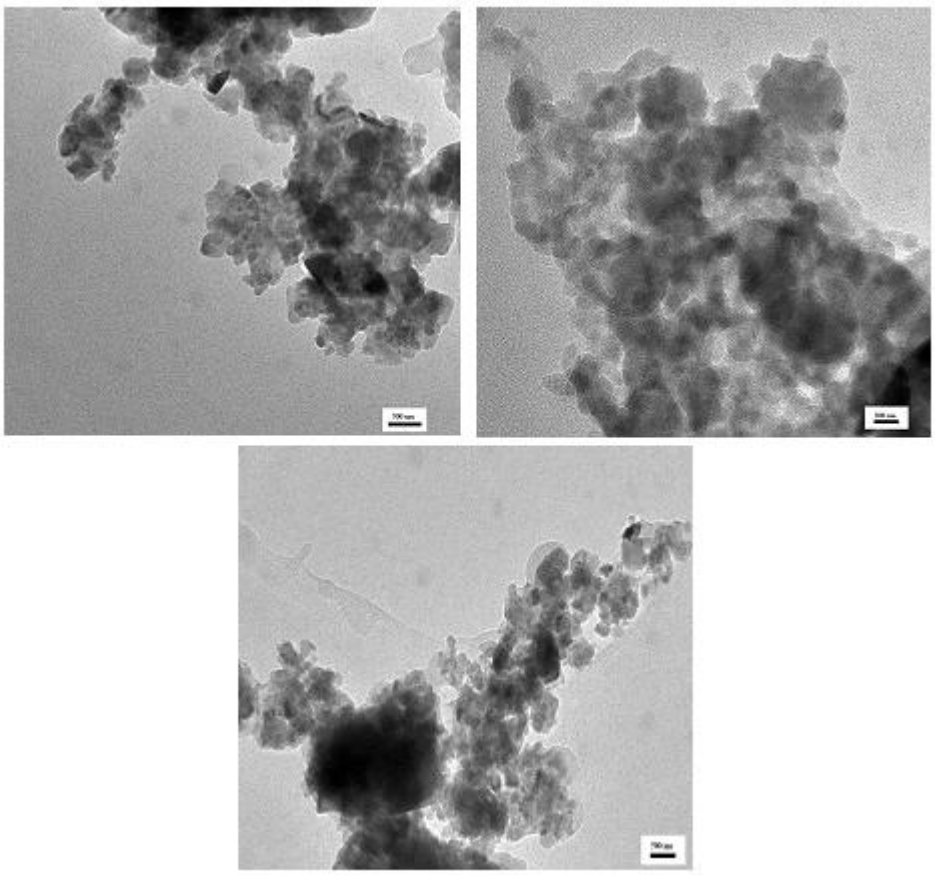

Figure IV.17 TEM images of BZN-4 sample (CA/MC: 0.5) that was synthesized by citrate gel method, heat treated at 300 °C for 2 hours and calcined at 1100 °C for 4 hours.

IV.2 EFFECT OF CITRIC ACID ON BZN PHASE FORMATION AND PARTICLE SIZE

The effect of citric acid content on phase formation, particle size and particle morphology is known in literature [65, 73, 74, 75]. In the present study, the effect of citric acid amount on BZN phase formation, BZN particle size and morphology was investigated.

At high citric acid contents (citric acid/metal cations mol ratio: 5; CA/MC: 5) although BZN phase started to form at 500 °C, single phase BZN structure could not be obtain at any temperature. In spite of higher amount of BZN phase at 1000 °C, there were some minor amounts of second phases. In addition, BZN phase decomposed to undefined phases at temperatures above 1000 °C probably due to the evaporation of ZnO. Therefore, it can be concluded that high citric acid contents are not appropriate for the production of BZN phase by citrate gel method. On the other

hand, low citric acid amounts (CA/MC: 0.5) caused formation of $Ba_4Nb_{14}O_{23}$ phase at 400 °C and 500 °C and BZN phase started to form at 600 °C. Single phase BZN structure occurred at 1100 °C. However, moderate citric acid/metal cations mol ratio of 1 and 2 are more appropriate for the BZN production that BZN phase formation and single phase BZN formation were relatively lower. Comparing the CA/MC mol ratio of 2 (BZN-2) and 1 (BZN-3), CA/MC: 2 is much more promising than the CA/MC: 1, since when CA/MC mol ratio equals to 2, BZN phase started to form at 400 °C and single phase BZN structure was obtained at 1000 °C. As a result, it can be concluded that the best citric acid to total metal cations mol ratios is 2 in the production of BZN powder by citrate gel method. Phase development during formation of BZN single phase structure is significantly different when citric acid content is different. This result proves that citric acid amount has considerable effect on production of single phase BZN by citrate gel method.

In the literature, in several studies it was determined that citric acid content had prominent effect on phase development. In a study of $SrFeO_{-2.85}$ production by Pechini method, the effect of citric acid mol ratios to metal cations (Fe+Sr) was studied by using ratios as 0.5, 1 and 1.5 [65]. The most appropriate ratio was determined as 1 as a result of calcination studies. In this study, the required heat treatment times for citric acid to metal cations mol ratios as 0.5, 1 and 1.5 was 30 hours, 5 hours and 50 hours respectively at 600 °C. This result also was a proof of significant effect of citric acid content on phase formation. Also, in $SrFeO_{-2.85}$ phase formation without carbonate in the structure, low citric acid amounts as 0.5 required longer time than production with high citric acid amounts as 1. In another study to produce $Ba_{0.70}Sr_{0.30}TiO_3$ by citrate gel method, citric acid/metal cations mol ratios were varied between 2.5 and 5 to investigate the effect of citric acid on phase formation and particle morphology [64]. The results showed that CA/MC mol ratio had important effect on phase formation that increased citric acid amount resulted in increased oxi carbonate inter phases in the system. In addition, in a study to produce cordierite structure by sol gel method, the effect of citric acid amount on cordierite phase formation was investigated using ratios of CA/Al^{3+}: 1 ,3 and 5. When the CA/Al^{3+} ratio was 1, the amount of cordierite phase was reported to be higher as it was compared with the amount in CA/Al^{3+}: 3 and 5 [73].

Investigations to determine the effect of citric acid amount on BZN powder particle size, shape and morphology showed that there is no significant effect of citric acid amount on particle morphology since almost all BZN powders produced at different citric acid/total metal cation (Ba+Zn+Nb) mol ratios (BZN-1: 5, BZN-2 : 2, BZN-3: 1, BZN-4: 0.5) had identical morphologies. However, citric acid amount had considerable effect on BZN particle size. Table IV.1 gives the TEM particle size of BZN powders produced using different citric acid/metal cation mol ratio. It is clearly seen from the table that while the powders produced with CA/MC: 5, 2 and 1, had identical particle size ranges, low citric acid content (CA/MC: 0.5) resulted in larger particles. Therefore, it can be concluded that while high citric acid contents may give smaller particle sizes, low citric acid contents may give larger particles. In addition to particle size, different citric acid amounts leads to different agglomeration levels in BZN powders. Especially for high CA/MC mol ratio of 5 and low CA/MC mol ratio of 0.5, powders have higher agglomeration than the samples with moderate level of CA/MC ratio. As it can be determined from TEM images that agglomeration degree is the lowest for ratios of CA/MC: 1 and CA/MC: 2 (Figure IV.18).

Table IV.1 Particle sizes measured using TEM images as reference for $Ba(Zn_{1/3}Nb_{2/3})O_3$ powders that were synthesized with different CA/MC mol ratios and calcined at 1100 °C for 4 hours.

BZN Powder Sample	**Particle Size**
BZN-1 (CA/MC: 5)	75-150 nm
BZN-2 (CA/MC: 2)	55-150 nm
BZN-3 (CA/MC: 1)	60-150 nm
BZN-4 (CA/MC: 0.5)	150-200 nm

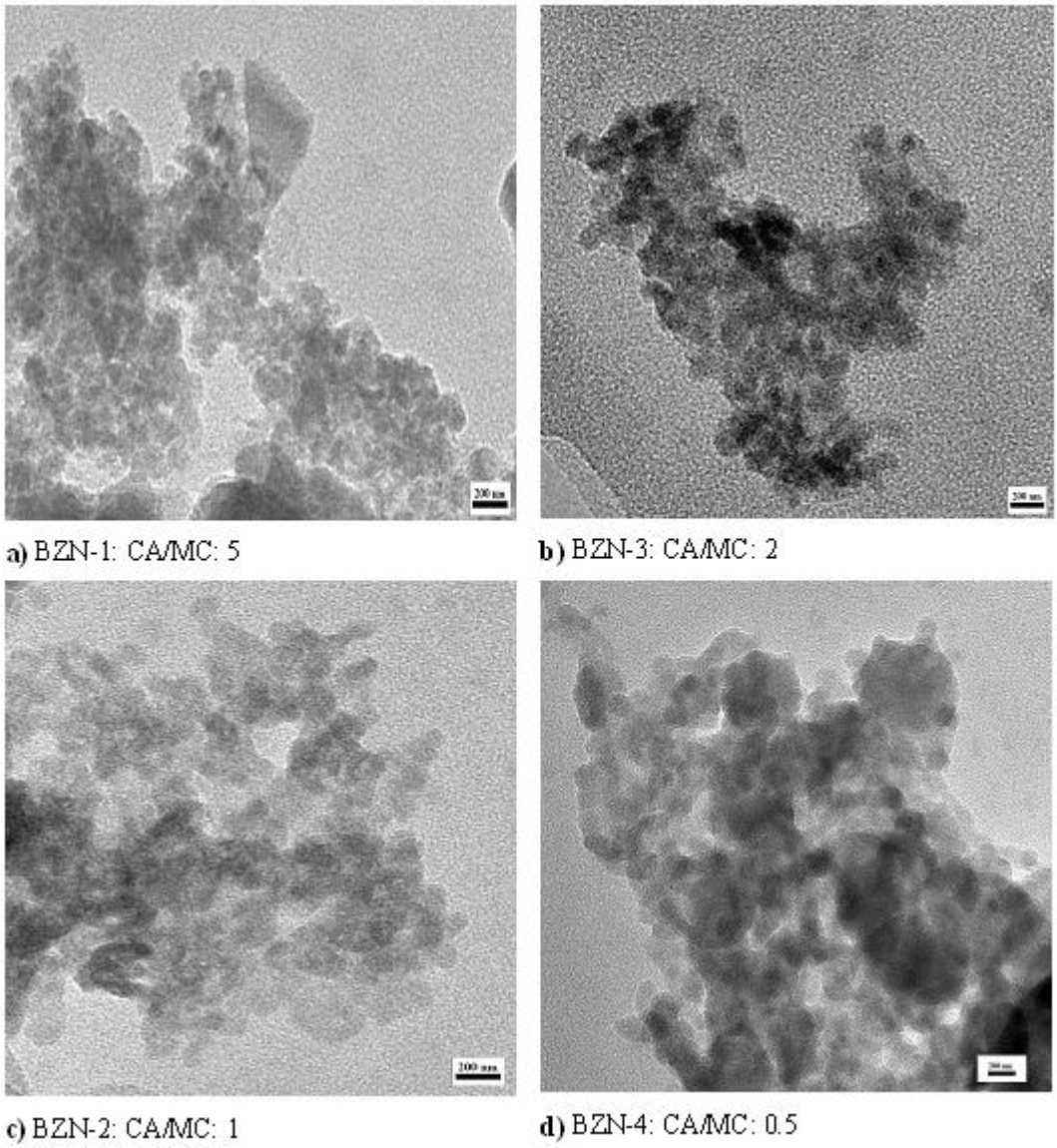

Figure IV.18 TEM images of $Ba(Zn_{1/3}Nb_{2/3})O_3$ powders that were synthesized by citrate gel method, heat treated at 300 °C for 2 hours and calcined at 1100 °C for 4 hours a) CA/MC: 5, b) CA/MC: 2, c) CA/MC: 1, d) CA/MC: 0.5.

In the literature, it is also evident that citric acid content had prominent effect on particle size. In the study, performed to produce $SrFeO_{-2.85}$ by Pechini method, citric acid effect on particle size was investigated by studying different citric acid/metal cations mol ratios (0.5, 1, 1.5) [65]. As a result of this study, it was reported that citric acid/metal cations mol ratios had significant effect on particle size of $SrFeO_{-2.85}$. Particle sizes of powders synthesized at 600 °C and 800 °C increased with decreasing citric acid amount (CA/MC: 0.5). In addition, in a study to produce $Ni/MgO.ZrO_2$ nanocrystals by citrate gel method, the effect of citric acid mol ratio to

total metal ions (1, 1.5, 2 and 3) on particle size was investigated and reported that imcreased citric acid amount caused smaller particle sizes [66]. In this study, results for particle size in CA/MC: 1 and 1.5 were close to each other and also results in CA/MC: 2 and 3 were rather similar as well. As a paralled study of producing $Ba_{0.70}Sr_{0.30}TiO_3$ by citrate gel method demonstrated the effect of CA/MC mol ratio as 2.5 and 5 on particle morphology and agglomeration degree [64]. Conclusion of the study was that different CA/MC mol ratios had significant effect on powder morphology that powders with CA/MC ratio of 5 were almost square in shape with lower degree of agglomeration.

In order to compare with the TEM results, crystallite sizes of BZN powder samples that were synthesized with different citric acid to metal cations mol ratios were measured by XRD and calculated using Scherrer equation (Table IV.2). It was determined from the XRD results that crystal sizes of powders commonly change from 18 to 47 nm and also increasing heat treatment temperature causes increased crystal size, as expected. As it is found fro TEM results, XRD results also indicated that as the citric acid content increased generally the crystallite size increased.

Tablo IV.2: Particle Sizes calculated by using Scherrer equation on XRD results for $Ba(Zn_{1/3}Nb_{2/3})O_3$ powders that were synthesized with different CA/MC mol ratios and heat treated at various temperatures.

Powder Particle Size (nm)						
Temperature (°C)	**700**	**800**	**900**	**1000**	**1100**	**1200**
BZN-1 (CA/MC: 5)	18	29	30	32	29	36
BZN-2 (CA/MC: 2)	30	31	32	34	37	47
BZN-3 (CA/MC: 1)	25	32	32	28	30	32
BZN-4 (CA/MC: 0.5)	24	29	30	33	36	37

IV.3 PRODUCTION AND CHARACTERIZATION OF $Ba(Zn_{1/3}Nb_{2/3})O_3$ PEROVSKITE CERAMICS

BZN-2 powders that were synthesized by citrate gel method with citric acid/metal cations ratios of 2 and calcined at 1100 °C for 4 hours were used in the production of BZN ceramics. After grinding the calcined powder in an agate mortar, they were made pellets which were sintered at various temperatures between 1250-

1400 °C for 4h to produce dense BZN ceramics. Sintering process was made in a tightly closed alumina crucible by embedding pellets into their own calcined powders to prevent ZnO evaporation. Densities of sintered pellets were measured with Archimed method and relative densities were calculated using theoretical density value of 6.516 g/cm^3 for $Ba(Zn_{1/3}Nb_{2/3})O_3$ ceramic [63].

BZN ceramics (CA/MC: 2) had a relative density of 95.8% at 1300 °C, while they had a relative density of around 94% at 1250 °C. Temperatures above 1300 °C caused a gradual decrease in density (Figure IV.19). Gradual decrease in density above 1300 °C is probably due to evaporation of ZnO [76]. Densities of BZN ceramics synthesized by citrate gel method are higher than the BZN ceramics produced by mixed oxide route [76, 77, 78, 79]. In the study of $Ba(Zn_{1/3}Nb_{2/3})O_3$ produced by solid state route with B_2O_3 and LiF additives by Roulland et al. [80] dictated that BZN requires a high temperature (1350 °C according to the literature) to reach a satisfactory density >90% of the theoretical one.

In another study made by Barwick et al. [76] who produced $Ba(Ni_{1/3}Nb_{2/3})O_3$–$Ba(Zn_{1/3}Nb_{2/3})O_3$ (BNN–BZN) preparation by mixed oxide route, it was reported that maximum density for BZN was achieved at sintering temperatures between 1450–1475 °C with relative density of 92% [76].

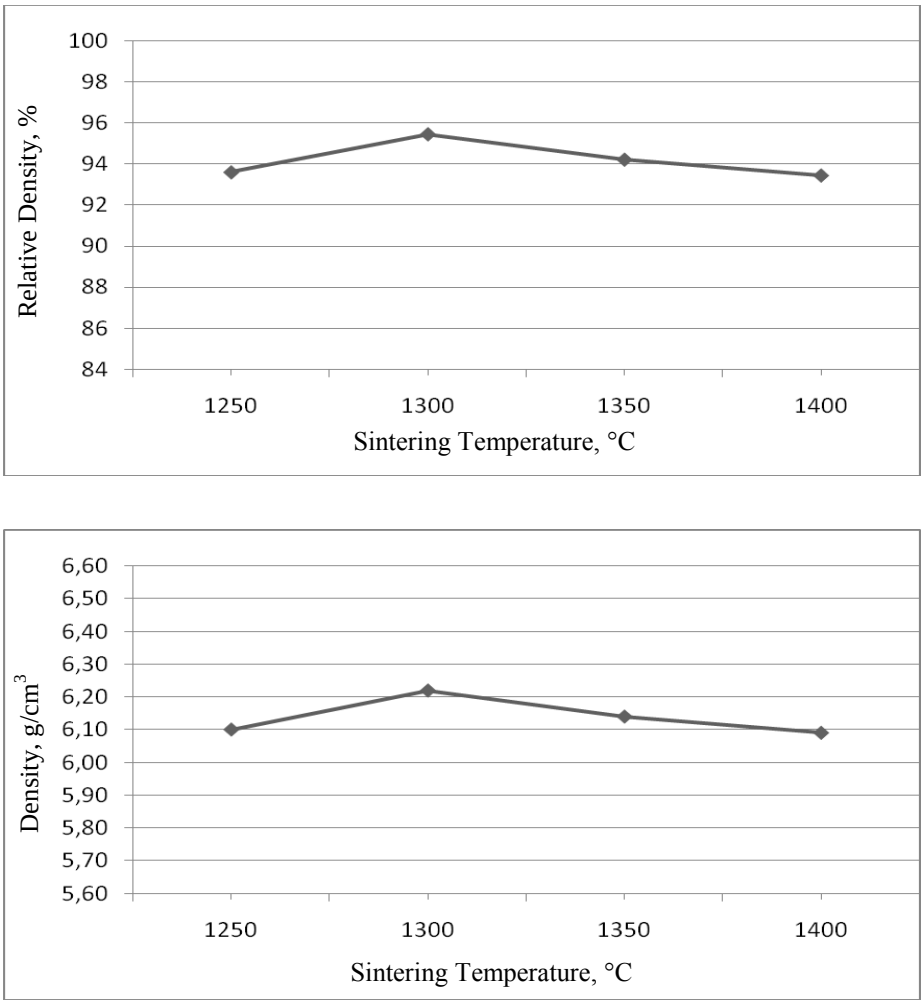

Figure IV.19 Densities of BZN ceramics produced from calcined BZN-2 powders (CA/MC: 2) versus temperature.

SEM images of BZN ceramics sintered at 1300 °C for 4 hours are given in Figure IV.20. Single phase BZN structure was determined in SEM as observed by XRD. BZN grain sizes vary from 0.5 to 4.5 μm. EDS analysis applied on BZN grains indicated that they had identical chemical composition with theoretical BZN composition.

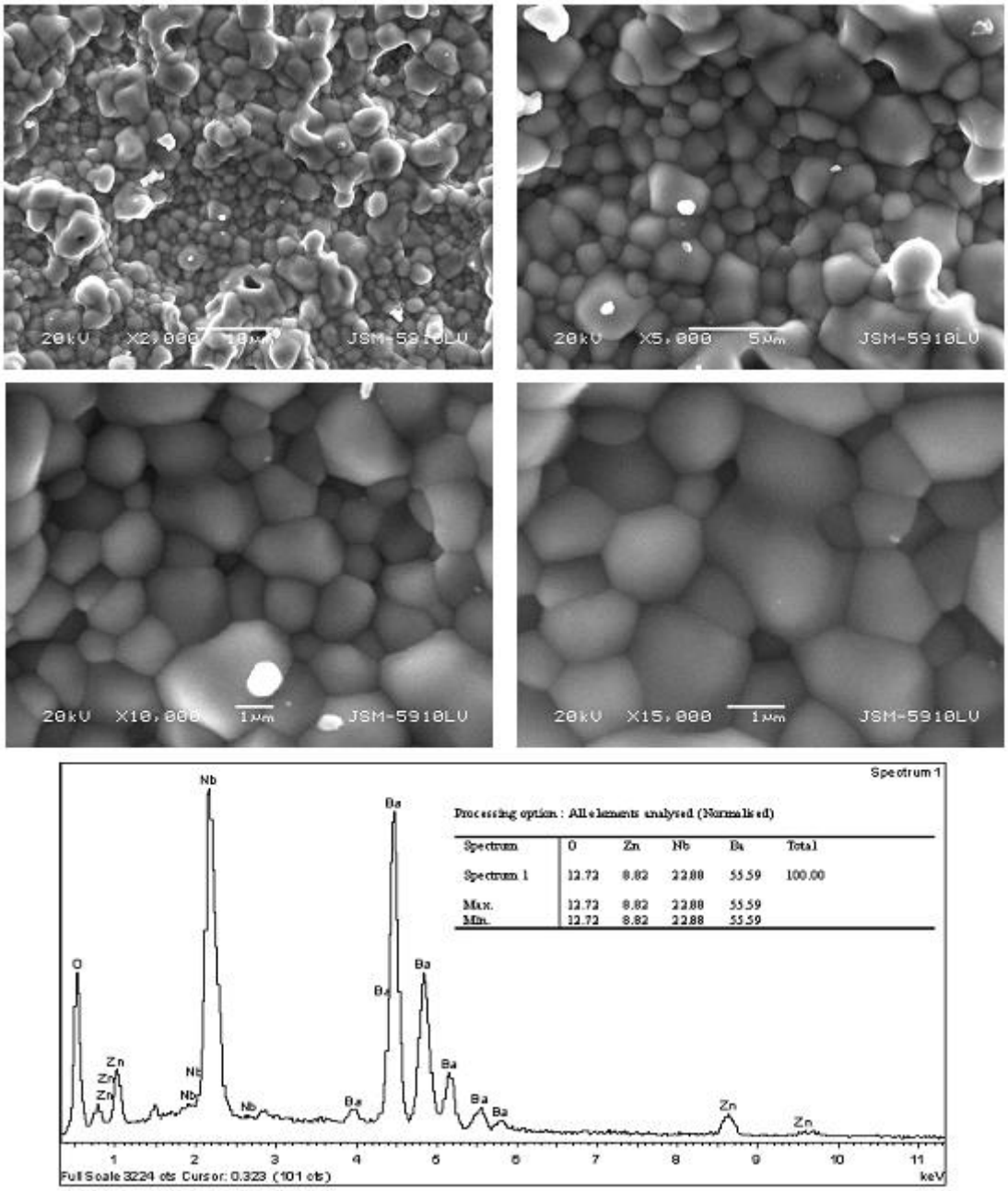

Figure IV.20 SEM images and EDS analysis of BZN ceramics that were produced from BZN-2 powder (CA/MC: 2) by citrate gel method and sintered at 1300 °C for 4 hours.

IV.4 DIELECTRIC PROPERTIES OF $Ba(Zn_{1/3}Nb_{2/3})O_3$ (BZN) PEROVSKITE CERAMICS

The dielectric properties of sintered BZN ceramics were also measured as a function of temperature and frequency. For dielectric measurements, BZN ceramic pellets were produced from BZN-2 powders that were synthesized by citrate gel

method with citric acid/metal cations ratios of 2 and calcined at 1100 °C for 4 hours. BZN ceramics sintered at 1300 °C for 4 hours had a relative density of 95.46%.

Dielectric constant and dielectric loss of BZN ceramics were measured between 1 kHz-2 MHz frequency and in the temperature range of 20-200 °C and the dielectric constant and dielectric loss curves are given in Figure IV.21. Dielectric constant of BZN ceramic changed from 36.6 to 37.7 between 1 kHz-2 MHz frequency range and 20-200 °C temperature ranges. There was a sharp decrease in dielectric constant at low frequencies below 50 kHz, but after that dielectric constant remained almost stable with frequency up to 500 kHz. On the other hand, at frequencies above 500 kHz dielectric constant started to increase. However, the increase in dielectric constant above 500 kHz was rather low and frequency dependency of dielectric constant was rather weak. As it was expected, dielectric constant decreased with increasing temperature in the range of 20-200 °C. But, decrease in dielectric constant with increasing temperature was quite limited. For instance, dielectric constant of 37.29 at 1 MHz and at 20 °C decreased to 36.78 at 1 MHz at 200 °C.

Dielectric loss values were below $2{,}5\times10^{-3}$ at any frequency and temperature values between 1 kHz-2 MHz and 20-200 °C (Figure IV.21). Sharp decrease in dielectric loss was observed below 100 kHz, then dielectric loss behaved almost independently with frequency up to 1 MHz and finally it increased from $1{,}25\times10^{-3}$ to $2{,}5\times10^{-3}$ until 2 MHz. Measured values have correlation with the ones in literature [80, 81, 82]. Veres et al. gave the dielectric constant and dielectric loss of BZN ceramic as 39.4 and $<10^{-3}$ at 1 MHz and 25°C, respectively in the study to produce $Ba(Mg,Zn)_{1/3}Nb_{2/3}O_3$ ceramic by mixed oxide route with addditives of B_2O_3 and LiF [81]. In addition, the study of $Ba(Zn_{1/3}Nb_{2/3})O_3$ production by solid state route with additives of B_2O_3 and LiF by Roulland et al. revealed that BZN samples had dielectric constant as 37.2 and dielectric loss values as $<10^{-3}$ [80].

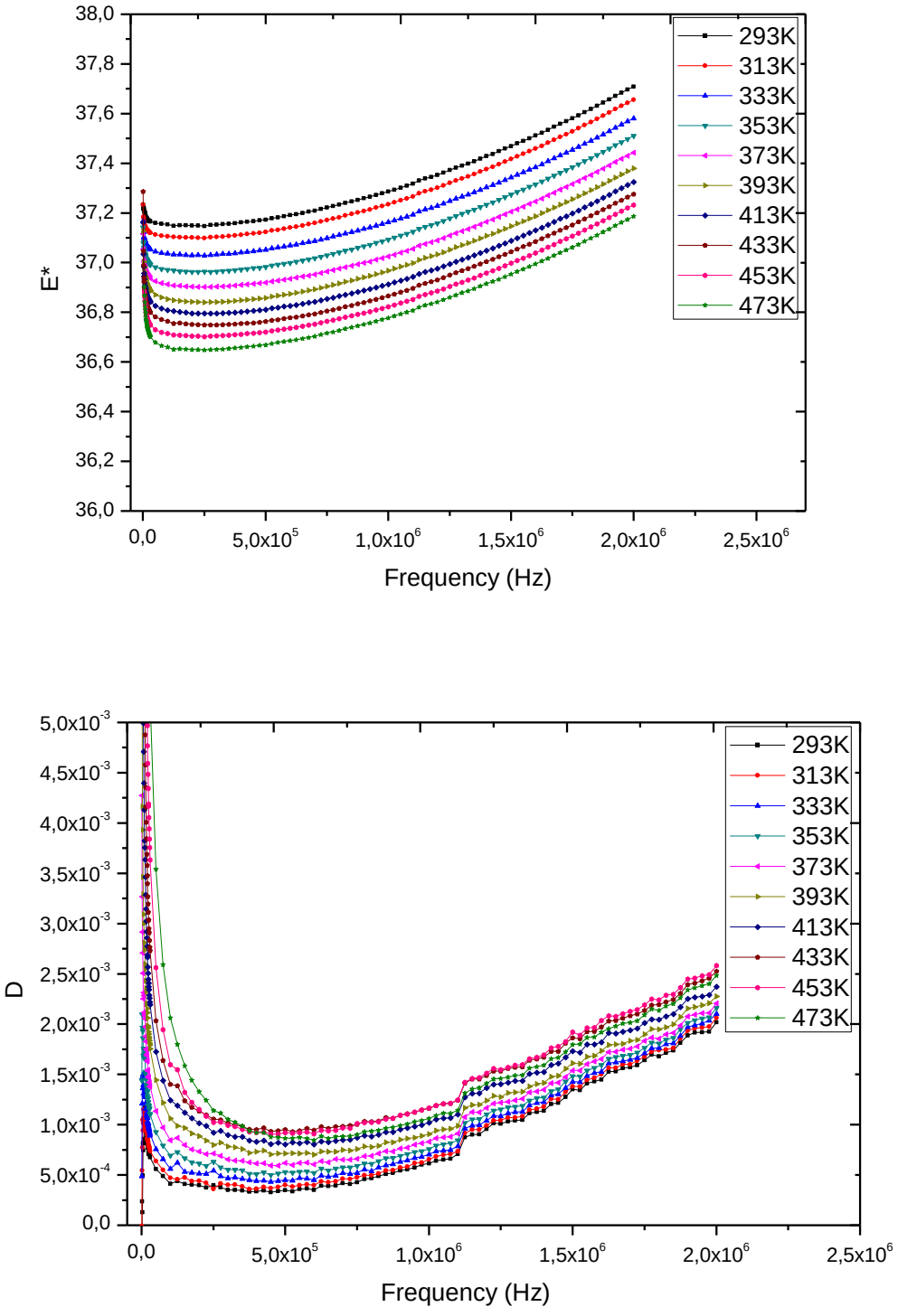

Figure IV.21 Dielectric constant (E) and dielectric loss (D) variation of BZN ceramics produced with CA/MC: 2 and sintered at 1300 °C for 4 hours versus frequency at various temperatures.

CHAPTER V

CONCLUDING REMARKS AND RECOMMENDATIONS

$Ba(Zn_{1/3}Nb_{2/3})O_3$ perovskite ceramic powders were synthesized by citrate gel method. Effect of citric acid content during production of BZN powders was examined by changing the citric acid to total metal cation (Ba+Zn+Nb) ratio as 5.0, 2.0, 1.0, 0.5 (CA/MC=5.0 BZN-1; CA/MC=2.0 BZN-2; CA/MC=1.0 BZN-3; CA/MC=0.5 BZN-4). $Ba(Zn_{1/3}Nb_{2/3})O_3$ ceramic powders, synthesized by citrate gel method were characterized in detail by different techniques (TG-DTA, XRD, FT-IR, SEM, TEM) and effect of citric acid content on phase development and size, shape and morphology of particles were investigated. Finally, $Ba(Zn_{1/3}Nb_{2/3})O_3$ perovskite ceramics with high density were produced by sintering and their microstructures were examined by SEM and their dielectric properties were measured at different frequencies and temperatures.

High citric acid content effected the BZN phase formation negatively because although BZN phase started to form at low temperature (500 °C), single phase BZN could not be obtained even at high temperatures. Although, the structure at 1000 °C was almost completely BZN phase, some secondary phases with low intensities existed as well. In addition, BZN phase decomposed into undefined phases at temperatures above 1000 °C probably due to the evaporation of ZnO. Therefore, it can be concluded that high citric acid amounts are not appropriate to produce BZN phase by citrate gel method. On the other hand, low citric acid contents (CA/MC: 0.5) led to formation of $Ba_4Nb_{14}O_{23}$ phase at 400 °C and 500 °C and BZN phase started to form at higher temperatures (600 °C). Moreover, single phase BZN structure was obtained relatively at high temperature (1100 °C). Therefore, besides high citric acid contents, low citric acid contents as CA/MC: 0.5 is not appropriate to produce BZN powder. However, moderate levels of citric acid to total metal cations ratio (CA/MC: 2 and CA/MC: 1) are more suitable for the production of BZN. Comparing these two ratios, CA/MC:2 is much more promising ratio than the

CA/MC: 1 because at this ratio BZN started to form at 400 °C and single phase BZN structure was obtained at 1000 °C. These results indicate that citric acid content has significant effect on BZN phase development.

In addition to phase development, effect of citric acid content on the size, shape and morphology and on the degree of agglomeration was also determined. SEM and TEM results revealed that although citric acid content did not have any considerable effect on particle morphology, it affected the size of particles. At all ratios near to spherical particles were obtained. While the size of BZN particles were identical for the CA/MC ratios of 5, 2 and 1 (between 55-150 nm), larger particles of between 150-200 nm were obtained at lower citric acid contents. Crystallite size measurement by XRD also confirms these results. Citric acid content also effects the degree of agglomeration that although for high (CA/MC:5) and low (CA/MC:0.5) ratios higher degree of agglomeration were observed, moderate citric acid contents (CA/MC: 2 and 1) have lower agglomeration.

BZN ceramics produced from powder with CA/MC ratio of 2 had a relative density of 95.5% at 1300 °C. Temperatures above 1300 °C caused a gradual decrease in density due to evaporation of ZnO. Densities of BZN ceramics synthesized by citrate gel method are higher than the BZN ceramics produced by mixed oxide route. SEM examination revealed only single phase structure as XRD. The size of BZN grains varied from 0.5 to 4.5 μm.

BZN ceramics sineterd at 1300 °C for 4h had a dielectric constant between 36.6 to 37.7 in the frequency range of 1 kHz-2 MHz and between 20-200 °C. The dielectric loss were below 1.,25$\times 10^{-3}$ above 100 kHz. Both dielectric constant and dielectric loss indicated rather a low frequency and temperature dependence between, 1 kHz-2 MHz and 20-200 °C.

Recommendations

Microwave frequency dielectric properties of chemically produced BZN should be measured.

Some additives could be doped into the BZN using complex polymerized technique to modify the dielectric properties.

Some surfactants could be used in polymerized complex method to reproduce BZN powders with less degree of agglomeration.

REFERENCES

[1] Hench, L.L.; West, J.K.: "Principles of Electronic Ceramics", *Principles of Electronic Ceramics*, **(1990)**

[2] Galasso, F.; Katz, R.W.: "Substitution in the Octahedrally Coordinated Cation Positions in Compounds of the Perovskite Type", *J. Am. Chem. Soc.*, 81 **(1959)** 820–823.

[3] Moulson, A.J.; Herbert, J.M.: "Electroceramics-Materials-Properties-Applications", *John Wiley and Sons*, 2nd Edition., England, **(2003)**.

[4] Wakino, K.; Minai, T. and Tamura, H.: "Microwave characteristics of (Zr,Sn)TiO_4 and BaO-PbO-Nd_2O_3-TiO_2 dielectric resonators", *J. Am. Ceram. Soc.*, 67 **(1984)** 278–281.

[5] Kawashima, S.; Nishida, M.; Ueda, I. and Ouchi, H.: "$BaZn_{1/3}Ta_{2/3}O_3$ Ceramics with Low Dielectric Loss at Microwave Frequencies", *J. Am. Ceram. Soc.*, 66 **(1983)** 421–423.

[6] Lu, C.H. and Tsai, C.C.: "Reaction kinetics, sintering characteristics, and ordering behavior of microwave dielectrics: Barium magnesium tantalate", *J. Mater. Res.*, 11 **(1997)** 1219–1227.

[7] Hong, K.S.; Kim, I.T. and Kim, C.D.: "Order-Disorder Phase Formation on the Complex Perovskite Compounds $Ba(Ni_{1/3}Nb_{2/3})O_3$ and $Ba(Zn_{1/3}Nb_{2/3})O_3$", *J. Am. Ceram. Soc.*, 79 **(1996)** 3218–3224.

[8] Reaney, I.M.; Iqbal, Y.; Zheng, H.; Feteira, A.; Hughes, H.; Iddles, D.; Muir, D. and Price, T.: "Order–disorder behavior in $0.9Ba([Zn_{0.60}Co_{0.40}]_{1/3}Nb_{2/3})O_3$–$0.1Ba(Ga_{0.5}Ta_{0.5})O_3$ microwave dielectric resonators", *J. Eur. Ceram. Soc.*, 25 **(2005)** 1183–1189.

[9] Khemakhem, L.; Kabadoua, A.; Maalej, A.; Ben Salah, A.; Simonc, A. and Maglione, M.: "New relaxor ceramic with composition $BaTi_{1-x}(Zn_{1/3}Nb_{2/3})_xO_3$", *J. Alloys Comp.*, 452 **(2008)** 451–455.

[10] Barwick, M.; Azough, F. and Freer, R..: "Structure and dielectric properties of perovskite ceramics in the system $Ba(Ni_{1/3}Nb_{2/3})O_3$-$Ba(Zn_{1/3}\ Nb_{2/3})O_3$", *J. Eur. Ceram. Soc.*, 26 **(2006)** 1767–1773.

[11] Carter, C.B. and Norton, M.G.: "Ceramic Materials Science and Engineering", *Springer Science+Business Media, LLC.*, New York, USA, **(2007).**

[12] Koch, C.C.: "Nanostructured Materials: Processing, Properties and Applications", *William Andrew Publishing*, 2nd Edition, New York, USA, **(2007)**.

[13] Chow, G.M. and Gonsalves, K.E.: "Particle Synthesis by Chemical Routes, (A. S. Edelstein, and R. C. Cammarata, eds.), Nanomaterials: Synthesis, Properties, and Applications", *Institute of Physics Publishing*, Bristol and Philadelphia, **(1996)** 55-71.

[14] Klein, L.C.: "Processing of Nanostructured Sol-Gel Materials, (A. S. Edelstein, and R. C. Cammarata, eds.), Nanomaterials: Synthesis, Properties, and Applications", *Institute of Physics Publishing*, Bristol and Philadelphia, **(1996)** 147-164.

[15] Sugimoto, T.; Zhou, X.P. and Muramatsu, A.: "Synthesis of Uniform Anatase TiO_2 Nanoparticles by Gel-sol Method 3. Formation Process and Size Control", *J. Colloid Interf. Sci.*, 259 **(2003)** 43-52.

[16] Barnard, A.S. and Curtiss, L.A.: "Prediction of TiO_2 Nanoparticle Phase and Shape Transitions Controlled by Surface Chemistry", *Nano Lett.*, 5 **(2005)** 1261–1266.

[17] Pierre, A.C.: "Sol-Gel Processing of Ceramic Powders", *Am. Ceram. Soc. Bull.*, 70 **(1991)** 1281-1288.

[18] Kozuka, H.: "HANDBOOK of SOL–GEL SCIENCE and TECHNOLOGY, Processing, Characterization and Applications", *Kluwer Academic Publishers*, Volume I.

[19] King, A.G.: "Ceramic Technology and Processing", *William Andrew Publishing/Noyes*, **(2002)**.

[20] Materials Evaluation and Engineering, Inc., *"Handbook of Analytical Methods for Materials"*, http://mee-inc.com/eds.html

[21] Moulson, A.J. and Herbert, J.M.: "Electroceramics", *John Wiley & Sons Ltd.*, 2nd Edition, Chichester, England, **(2003)**.

[22] Sebastian, M.T.: "Dielectric Materials for Wireless Communication", *Elsevier*, 1st Edition, Netherlands, **(2008)**.

[23] Moulson, A.J. and Herbert, J.M.: "Electroceramics", *Chapman and Hall*, London, **(1990)**.

[24] Halli, B.W. and Coleman, P.D.: "A dielectric resonator method of measuring inductive capacities in the millimeter range", *IRE Trans. Microw. Theory Tech. MTT,* 8 **(1960)** 402-410.

[25] Courtney, W.E.: "Analysis and evaluation of a method of measuring complex permittivity and permeability of microwave materials", *IEEE Trans. Microw. Theory Tech. MTT*, 18 **(1970)** 476–485.

[26] Krupka, J.: "Frequency domain complex permittivity measurements at microwave frequencies", *Meas. Sci. Technol.*, 16 **(2005)** 1–16.

[27] Gurevich, G.L. and Tagantsev, A.K.: "Intrinsic dielectric loss in crystals", *Adv. Phys.*, 40 **(1991)** 719–767.

[28] Kajfezz, D. and Guillon, P.: "Dielectric Resonators", *Noble Publishing Corporation*, Georgia, USA, **(1998)**.

[29] Kajfezz, D. and Guillon, P.: "Dielectric Resonators", *Noble Publishing Corporation*, Georgia, USA, **(1998)**.

[30] Navrotsky, A. and Weidner, D.J.: "Perovskite: A Structure of Great Interest to Geophysics and Materials Science", *American Geophysics Union*, Washington, DC, **(1989)**, Vol. 45.

[31] Megaw, H.D.: "Crystal structure of double oxides of the perovskite type", *Proc. Phys. Soc.*, 58 **(1946)** 133–152.

[32] Roy, R.: "Multiple ion substitution in perovskite lattice", *J. Am. Ceram. Soc.*, 37 **(1954)** 581–588.

[33] Roy, R.: "Multiple ion substitution in the perovskite lattice", *J. Am. Ceram. Soc.*, 27 **(1954)** 581–588.

[34] Galasso, F.S.; Katz, L. and Ward, R.: "Substitution in the octahedrally coordinated cation positions in compounds of perovskite type", *J. Amer. Chem. Soc.*, 81 **(1959)** 820–823.

[35] Galasso, F.S.; Barrante, J.R. and Katz, L.: "Alkaline earth tantalum oxygen phases including the crystal structure of an ordered perovskite compound $Ba_3SrTa_2O_9$", *J. Amer. Chem. Soc.*, 83 **(1961)** 2830–2832.

[36] Galasso, F.S.: "Structure and properties of perovskite compounds", *Pergamon Press*, Headington Hill, Oxford, **(1969)**.

[37] Galasso, F. and Pyle, J.: "Ordering in compounds of the $A(B_{0.33}Ta_{0.67})O_3$ type", *Inorg. Chem.*, 23 **(1963)** 482–484.

[38] Kawashima, S.; Nishida, M.; Ueda, I.; Ouchi, H. and Hayakawa, S.: "Dielectric properties of $Ba(Zn_{1/3}Nb_{2/3})O_3$–$Ba(Zn_{1/3}Ta_{2/3})O_3$ ceramics", *Keihin Printing Co., Ltd.*, Kyoto, Tokyo, **(1977)** 293–296.

[39] Nomura, S.: "Ceramics for microwave dielectric resonator", *Ferroelectrics*, 49 **(1983)** 61–70.

[40] Roulland, F. and Marinel, S.: "Effects of glass phase additives and stoichiometry on the $Ba(Zn_{1/3}X_{2/3})O_3$ (X=Ta or Nb) sinterability and dielectric properties", *J. Electroceram*, 14 **(2005)** 239–246.

[41] Roulland, F. and Marinel, S.: "$Ba(Zn_{1/3}Nb_{2/3})O_3$ sintering temperature lowering for silver co-sintering applications", *Ceram. Int*, 32 **(2006)** 377–383.

[42] Liou, Y.C.; Chen, J.H.; Wang and Liu, C.Y.: "Synthesis of $Ba_xSr_{1-x}(Zn_{1/3}Nb_{2/3})O_3$ ceramics by reaction sintering process and microstructure", *Mater. Res. Bull*, 41 **(2006)** 455–460.

[43] Kolodiazhnyi, T.; Annino, G.; Younker, A.; Malysz, P.; Maschen, P. and Haneda, H.: "Probing point defects in $Ba(B'_{1/3}B''_{2/3})O_3$ by ESR, PAS and dielectric spectroscopy", *J. Eur. Ceram. Soc.*, 26 **(2006)** 1921–1924.

[44] Onada, M.; Kuwata, J.; Kaneta, K.; Toyoma, K. and Nomura, S.: "$Ba(Zn_{1/3}Nb_{2/3})O_3$–$Sr(Zn_{1/3}Nb_{2/3})O_3$ solid solution ceramics with temperature stable high dielectric constant and microwave loss", *Jpn. J. Appl. Phys*, 21 **(1982)** 1707–1710.

[45] Liang, M.H.; Hu, C.T.; Chang, H.Y. and Lin, I.N.: "$Ba(Zn_{1/3}Nb_{2/3})O_3$ ceramics synthesized by spray pyrolysis techniques, *Ferroelectrics*, 231 **(1999)** 243–248.

[46] Varma, M.R; Biju, S. and Sebestian, M.T.: "Preparation of phase pure $Ba(Zn_{1/3}Ta_{2/3})O_3$ nanopowders for microwave dielectric resonator applications", *J. of the Euro. Ceram. Soc.*, 26 **(2006)** 1903-1907.

[47] Lu, C.H. and Tsai, C.C.: "A new sol–gel route using inorganic salts for synthesizing barium magnesium tantalate ceramics", *Mater. Lett.*, 31 **(1997)** 271–274.

[48] Ravichandran, D.; Meyer, R.; Roy, R.; Guo, R.; Bhalla, A.S. and Cross, L.E.: "Sol–gel synthesis of $Ba(Mg_{1/3}Ta_{2/3})O_3$: phase pure thin films", *Mater. Res. Bull.*, 31 **(1996)** 817–825.

[49] Liang, M.H.; Wu, S.Y.; Hu, C.T. and Lin, I.N.: "Enhancing the sinterability of $Ba(Mg_{1/3}Ta_{2/3})O_3$ dielectrics by using chemically-derived powders", *Mater. Chem. and Phys.*, 79 **(2003)** 276-281.

[50] Tsai, C.C. and Teng, H.: "Synthesis of $Ba(Mg_{1/3}Ta_{2/3})O_3$ microwave ceramics through a sol-gel route using acetate salts", *J. Am. Ceram. Soc.*, 87 **(2004)** 2080-2085.

[51] Liang, M.H.; Hu, C.T.; Chang, H.Y. and Lin, I.N.: "$Ba(Zn_{l/3}Nb_{2/3})0_3$ Ceramics Synthesized by Spray Pyrolysis Technique", *Ferroelectrics*, 231 **(1999)** 243-248.

[52] Mergen, A. and Sert, D.: "Production of $Ba(Zn_{1/3}Nb_{2/3})O_3$ Ceramic by Coprecipitation" submitted to Materials Characterization, 2010.

[53] Noh, S.Y.; Yoo, M.J.; Nahm, S.; Choi, C.H.; Park, H.M. and Lee, H.J.: "Effect of structural changes on the microwave dielectric properties of $Ba(Zn_{1/3}Nb_{2/3})O_3$ ceramics, *Jpn. J. Appl. Phys*, 41 **(2002)** 2978–2981.

[54] Wu, H. and Davies, P.K.: "Influence of non-stoichiometry on the structure and properties of $Ba(Zn_{1/3}Nb_{2/3})O_3$ microwave dielectrics", J. *Am. Ceram. Soc.*, 89 **(2006)** 2264–2270.

[55] Scott, R.I.; Thomas, M. and Hapson, C.: "Development of low cost, high performance $Ba(Zn_{1/3}Nb_{2/3})O_3$ based materials for microwave resonator applications", *J. Eur. Ceram. Soc.*, 23 **(2003)** 2467–2471.

[56] Yue, Z.; Zhao, F.; Zhang, Y.; Gui, Z. and Li, L.: "Microwave dielectric properties of $Ba[(Zn_{1-x}Co_x)_{1/3}Nb_{2/3}]O_3$ ceramics", *Mater. Lett.*, 58 **(2004)** 1830–1834.

[57] Galasso, F.S. and Pyle, J.: "Preparation and study of ordering in $A(B_{0.33}Nb_{0.67})O_3$ perovskite type", *J. Phys. Chem.*, 67 **(1963)** 1561–1562.

[58] Colla, E.L.; Reaney, I.M. and Setter, N.: "Effect of structural changes in complex perovskites on the temperature coefficient of the relative permittivity", J. *Appl. Phys.*, 74 **(1993)** 3414–3425.

[59] Kim, J.S.; Lee, J.H.; Lim, Y.S.; Jang, J.W. and Kim, I.T.: "Revisit to the anomaly in dielectric properties of $Ba_{1-x}Sr_x(Zn_{1/3}Nb_{2/3})O_3$ solid solution systems", *Jpn. J. Appl. Phys.*, 36 **(1997)** 5558–5581.

[60] Reaney, I.M.; Colla, E.L. and Setter, N.: "Dielectric and structural characteristics of Ba and Sr based complex perovskites as a function of tolerance factor", *Jpn. J. Appl. Phys.*, 33 **(1994)** 3984–3990.

[61] Glazer, A.M.: "The classification of tilted octahedra in perovskites", *Acta Crystallogr.*, 28 **(1972)** 3384–3392.

[62] Sianou, A.K.; Stergioudis, G.A.; Efthimiadis, K.G.; Kalogirou, O. and Tsoukalas, I.A.: "Detection by Means of Electrical and Magnetic Measurements of Cr^{n+} (n>3) Ions in Polycrystalline $ZnCr_2O_4$ Samples Prepared by Heating in Air", *Journal of Alloys and Compounds*, 392 **(2005)** 310-316.

[63] Wu, H. and Davies, P.K.: "Influence of Non-Stoichiometry on the Structure and Properties of $Ba(Zn_{1/3}Nb_{2/3})O_3$ Microwave Dielectrics: I. Substitution of $Ba_3W_2O_9$", *J. Am. Ceram. Soc.*, 89 **(2006)** 2239-2249.

[64] Mao, C.; Dong, X.; Zeng, T.; Wang, G. and Chen, W.S.: "Formation and Control of Mechanism for the Preparation of Ultra-Fine Barium Strontium Titanate Powders by the Citrate Precursor Method", *Mat. Res. Bull.*, 42 **(2007)** 1602-1610.

[65] Majid, A.; Tunney, J.; Argue, S.; Wang, D.; Post, M. and Margeson, J.: "Preparation of $SrFeO_{\sim 2.85}$ Perovskite Using a Citric Acid Assisted Pechini-Type Method", *J. of Alloys and Comp.*, 398 **(2005)** 48–54.

[66] Trakarnpruk, W. and Sukkaew, C.: "Preparation of $Ni/MgO.ZrO_2$ Nanocrystals by Citrate Sol–Gel Method", *J. of Alloys and Comp.*, 460 **(2008)** 565–569.

[67] Mali, A. and Ataie, A.: "Structural Characterization of Nano-Crystalline $BaFe_{12}O_{19}$ Powders Synthesized by Sol–Gel Combustion Route", *Scripta Materialia*, 53 **(2005)** 1065–1070.

[68] Lee, C.T.; Lin, Y.C.; Huang, C.Y. and Su, C.Y.: "Ordering and Dielectric Characteristics in Barium Zinc Niobate, *J. Am. Ceram. Soc.*, 90 **(2007)** 483-489.

[69] Hobbs, V.; Chapman, E.N. and Craven, A.J.: "Radiation Effects in Analysis in TEM in Quantitative Electron Microscopy", *SUSSP Publishing*, **(1984)**.

[70] Mclaren, A.C.: "Transmission Electron Microscopy of Minerals and Rocks", *Cambridge University Publishing*, Cambridge, **(1991)**.

[71] Duran, P.; Gutierrez, D.; Tartaj, J.; Banares, M.A. and Moure, C.: "On the formation of an oxycarbonate intermediate phase in the synthesis of $BaTiO_3$ from (Ba,Ti)-polymeric organic precursors", *J. Eur. Ceram. Soc.*, 22 **(2002)** 797–807.

[72] Colthup, N.B.; Daly, L.H. and Wiberley, S.E.: "Introduction to Infrared and Raman Spectroscopy", *Academic Press*, 3rd Edition, New York, **(1990)**.

[73] Bertran, C.A.; Silva, N.T. and Thim, G.P.: "Citric Acid Effect on Aqueous Sol-Gel Cordierite Synthesis", *Journal of Non-Crystalline Solids*, 273 **(2000)** 140-44.

[74] Chandradass, J.; Kim, M.H. and Bae, D.S.: "Influence of Citric Acid to Aluminum Nitrate Molar Ratio on the Combustion Synthesis of Alumina–Zirconia Nanopowders", *J. Alloys and Comp.*, 470 **(2009)** L9–12.

[75] Mali, A. and Ataie, A.: "Influence of the Metal Nitrates to Citric Acid Molar Ratio on the Combustion Process and Phase Constitution of Barium Hexaferrite Particles Prepared by Sol–Gel Combustion Method", *Ceram. Int.*, 30 **(2004)** 1979–83.

[76] Barwick, M.; Azough, F. and Freer, R.: "Structure and Dielectric Properties of Perovskite Ceramics in the System $Ba(Ni_{1/3}Nb_{2/3})O_3$-$Ba(Zn_{1/3}Nb_{2/3})O_3$, *J. Euro. Ceram. Soc.*, 26 **(2006)** 1767-73.

[77] Yue, Z.; Zhao, F.; Zhang, Y.; Gui, Z. and Li, L.: "Microwave Dielectric Properties of $Ba[(Zn_{1-x}Co_x)_{1/3}Nb_{2/3}]O_3$ Ceramics", *Materials. Letters*, 58 **(2004)** 1830-1834.

[78] Kim, I.T.; Hong, K.S. and Yoon, S.J.: "Effect of Nonstoichiometry and Chemical Inhomogeneity on the Order–Disorder Phase Formation in the Complex Perovskite Compounds, $Ba(Ni_{1/3}Nb_{2/3})O_3$ and $Ba(Zn_{1/3}Nb_{2/3})O_3$", *J. Mater. Sci.*, 30 **(1995)** 514–521.

[79] Park, J.K. and Kim, D.Y.: "Effect of Grain Size on Diffusion-Induced Grain Boundary Migration in $Ba(Zn_{1/3}Nb_{2/3})O_3$ Ceramics", *J. Am. Ceram. Soc.*, 79 **(1996)** 1405-1408.

[80] Roulland, F. and Marinel, S.: "$Ba(Zn_{1/3}Nb_{2/3})O_3$ Sintering Temperature Lowering for Silver Co-Sintering Applications", *Ceram. Int.*, 32 **(2006)** 377–383.

[81] Veres, A.; Marinel, S. and Roulland, F.: "Dielectric Properties of $Ba(Mg,Zn)_{1/3}Nb_{2/3}O_3$ and Effect of B_2O_3 and LiF Addition", *J. Eur. Ceram. Soc.*, 25 **(2005)** 2759–62.

[82] Varma, M.R. and Sebastian, M.T.: "Effect of Dopants on Microwave Dielectric Properties of $Ba(Zn_{1/3}Nb_{2/3})O_3$ Ceramics*", J. Eur. Ceram. Soc.*, 27 **(2007)** 2827-33.

BIOGRAPHY

Duygu SERT was born on July, 1984 in İzmit. She raised in İzmit, KOCAELİ. Following her high school education in Kocaeli Anatolian High School in 2002, she attended to Marmara University and she was graduated from Metallurgical and Materials Enginnering programme in 2007. In addition to her major education in Metallurgical and Materials Engineering, she attended Mechanical Engineering in Marmara University as a minor programme and completed in 2007. She has been studying her M.Sc. eduacation in Marmara University, Pure and Applied Sciences Institute, Metallurgy and Materials Engineering programme since 2007. During her M.Sc. education, she has been working as research student in the project (Grant Number 107M372) of The Scientific and Technological Research Council of Turkey (TUBITAK).

Currently, she is working as Quality Control Engineer (NDT Engineer) in General Electric, Aviation, Marmara Technology Center since January, 2009.

Publication;

1. Sert, D. and Mergen, A.: "Production of nanoscale $Ba(Zn_{1/3}Nb_{2/3})O_3$ microwave dielectric ceramics by polymerised complex method", *Journal of Alloys and Compounds*, 482 **(2009)** 396-399.

2. Sert, D. and Mergen, A.: "Production of Nano Scale $Ba(Zn_{1/3}Nb_{2/3})O_3$ Microwave Dielectric Ceramics by Polymerized Complex Method", *7th International Ceramic Congress, Afyonkarahisar*, Turkey, 26-28 November **(2008)**.

3. Mergen, A. and Sert, A.: "Production of $Ba(Zn_{1/3}Nb_{2/3})O_3$ Ceramic by Coprecipitation", submitted to Materials Characterization, 2010.

MARMARA UNIVERSITY

THE INSTITUTE FOR

GRADUATE STUDIES IN PURE AND APPLIED SCIENCES

ACCEPTANCE AND APPROVAL DOCUMENT

The jury established by the Executive Board of the *INSTITUTE FOR GRADUATE STUDIES IN PURE AND APPLIED SCIENCES* on 07.07.2010 (Resolution no:2010/11-08) has accepted Ms Duygu SERT 's thesis titled "Production of Nanoscale $Ba(Zn_{1/3}Nb_{2/3})O_3$ Microwave Dielectric Ceramics by Polymerised Complex Method" as Master of Science thesis in Department of Materials Science and Engineering, Materials Science and Engineering Programme.

Advisor	: Assoc. Prof. Dr. Ayhan MERGEN	Marmara University
1. Member of the jury	: Prof. Dr. Arif N. GULLUOGLU	Marmara University
2. Member of the jury	: Prof. Dr. Ugur YAHSI	Marmara University

Date : 07.07.2010

APPROVAL

Ms. Duygu SERT has satisfactorily completed the requirements for the degree of Master of Science in Metallurgy and Materials Engineering at Marmara University. The Executive Commitee approves that she be granted the degree of Master of Science on 09.08.2010 (Resolution no:2010/15-02)

DIRECTOR OF THE INSTITUTE

Prof. Dr. Meral ÜNAL
Müdür